



**ANA RITA FUTRE
CARREIRA**

**SÍNTESE E AVALIAÇÃO DE NOVOS DERIVADOS
DE PIRAZOL PARA ATIVIDADE CITOTÓXICA**

**SYNTHESIS AND EVALUATION OF NOVEL
PYRAZOLE DERIVATIVES FOR CYTOTOXIC
ACTIVITY**



**ANA RITA FUTRE
CARREIRA**

**SÍNTESE E AVALIAÇÃO DE NOVOS DERIVADOS
DE PIRAZOL PARA ATIVIDADE CITOTÓXICA**

**SYNTHESIS AND EVALUATION OF NOVEL
PYRAZOLE DERIVATIVES FOR CYTOTOXIC
ACTIVITY**

Dissertação apresentada à Universidade de Aveiro para cumprimento dos requisitos necessários à obtenção do grau de Mestre em Bioquímica, ramo Métodos Biomoleculares, realizada sob a orientação científica da Doutora Susana Santos Braga, Investigadora Principal do Departamento de Química da Universidade de Aveiro e co-orientação da Doutora Paula Andrade, Professora Associada com Agregação do Departamento de Ciências Químicas da Faculdade de Farmácia da Universidade do Porto.

o júri

presidente

Doutor Francisco Manuel Lemos Amado

Professor associado com agregação do Departamento de Química da Universidade de Aveiro

Doutora Susana Isabel Fonseca de Almeida Santos Braga

Investigadora principal do Departamento de Química da Universidade de Aveiro

Doutor David Alexandre Micael Pereira

Professor auxiliar da Faculdade de Farmácia da Universidade do Porto

agradecimentos

Em primeiro lugar, agradeço à minha orientadora, Doutora Susana Braga, pelo acompanhamento, paciência e boa disposição do costume. À minha coorientadora, Doutora Paula Andrade, por me ter recebido na Faculdade de Farmácia do Porto e por ter disponibilizado todos os recursos necessários para a execução dos ensaios biológicos. À Doutora Vera Silva por todos os conselhos, pela dedicação e por todos os ensinamentos sobre síntese orgânica. Ao Doutor David Pereira, pela disponibilidade e revisão dos resultados dos ensaios biológicos. Ao Doutor Artur Silva, pela retificação da estrutura química dos compostos orgânicos. Agradeço também à Universidade de Aveiro e a todos os professores que fizeram parte do meu percurso académico.

A todos os amigos que fiz ao longo dos últimos anos, em especial ao Luís Figueiredo e à Bruna Pereira. Agradeço também a inspiração artística que me tentaram transmitir, um dia ainda vou ser capaz de desenhar qualquer coisa em condições.

À minha família, pela força, amor e paciência. Sei que nem sempre sou fácil de aturar. À minha mãe por todas as lições de vida, ao meu pai por me proporcionar esta oportunidade, aos meus irmãos por me deixarem implicar com eles e à minha avó por me considerar, certamente, a neta preferida.

Por fim, ao Diogo por estar sempre presente na minha vida, pelo apoio, carinho e compreensão.

palavras-chave

Hidroxifenilestirilpirazóis, Complexos de Ruténio, Atividade citotóxica

resumo

O número crescente de pessoas afetadas mundialmente pelo cancro tem levado a comunidade científica a ampliar os esforços de pesquisa nesta área. O desenvolvimento de novos fármacos com potencial aplicação no tratamento do cancro tem sido amplamente estudado. Os pirazóis e os seus derivados são uma classe promissora devido ao seu variado espectro de atividades, que inclui a ação anticancerígena.

Neste trabalho são preparados derivados de uma família de (*E*)-3(5)-(2-hidroxifenil)-4-estiril-1*H*-pirazóis através de reações de glicosilação ou pela formação de complexos de coordenação de ruténio tritriacilononano, com o objetivo de obter novos compostos com ação citotóxica contra células tumorais. Os compostos sintetizados são caracterizados recorrendo a técnicas espectroscópicas de RMN 1D (¹H e ¹³C) e 2D (HSQC, HMBC, COSY e NOESY), espectrometria de massa e espectroscopia de infravermelho no caso dos complexos de ruténio. Sempre que possível, a pureza dos compostos foi ainda avaliada através da determinação do ponto de fusão.

Os compostos sintetizados são avaliados contra uma linha celular de cancro do estômago (AGS) e contra uma linha celular saudável de fibroblastos do pulmão (MRC-5), de modo a averiguar tangencialmente a sua seletividade. Dos compostos sintetizados, o mais potente é o complexo de ruténio contendo o ligando pirazol com um grupo metoxilo na posição *-para-* do estirilo. Este composto apresentou um IC₅₀ de 18.3 µM contra a linha celular tumoral AGS e um IC₅₀ de 62.2 µM contra a linha celular saudável MRC-5. A inserção do ligando no complexo de ruténio melhorou a seletividade quando comparada com o ligando isolado.

keywords

Hydroxyphenylstyrylpyrazoles, Ruthenium complexes, Cytotoxic activity.

abstract

The growing number of cancer patients worldwide has led the scientific community to strengthen research efforts in this field. The development of novel drug candidates for cancer treatment has been largely studied. Among these, pyrazoles derivatives are a promising class for their wide range of pharmacological activities, including antitumoral action.

This work describes the preparation of (*E*)-3(5)-(2-hydroxyphenyl)-4-styryl-1*H*-pyrazole derivatives, either by glycosylation reactions or by the formation of ruthenium trithiacyclononane complexes. The new compounds aim at having antitumoral activity. Full characterization of the compounds is carried out by NMR 1D (¹H and ¹³C) and 2D (HSQC, HMBC, COSY and NOESY) spectroscopies and by mass spectrometry. The new ruthenium-pyrazoles are also studied by infrared spectroscopy. Whenever appropriate, the purity of the synthesized compounds is evaluated by melting point measurements.

The compounds are evaluated against a gastric cancer cell line (AGS) and against a lung fibroblast cell line (MRC-5) to roughly assess their selectivity. The most potent compound is the ruthenium complex with the pyrazole having a *-para*-OCH₃ substituted styryl. This compound features an IC₅₀ value of 18.3 μM against the cancer cell line AGS and an IC₅₀ value of 62.2 μM on the healthy cell line MRC-5. Furthermore, the selectivity of this complex with this ligand is higher in comparison to that of ligand alone.

List of abbreviations and cell line codes

[9]aneS ₃	1,4,7-trithiacyclononane
5-phpz-OMe	(<i>E</i>)-3(5)-(2-hydroxyphenyl)-5(3)-(4-methoxystyryl)-1 <i>H</i> -pyrazole
8701-BC	Human breast cancer cell line
A2780	Human ovarian carcinoma cell line
A549	Human lung carcinoma cell line
AGS	Human gastric adenocarcinoma cell line
BGC823	Human gastric adenocarcinoma cell line
CARM1	Coactivator-associated arginine methyltransferase 1
c-Src	Cellular Src
DMEM	Dulbecco's Modified Eagle Medium
DNA	Deoxyribonucleic acid
EAC	Ehrlich ascites carcinoma
ELISA	Enzyme-Linked Immunosorbent Assay
equiv.	Molar equivalent
FBS	Fetal bovine serum
GES-1	Human normal gastric mucosa cell line
GI ₅₀	Growth half-maximal inhibitory concentration
HCT116	Human colon carcinoma cell line
HepG2	Human liver carcinoma
HT29	Human colon adenocarcinoma cell line
IC ₅₀	Half-maximal inhibitory concentration
<i>J</i>	Coupling constant (Hz)
KP1019	Indazolium <i>trans</i> -[tetrachlorobis(1 <i>H</i> -indazole)ruthenate(III)]
L-02	Human normal hepatocyte cell line
m.p.	Melting point
MCF7	Human breast adenocarcinoma cell line
MDA-MB-231	Human breast adenocarcinoma cell line
MEM	Minimum Essential Media
MGC-803	Human gastric carcinoma cell line
MRC-5	Human lung fibroblast cell line

MTT	3-(4,5-dimethylthiazol-2-yl)-2,5-diphenyltetrazolium bromide
NCI-H460	Human lung carcinoma cell line
NF- κ B	Nuclear factor kappa B
NKP-1339	Sodium trans-[tetrachloridobis(1 <i>H</i> -indazole)ruthenate(III)]
NOESY	Nuclear Overhauser effect spectroscopy
p53	Tumor suppressor protein 53
PBS	Phosphate-buffered saline
PC-3	Human prostate cancer cell line
PCR	Polymerase Chain Reaction
PDB ID	Protein data bank identity
PP2	4-amino-1-(<i>tert</i> -butyl)-3-(4-chlorophenyl)-pyrazolo[3,4- <i>d</i>]pyrimidine
PRMT	Protein arginine methyl transferase
r.f.	Retardation factor
S180	Murine sarcoma cancer
SEM	Standard error of mean
Src	Non-receptor protein tyrosine kinase family
TRAP	Telomeric repeat amplification protocol

Index

Introduction	1
1.1. Pyrazole derivatives	3
1.1.1. Telomerase as a cytotoxic target for pyrazoles	4
1.1.2. Pyrazole derivatives targeting CARM1	8
1.1.3. Pyrazoles as Src inhibitors	9
1.2. Pyrazoles with cytotoxic activity against tumor cell lines	11
1.2.1. Inhibitory action against human colon cancer cell lines	11
1.2.2. Pyrazoles active against human lung carcinoma	13
1.2.3. Disubstituted pyrazoles active against human gastric adenocarcinoma	14
1.3. Ruthenium complexes	16
1.3.1. Ru(II)[9]aneS ₃ – pyrazole complexes as chemotherapeutic drugs	18
Glycosylation of (<i>E</i>)-3(5)-(2-hydroxyphenyl)-4-styryl-1 <i>H</i> -pyrazoles	21
2.1. Nomenclature adopted for the synthesized compounds	22
2.1.1. (<i>E</i>)-3-Styryl-4 <i>H</i> -chromen-4-ones	22
2.1.2. (<i>E</i>)-3(5)-(2-Hydroxyphenyl)-4-styryl-1 <i>H</i> -pyrazoles	23
2.1.3. Pyrazoles containing sugar moieties at position N1	23
2.2.1. Synthesis of (<i>E</i>)-3-styryl-4 <i>H</i> -chromen-4-ones	26
2.2.2. Synthesis of (<i>E</i>)-3(5)-(2-hydroxyphenyl)-4-styryl-1 <i>H</i> -pyrazoles	26
2.2.3. Novel glycosylated (<i>E</i>)-3(5)-(2-hydroxyphenyl)-4-styryl-1 <i>H</i> -pyrazoles obtained by Koenigs-Knorr method	27
2.2.3.1. Removal of the protecting groups of the glycosylated products	33
2.3. Structural characterization of the synthesised compounds	35
2.3.1. (<i>E</i>)-3(5)-(2-Hydroxyphenyl)-4-styryl-1 <i>H</i> -pyrazoles	35
2.3.2. (<i>E</i>)-1-[β-D-(2,3,4,6-Tetra- <i>O</i> -acetylglucose-1-yl)]-3-(2-hydroxyphenyl)-4-styryl-1 <i>H</i> -pyrazoles	37
2.3.3. 1-[(2 <i>R</i> ,3 <i>aR</i> ,5 <i>R</i> ,6 <i>S</i> ,7 <i>S</i> ,7 <i>aR</i>)-6,7-diacetoxy-5-acetoxymethyl-2-methyltetrahydro-5 <i>H</i> -[1,3]dioxolo[4,5- <i>b</i>]pyran-2-yl)]-(<i>E</i>)-3-(2-hydroxyphenyl)-4-styryl-1 <i>H</i> -pyrazoles	42
2.3.4. (<i>E</i>)-1-[β-D-(glycose-1-yl)]-3-(2-hydroxyphenyl)-4-styryl-1 <i>H</i> -pyrazoles	47
2.3.5. 1-[(2 <i>R</i> ,3 <i>aR</i> ,5 <i>R</i> ,6 <i>S</i> ,7 <i>S</i> ,7 <i>aR</i>)-6,7-dihydroxy-5-hydroxymethyl-2-methyltetrahydro-5 <i>H</i> -[1,3]dioxolo[4,5- <i>b</i>]pyran-2-yl)]-(<i>E</i>)-3-(2-hydroxyphenyl)-4-styryl-1 <i>H</i> -pyrazoles	50
Synthesis of ruthenium complexes with pyrazoles	55
3.1. Nomenclature adopted for the ruthenium-pyrazole complexes	56
3.2. Preparation of the complexes	56
3.3. Structural characterization of the ruthenium-pyrazole complexes	57
3.4. Mass spectrometry of the ruthenium-pyrazole complexes	60

3.5. Fourier-transform infrared of the ruthenium-pyrazole complexes	61
Biological assays	63
4.1.1. AGS cancer cell line.....	64
4.1.2. MRC-5 cell line.....	68
Experimental section	73
5.1. Equipment, materials and solvents.....	74
5.2. Protocols.....	75
5.2.1. Synthesis of (<i>E</i>)-3-styryl-4 <i>H</i> -chromen-4-ones	75
5.2.2. Synthesis of (<i>E</i>)-3(5)-(2-hydroxyphenyl)-4-styryl-1 <i>H</i> -pyrazoles	77
5.2.3. Glycosylation of (<i>E</i>)-3(5)-(2-hydroxyphenyl)-4-styryl-1 <i>H</i> -pyrazoles	78
5.2.4. Deprotection of the glycosylated products 5 and 6	84
5.2.5. Synthesis of the complexes [Ru([9]aneS ₃)(<i>E</i>)-3(5)-(2-hydroxyphenyl)-4-styryl-1 <i>H</i> -pyrazole)(DMSO)Cl]Cl.....	89
5.2.6. Biological assays	93
5.2.6.1. Preparation of the stock solutions	93
5.2.6.2. Thaw of the cell lines	93
5.2.6.3. Cell culture	93
5.2.6.4. MTT assay.....	94
5.2.6.5. Statistical analysis	95
Conclusions and future perspectives	97
References	99

Preamble

This work is divided into five chapters. The first chapter presents a review of the reported pyrazole derivatives regarding their cytotoxic activity. Some pyrazole derivatives have well-known molecular targets, that are briefly described. The cytotoxic action of the most relevant reported pyrazole derivatives against colon, stomach and lung cancer cell lines are also presented. This chapter further contemplates the cytotoxic activity of ruthenium complexes and the potential benefits of the complexation of pyrazole derivatives with Ru(II)([9]aneS₃) concerning their cytotoxic action. Chapter two starts by presenting the adopted nomenclature for the novel glycosylated products and their precursors, followed by a brief description of the synthesis method for these compounds and their structural characterization by NMR. Chapter three is devoted to the nomenclature, synthetic route and structural characterization of the new pyrazole-ruthenium complexes. Chapter four displays the results of the *in vitro* cytotoxic action of the synthesised pyrazole derivatives. Finally, chapter five refers to the materials and methods including equipment, reactants, solvents, and the extensive description of the protocols herein employed.

Objectives

The main objectives of this work are the synthesis of novel glycosylated (*E*)-3(5)-(2-hydroxyphenyl)-4-styryl-1*H*-pyrazole derivatives and new ruthenium-pyrazole complexes and their cytotoxic evaluation on AGS stomach cancer cell line, as well as their preliminary safety assessment using the MRC-5 cell line. These goals were achieved by carrying out the following steps: (i) synthesis of (*E*)-3-styryl-4*H*-chromen-4-ones and (*E*)-3(5)-(2-hydroxyphenyl)-4-styryl-1*H*-pyrazoles; (ii) glycosylation of the synthesized (*E*)-3(5)-(2-hydroxyphenyl)-4-styryl-1*H*-pyrazoles; (iii) deprotection of the sugar moiety by cleavage of the acetyl protecting groups; (iv) complexation of the free pyrazole derivatives with [Ru(II)([9]aneS₃)(DMSO)Cl₂]; (v) full structural characterization of the novel compounds by 1D (¹H and ¹³C) and 2D (HSQC, HMBC, NOESY) NMR, mass spectrometry, and high resolution mass spectrometry or elemental analysis; (vi) characterization of the ruthenium-pyrazole complexes by infrared; (vii) cytotoxic evaluation of the compounds by MTT assays, resorting to AGS and to MRC-5 cell lines.

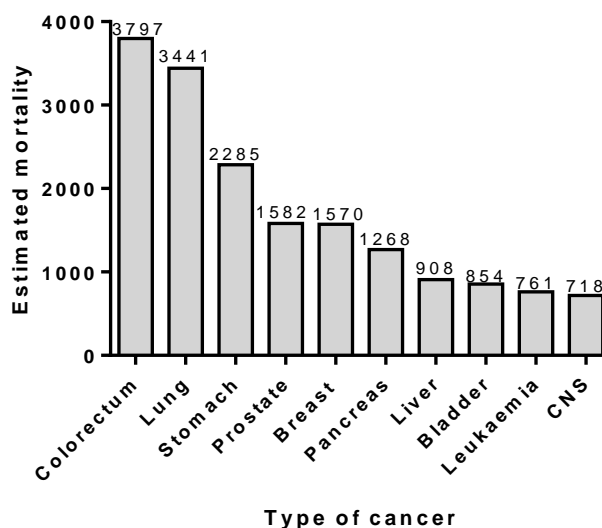
Chapter 1

Introduction

Cancer is a major public health problem worldwide, generally affecting more men than women.¹ This set of pathologies is highly known by the hyper-proliferative activity of cells, that is, they have an abnormal and nonstop growth.² This is attributed to the fact that malignant cells ignore the signals sent to trigger their own apoptosis, a deregulation associated with mutations in the genes responsible for the control of cell growth and proliferation, namely in pro-oncogenes,² tumor suppressor genes³ and/or DNA repair genes.

Among the different kinds of cancer, lung cancer is the most prevalent type globally, with an estimated incidence of approximately 1.8 million cases for both sexes in 2012.¹ In fact, statistics show that lung cancer is the deadliest form of cancer, accounting for about 1.5 million deaths worldwide in the same period. Concerning Portugal, statistics for both sexes in 2012 (see Graphic 1.1) reveal that colorectal cancer is the most mortal, with an estimated mortality of 3797 cases, followed by lung and stomach cancer with an estimated mortality of 3441 and 2285 cases, respectively.

Graphic 1.1 – Estimated mortality cases in Portugal in 2012 for both sexes organized by descending prevalence. The NHL acronym stands for Non-Hodgkin lymphoma.



Statistics provided by DGS (Direção-Geral da Saúde) show that in 2014 colon cancer and lung cancer remained the deadliest in Portugal, although the number of lung cancer deaths surpassed those of colorectal cancer.⁴ The numbers depicted in the Graphic 1.1 highlight

the need of improved chemotherapeutic drugs, which should have lower cytotoxicity to healthy cells and higher cytotoxicity towards malignant cells.⁵

The work presented in this dissertation addresses the challenges in cancer chemotherapy by developing new cytotoxic drug candidates. The structures are based on 3,4-disubstituted pyrazoles, and include glycosylated derivatives and ruthenium-pyrazole complexes, and their synthesis and *in vitro* cytotoxic evaluation is herein presented. Several pyrazoles are already reported to feature cytotoxic bioactivity,^{6,7} as detailed in the subsection 1.1.

1.1. Pyrazole derivatives

Pyrazole (1*H*-pyrazole, **1**, Figure 1.1) is a five-membered heteroaromatic ring containing two nitrogen atoms at positions 1 and 2 and three carbon atoms.⁸ *N*-unsubstituted pyrazoles may present three identical and non-separable tautomers, due to rapid interconversion in solution. Usually it is impossible to unequivocally assign the proton resonances of the pyrazole core in the proton-nuclear magnetic resonance (¹H NMR) spectra of these compounds.

Pyrazole derivatives span a wide range of bioactivities, such as cytotoxic,⁸ anti-inflammatory,⁹ analgesic, antimicrobial,¹⁰ antihypertensive and antiviral¹¹ activities.^{12,13} The versatility of pyrazole derivatives led to the exploration of their activities in several fields, including medicine, pharmacology and agrochemical industry.¹⁰ Celecoxib **2**, represented in the Figure 1.2, is a noteworthy example of a drug possessing a *N*-substituted pyrazole scaffold that succeeded in the pharmaceutical field.^{14,15}

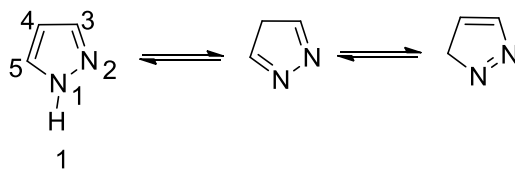


Figure 1.1 – Chemical structures and numbering of pyrazole **1**.

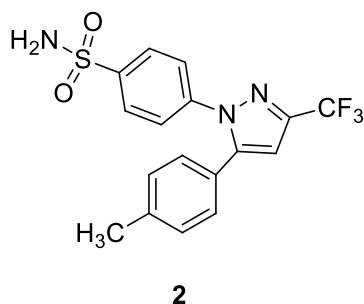


Figure 1.2 – Chemical structure of the NSAID drugs Celecoxib **2**.

Compound **2** is a nonsteroidal anti-inflammatory drugs (NSAID) that works by inhibiting cyclooxygenase-2. Nevertheless, the activity of *N*-substituted pyrazoles is not restricted to the anti-inflammatory action.^{14,16} Evidence shows that *N*-substituted pyrazole derivatives have an important role as anti-proliferative,¹⁷ autophagy stimulation,¹⁸ inhibition of cell growth, pro-apoptotic, anti-angiogenic and anti-leukemic drugs.¹⁹ Unfortunately, the vast majority of the pyrazole derivatives reported so far does not have a specific mechanism of activity associated.^{8,20,21} Still, whenever it's possible to determine the action mechanism of the pyrazole derivative of interest, scientists determine which pyrazole derivative is the most effective and they optimize the structure to achieve better bioactivities.^{7,22} Note also that, for a few number of pyrazole derivatives, targets of cytotoxic action have already been identified, and these include telomerase,²³ CARM1⁷ and Src.²⁴

1.1.1. Telomerase as a cytotoxic target for pyrazoles

Telomerase is an enzyme that monitors the stability of the genome by maintaining and repairing telomeres, repetitive TTAGGG sequences present at the chromosome's end. Telomerase activity is absent or undetected in the majority of adult human tissues.^{25,26} The limited telomerase action conjugated with the inability of the DNA replication machinery to fully copy the telomeres sequences results in a progressive shrinkage of telomeres in a normal adult somatic cell whenever cell division occurs. Subsequently, with aging, telomeres reach a critical length causing cells to lose their ability to divide which ultimately prevents the endless proliferation of somatic cells.²⁷ However, telomerase is active in the majority of tumor cells, allowing them to maintain or lengthen telomeres in order to remain able to divide virtually indefinitely.²⁸ This is believed to be a critical step in carcinogenesis. Targeting telomerase is thus a trending strategy for the development of

novel active therapies against malignant cells with minimal toxicity for healthy tissues.²⁹ The pyrazole derivatives with known telomerase-inhibiting ability are depicted in the Figure 1.3.^{23,30,31}

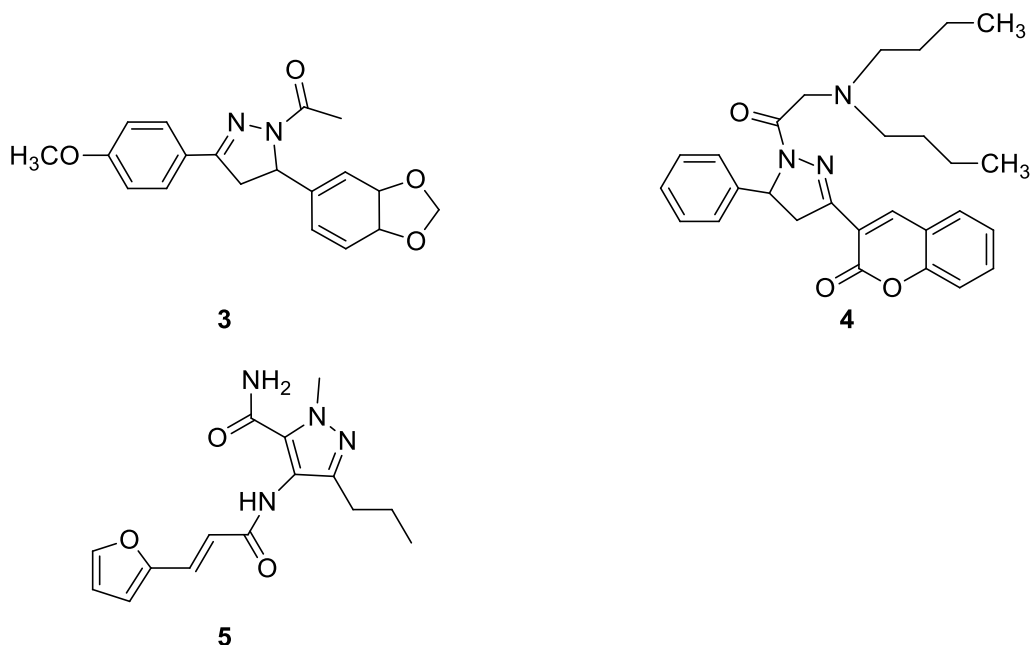


Figure 1.3 – Structures of the most active pyrazole derivatives against telomerase, reported by Luo *et al*, Wang *et al* and Shi *et al*.^{23,30,31}

Compounds **3**,²³ **4**³⁰ and **5**³¹ were tested against telomerase by the modified telomeric repeat amplification protocol (TRAP)^{23,30} or by the TRAP-PCR-ELISA³¹ protocol. Telomerase inhibition IC₅₀ values for compounds **3**, **4** and **5** were, respectively, 0.90, 0.98 and 1.02 μM . All the compounds showed better performance than the reference drugs used in the respective studies (see Figure 1.4). Compound **3** was far better than the control, ethidium bromide **6**, with an IC₅₀ of 2.6 μM ,²³ and compound **4** was also more potent than the control, staurosporine **7**, with an IC₅₀ of 9.0 μM .³⁰ Finally, compound **5** also surpassed the IC₅₀ value of ethidium bromide, of 2.1 μM in that study.³¹

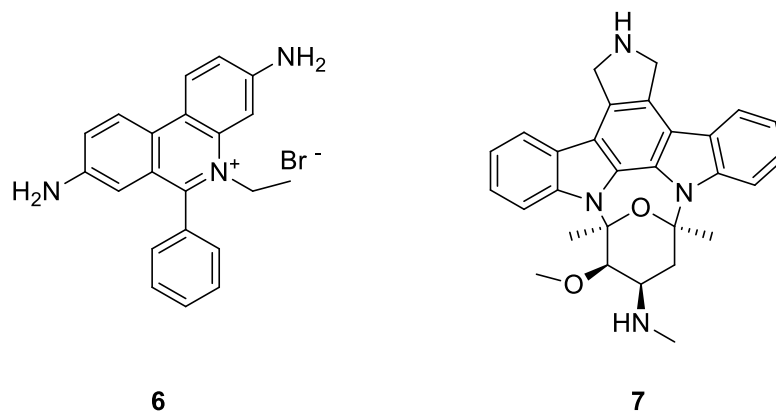


Figure 1.4 – Representation of ethidium bromide **6** and staurosporine **7**.

Compound **4** was also tested against several cancer cell lines, including the gastric cancer cell line MGC-803, against which it featured an IC_{50} value of $2.96 \pm 0.15 \mu\text{M}$.³⁰ To assess its selectivity toward cancer cells, compound **4** was also tested against human normal gastric mucosa (GES-1) and human normal hepatocyte (L-02) cell lines, having IC_{50} values of 1.64 ± 0.17 and $1.62 \pm 0.24 \text{ mM}$. Further *in vivo* tests with **4** on mice affected by S180 or HepG2 tumors revealed that this compound can inhibit the tumor growth of mice affected by S180 or HepG2 tumors. Adding to these outstanding results, the administration of compound **4** to mice with EAC tumors increased their survival rate.

Compounds **3-5** were also studied by molecular docking studies. All were shown to bind strongly to the Tert catalytic subunit of telomerase, establishing four to six connections of the hydrogen bonds and electrostatic interaction kind.^{23,30,31} The four bridging sites of compound **3** are depicted in the Figure 1.5.

Compound **4** binds *via* the coumarin residue with Lys 710 and Lys 902, *via* pi-cation interactions, and Val 904 and Pro 929, *via* hydrophobic interactions. Moreover, one aliphatic chain forms a pi-cation interaction with Phe 568, and the dihydropyrazole ring, along with benzene ring, make a hydrophobic interaction with Pro 627.

Compound **5** also has six binding interactions, as depicted in Figure 1.6.³¹

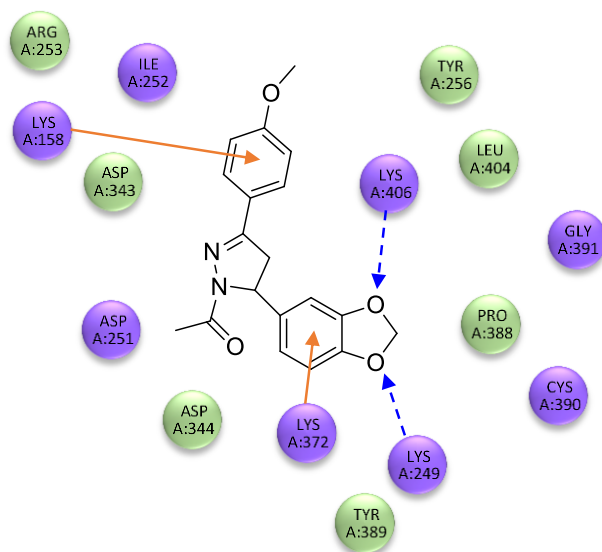


Figure 1.5 – Interaction diagram of compound **3** with Tert catalytic subunit (PDB ID: 3DU6), adapted from Luo *et al.*²³ The labelled circles represent essential amino acid residues at the binding site, with purple for those involved in hydrogen bonding, electrostatic or hydrophilic interactions and green for those involved in Van der Waals interactions. The orange arrows represent the pi-cation interactions and the blue arrows represent the hydrogen bond interactions.

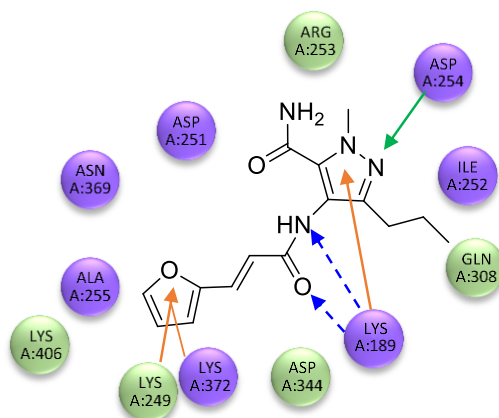


Figure 1.6 – Interaction diagram of compound **5** with Tert catalytic subunit (PDB ID: 3DU6), adapted from Shi *et al.*³¹ The orange arrows represent the pi-cation interactions and the blue arrows represent the hydrogen bond interactions. The green arrow stands for the interaction between the backbone amino groups of Asp 254 and the *N* atom of the pyrazole scaffold. The green circles show the amino acids which participate in the Van der Waals interactions.

Compounds **3**²³ and **4**³⁰ share common structural features, both being 3,5-diarylpyrazoles. The presence of aromatic groups in these positions seem to be important for the formation of pi-cation interactions with Tert's Lys residues.^{23,30}

Consequently, variations of pyrazole scaffolds substituted in positions 3 and 5 with aromatic groups may be a good start for the design of a novel telomerase inhibitors family.

1.1.2. Pyrazole derivatives targeting CARM1

The coactivator-associated arginine methyltransferase 1 (CARM1) is a member of the protein arginine methyltransferase (PRMT) family.³² CARM1 can methylate histone H3 and p300/CBP, triggering the alteration of chromatin architecture and, therefore, influencing the transcriptional initiation.^{33,34} Whenever CARM1 is recruited to the promoter sequences, histone H3 is methylated and chromatin becomes more accessible to the transcriptional machinery, ultimately leading to increased gene expression.³⁴

CARM1 acts as a co-activator of cancer-related proteins such as the nuclear factor kappa B (NF- κ B)³⁵ and the tumor suppressor protein p53.³⁶ Also, CARM1 is up-regulated in several types of cancer, namely, colorectal³⁷ and lung³⁸ cancer. The co-activation of substrates linked to tumorigenesis by CARM1 and its overexpression in numerous cancer types makes it an interesting chemotherapeutic target. Attempts to find a suitable CARM1 inhibitor leaned toward small molecules,^{39,40} including pyrazole derivatives.^{7,41,42,43} The compounds exhibiting the most relevant CARM1 inhibitory action are depicted in the Figure 1.7. The IC₅₀ values obtained for compounds **8**,⁴² **9**⁴³ and **10**⁷ were, respectively 0.04, 0.06 and 0.08 μ M. The compounds **8-10** were tested against other PRMT family members, namely PRMT1 and PRMT3. Their inhibitory activity was lower against PRMT1 and PRMT3, suggesting that compounds **8-10** are selective toward CARM1.

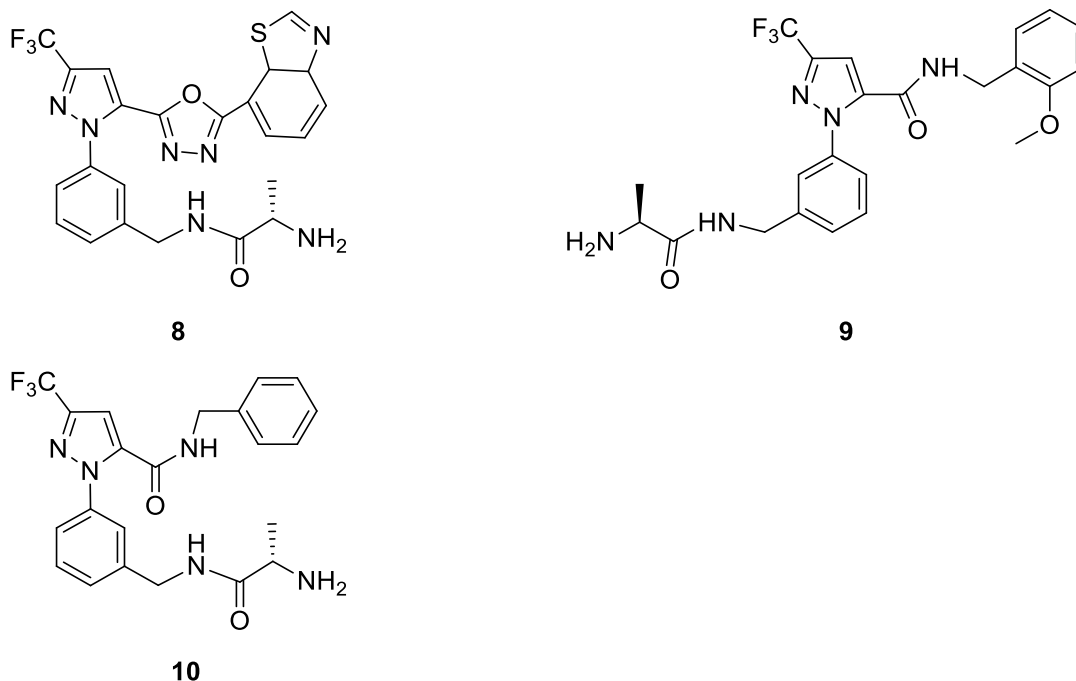


Figure 1.7 – Selection of pyrazole derivatives with good inhibitory activity against CARM1, reported by Purandare *et al.*,⁷ Huynh *et al.*⁴² and Therrien *et al.*⁴³

1.1.3. Pyrazoles as Src inhibitors

Pro-oncogene tyrosine-protein kinases (Src) are a family of non-receptor tyrosine-kinases composed by several members, such as, Blk, Fyn, Fgr, Hck, Lyn, Lck, c-Src, Yrk, Yes, Brk and Srm.^{44,45} The Src protein family is involved in many key processes required for the modulation of cell behavior and viability, such as, cell adhesion, spreading, motility, division, differentiation and apoptosis.⁴⁶ Furthermore, Src family can phosphorylate key molecules involved in tumor invasion and metastasis, which implies a role in the conduct of malignant cells.

The deregulation of Src members is often associated with uncontrolled cell growth and differentiation.⁴⁷ The protein family member c-Src is the most linked to tumorigenesis and cancer progression.⁴⁸ In fact, c-Src is up-regulated in several types of cancer, including pancreatic,⁴⁹ breast,⁵⁰ ovarian⁵¹ and colorectal⁵² cancer. The Src involvement in oncologic diseases triggered the quest for efficient Src family inhibitors.⁵³ Two pyrazolo-pyrimidine compounds, **11** and **12** (Figure 1.8), were tested against breast cancer 8701-BC cells, characterized by a significant overexpression of c-Src.⁵⁴ Their IC₅₀ values (expressed as the mean ± SEM) were 31.2 ± 0.5 and 38.8 ± 0.5 μM, respectively. The used reference

1.2. Pyrazoles with cytotoxic activity against tumor cell lines

Tumor bi-dimensional cell lines are the most commonly used approach to test the biological properties of a drug candidate.⁵⁵ Cultured cells are able to mimic the biological properties of the corresponding *in vivo* cells and to display the same characteristics of the pathology under study.⁵⁶ Over time, cell lines tend to adapt to their culture environment, suffering genotypic modifications that often translate into the phenotype, that is, they lose some of their *in vivo* functions and properties.^{56,55} Moreover, since cell lines lack their *in vivo* neighboring environment and interactions with other cell types, they tend to neglect their conduct within the tissue and behave differently *in vitro*. *In vitro* experiments will always have their setbacks; still, they provide useful information about the drugs' cytotoxic potential. In what concerns *N*-substituted pyrazole derivatives, growth inhibitory activity has already been reported on a few human cancer cell lines, including colon adenocarcinoma (HT29),⁵⁷ lung cancer (NCI-H460),⁵⁸ gastric cancer (AGS),⁵⁹ breast adenocarcinoma (MCF7),⁵⁸ ovarian carcinoma (A2780), among others.⁶⁰ Herein, reports on the activity of pyrazole derivatives against lung, colorectal and gastric cancer cell lines are presented, as these represent the most deadly types of cancer worldwide.¹

1.2.1. Inhibitory action against human colon cancer cell lines

Colorectal cancer incidence risk is increased by a poor diet, sedentarism, obesity, unbalanced alcohol intake and age.⁶¹ The incidence risk is also associated with multiple genetic variants identified by the genome-wide association study.⁶²

Despite the intricate background of this pathology, there are reports of pyrazole derivatives possessing good inhibitory action against human colon adenocarcinoma cell lines, namely against HCT29^{57,63} and HCT116 cell lines.⁶⁴ The most effective pyrazoloacridines reported by Antonini *et al* against HCT29 are compounds **15** and **16** (represented in the Figure 1.10), with IC₅₀ values of 3.9 and 31.0 nM, respectively.⁵⁷ These values are nonetheless higher than those of the reference drugs, mitoxantrone (**17**) and doxorubicin (**18**), with respective IC₅₀ values of 1.0 and 2.6 nM, albeit compound **15** is within the same order of magnitude.

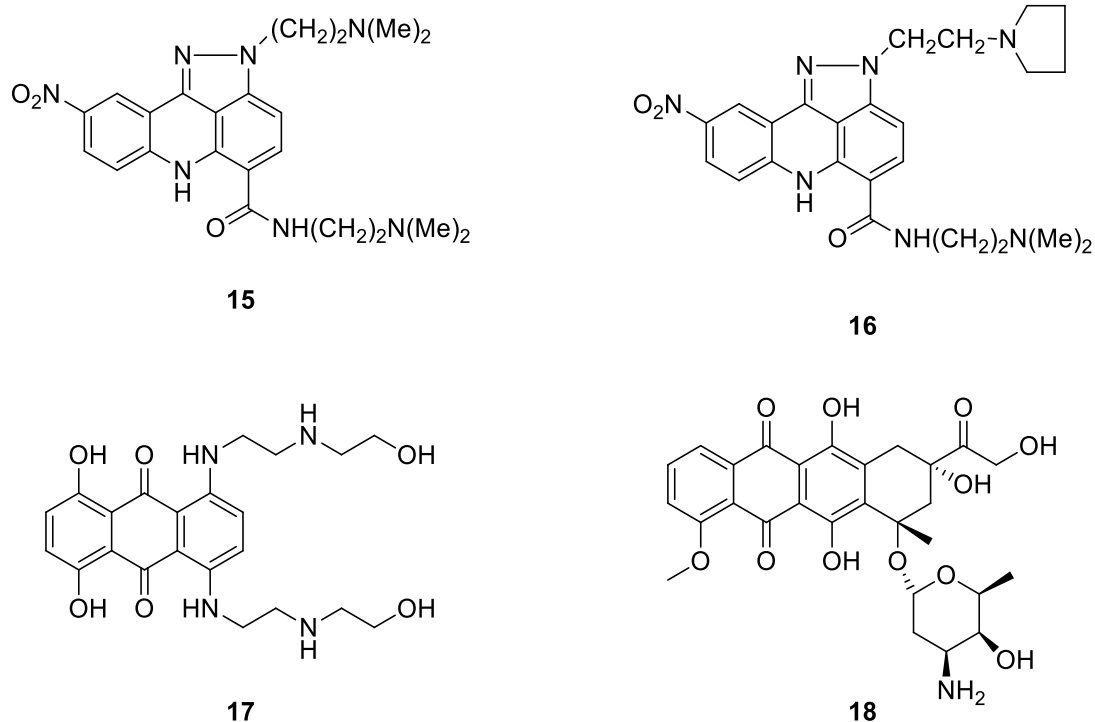


Figure 1.10 – Structure of the most potent compounds reported by Antonini *et al*⁵⁷ (top line) and of the reference drugs, mitoxantrone (**17**) and doxorubicin (**18**), used in the same study (bottom).

Competitive ethidium bromide displacement indicates that both **15** and **16** have Guanine-Cytosine as binding site preference. Further modifications on the structure of **15**, the one with the best performance, may afford some interesting compounds with higher cytotoxic activity.

In another study by Lukasik *et al*, the synthesized pyrazole derivatives were tested against the HCT116 cell line, being compounds **19** and **20** (Figure 1.11) the most efficient with GI₅₀ values of 0.49 and 0.59 μ M, respectively.⁶⁴

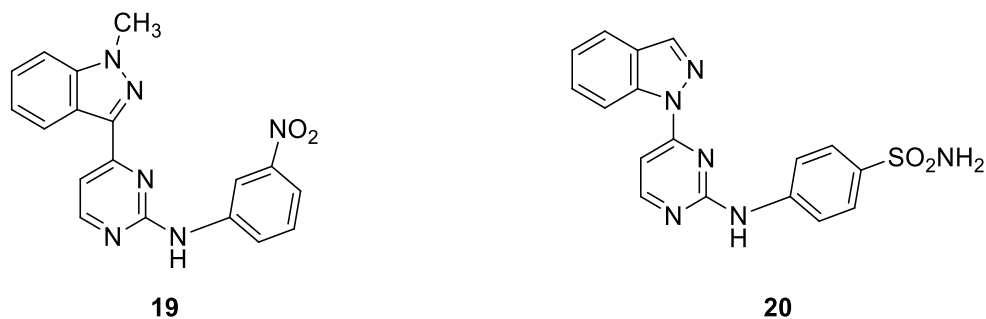


Figure 1.11 – Structures of the most relevant cytotoxic compounds against HCT-116 cell line reported by Lukasik *et al*.⁶⁴

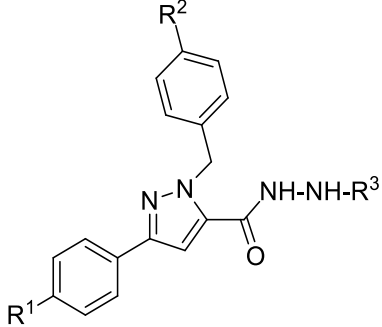
It is important to mention that the pyrazole derivatives reported by Antonini *et al* and Lukasik *et al* were not tested against healthy cell lines. Thus, their cytotoxicity towards healthy cells is unknown and a selectivity and safety profile remains to be established.

1.2.2. Pyrazoles active against human lung carcinoma

Lung cancer was, statistically, the most lethal type of cancer for both sexes worldwide, in 2012.¹ Among the acknowledged risk factors, cigarette smoking is the most relevant one in the development of lung cancer.⁶⁵ Mutations in the epidermal growth factor receptor (EGFR), kirsten rat sarcoma viral oncogene homolog (KRAS), and anaplastic lymphoma kinase (ALK) are also risk factors for this pathology.⁶⁶

Among the reported drugs possessing *in vitro* inhibitory action against lung cancer cell lines, some tri-substituted pyrazole derivatives featuring a cytotoxic activity against lung cancer A549 cell line are of interest.^{67,68} Two families of tri-substituted pyrazoles, reported by Xia *et al*⁶⁷ and Lian *et al*,⁶⁸ present cytotoxic action against the A549 lung cancer cell line. Xia *et al* study consisted in the synthesis of *N*-substituted pyrazole derivatives⁶⁷ and, in a follow-up research made by Lian *et al*, a sugar moiety (a glucosyl or a xylosyl unit, depending on the compound) was attached to the previously tested tri-substituted pyrazole derivatives.⁶⁸ The mentioned pyrazole derivatives are substituted in their pyrazole scaffold at position 1, 3 and 5. Their general structure and IC₅₀ values may be consulted in the Table 1.1. Among the compounds without a sugar moiety, compounds **21** and **25** weren't active towards A549 cell line.⁶⁷ Note how the IC₅₀ values of the compounds linked to a sugar moiety are, for the majority, lower than the IC₅₀ values achieved by their parent compounds.⁶⁸ The exceptions were compound **26**, having a lower IC₅₀ value than compounds **32** and **33**; and compound **24**, having a lower IC₅₀ value than compound **31**. Altogether, these two studies disclose the cytotoxic benefits employed by the attachment of a sugar moiety to a pyrazole scaffold.

Table 1.1 – General structure of the tri-substituted pyrazoles and their glycated derivatives, followed by their respective substituents (R¹, R² and R³, being the last one only valid for the glycated pyrazoles). The IC₅₀ values against A549 cell line, after 48 hours of compound's incubation, are also presented.

				
Compound	R ¹	R ²	R ³	IC ₅₀ (μM)
21	H	H	–	n.d. ^[a]
22	H	t-Bu	–	26.5
23	Cl	H	–	38.7
24	Cl	t-Bu	–	18.5
25	OCH ₃	H	–	n.d. ^[a]
26	OCH ₃	t-Bu	–	23.9
27	H	t-Bu	Xylosyl	15.2
28	H	t-Bu	Glucosyl	21.6
29	Cl	H	Glucosyl	31.8
30	Cl	t-Bu	Xylosyl	13.9
31	Cl	t-Bu	Glucosyl	26.6
32	OCH ₃	t-Bu	Xylosyl	24.9
33	OCH ₃	t-Bu	Glucosyl	38.9

[a] n.d. = not determined.

1.2.3. Disubstituted pyrazoles active against human gastric adenocarcinoma

Gastric cancer is directly related to the infectious organism *Helicobacter pylori*.⁶⁹ *H. pylori* is a risk factor for the development of non-cardia gastric cancer.⁷⁰ Also, nutrition has been implicated in the development of this disease. High consumptions of salt and nitrates are associated with a higher risk of gastric cancer development.

Despite the intricacy of this multifactorial pathology, there are some promising studies showing the cytotoxic activity of pyrazole derivatives against stomach cancer cell lines, explicitly against AGS⁵⁹ and BGC823 cell lines.^{71,72} In fact, a family of 3,5-diaryl-1*H*-pyrazoles studied against the AGS cell line afforded interesting results.⁵⁹ The structures of the mentioned 3,5-diaryl-1*H*-pyrazoles, numbered from **34** to **36**, are represented in the Figure 1.12. The type and position of the substituent groups allows to establish structure – activity correlations.

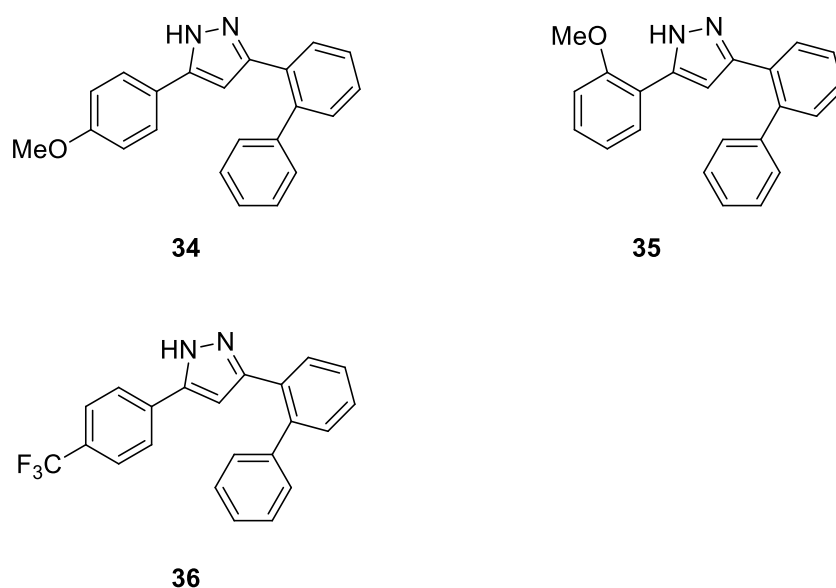


Figure 1.12 – Structure of a family of 3,5-disubstituted pyrazoles active against stomach cancer AGS cells.⁵⁹

Compound **34**, having a 4-methoxyphenyl in position 5 of the pyrazole, is the most active, with an GI₅₀ of $0.79 \pm 0.08 \mu\text{M}$. In turn, when the substituent is a 2-methoxyphenyl (compound **35**), the activity is lost (no action at the highest concentration tested, 40 μM). This shows that the position of the functional group is of high relevance for the cytotoxic activity. The type of functional group also plays an important role in the cytotoxic action. Compound **36**, with a 4-CF₃-phenyl in position 5, had a GI₅₀ of $6.9 \pm 0.7 \mu\text{M}$, which is around ninefold higher than that of compound **34**. These results point towards the relevance of *para*-substituted aryl groups on cytotoxic action against gastric cancer, further suggesting that a methoxy group, with electron-donating properties, contributes to higher efficacy.

A set of 3-(1*H*-indole-3-yl)-1*H*-pyrazole-5-carbohydrazide derivatives were tested against the stomach cancer cell line BGC823.⁷¹ The structure of the most active compounds reported by this study (**37** to **39**) and the structure of the used reference drug (**40**) are depicted in the Figure 1.13.

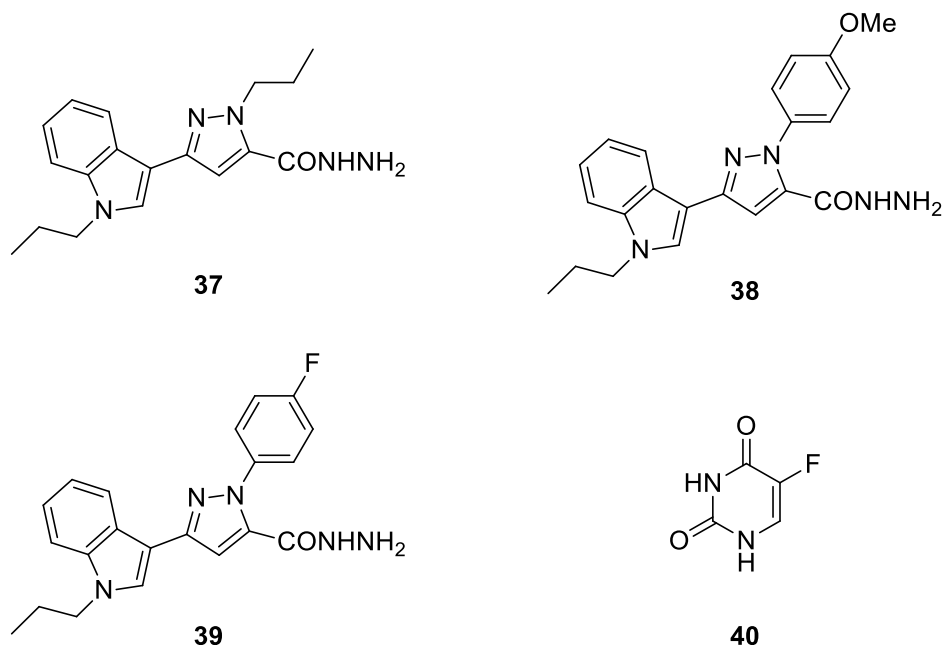


Figure 1.13 – Representation of some of the synthesized 3-(1*H*-indole-3-yl)-1*H*-pyrazole-5-carbohydrazide derivatives (**37-39**) reported by Zhang *et al.*⁷¹ Fluorouracil (**40**) was used as a reference drug.

The IC₅₀ of compounds **37-40** was, respectively, 1.94 ± 0.46, 1.89 ± 0.24, 0.71 ± 0.14 and 6.15 ± 0.59 μM. Note that **38**, with a 4-methoxyphenyl group in the position 1 of the pyrazole, had a slightly better activity than **37**, which features an aliphatic chain in the same position. Still, the highlight goes to **39** with a 4-fluorophenyl in position 1 and activity within the nanomolar range. Thus, the family of 3-(1*H*-indol-3-yl) pyrazole-5-carbohydrazide has a substituent effect opposite to that of the previously described 3,5-diaryl-1*H*-pyrazoles, that is, in this case the activity against stomach cancer is not significantly increased by the presence of the *-para*-OMe group.

1.3. Ruthenium complexes

The modification of substituents and their positioning is a widely used strategy for attempting to enhance the cytotoxic potential of a certain compound.^{59,71} Over the years several approaches were employed with this same purpose.^{73,74} One interesting approach is

the complexation of ruthenium with organic compounds, aiming at a higher cytotoxic activity and a lower toxicity.⁵ Ruthenium is a transition metal with several possible oxidation states, such as +2 (Ru(II)), +3 (Ru(III)) and, less frequently, +4 (Ru(IV)).⁷⁵ Of these, Ru(IV) is the most unstable and, consequently, the less explored. Ruthenium can mimic iron and, therefore, it can attach to plasma proteins like transferrin and albumin.⁷⁶ These plasma proteins are responsible for the solubilization and transportation of iron.⁷⁷ Therefore, the attachment of ruthenium to transferrin and albumin is deemed to reduce its interaction with the healthy tissue when compared to other drugs, such as cisplatin. Cisplatin is a platinum-based drug widely used as a chemotherapeutic drug but its cytotoxicity towards healthy cells, drug resistance and undesired side effects have limited its attractiveness.⁷⁸

Some reported ruthenium complexes exhibit excellent cytotoxic activity both *in vitro* and *in vivo*,⁷⁹ which highlights their potential to overcome the issues associated with cisplatin.⁸⁰ Indeed, two Ru(III) inorganic complexes have already entered human clinical trials: indazolium *trans*-[tetrachlorobis(1*H*-indazole)ruthenate(III)] (KP1019)⁸¹ and sodium *trans*-[tetrachloridobis(1*H*-indazole)ruthenate(III)] (NKP-1339), presented in the Figure 1.14.⁸² KP1019 is particularly effective towards colorectal cancer cells, as demonstrated by *in vivo* studies in rats. KP1019 decreased the volume of colorectal chemically induced tumors.⁸³ Its mechanism of action is based on the induction of malignant cell death by p53-independent apoptosis. This compound successfully passed phase I clinical trials and the phase II trials are still ongoing.^{84,85} Compound NKP-1339 was shown to be effective *in vivo* against solid tumors, including colorectal carcinoma, non-small cell lung cancer and gastrointestinal neuroendocrine tumors.⁸⁶ NKP-1339 also successfully passed phase I clinical trials and it is currently under phase II clinical trials.

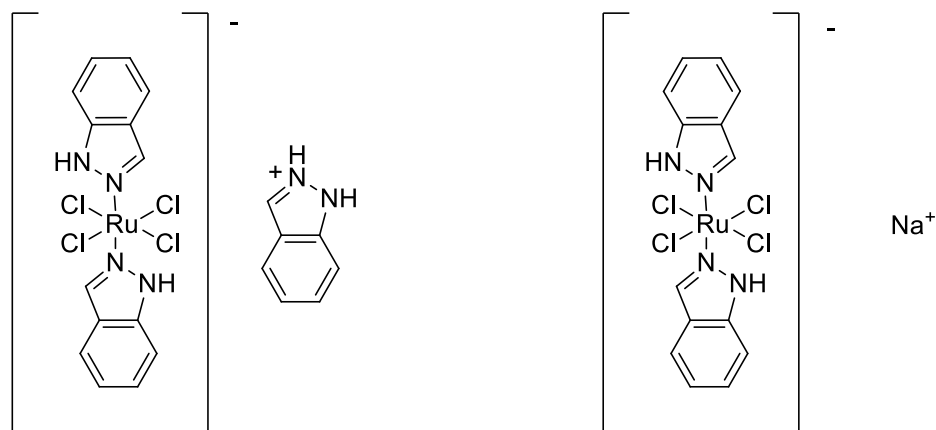


Figure 1.14 – Structure of KP1019, on the left, and its sodium salt analogue, NKP-1339 on the right.

1.3.1. Ru(II)[9]aneS₃– pyrazole complexes as chemotherapeutic drugs

In the literature there is a single published study, reported by Marques *et al*, on the cytotoxic activity of one Ru(II) trithiacyclononane complex bearing a 5-(2-hydroxyphenyl)-3-[(4-methoxystyryl)pyrazole] as a monodentate ligand (see Figure 1.15).²⁰

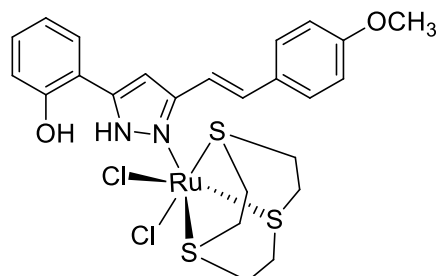


Figure 1.15 – Structure of the Ru(II)([9]aneS₃)(5-phpz-OMe)Cl₂ complex.

This Ru-pyrazole derivative complex was evaluated against human prostate adenocarcinoma (PC-3) and human breast adenocarcinoma (MDA-MB-231) cell lines. Cisplatin was used as control and the free 5-phpz-OMe [(*E*)-3(5)-(2-hydroxyphenyl)-5(3)-(4-methoxystyryl)-1*H*-pyrazole] was used to evaluate if complexation improved the cytotoxic activity. The IC₅₀ values of the free 5-phpz-OMe, Ru(II)([9]aneS₃)(5-phpz-OMe)Cl₂ complex and cisplatin were, respectively, 9.9, 32.3 and 6.6 μM, against PC-3 cell line. Concerning the MDA-MB-231 cell line, the IC₅₀ values were respectively of 10.2, 19.2 and 9.5 μM. Note that the cytotoxic action of the free 5-phpz-OMe was comparable to

cisplatin, which emphasizes the cytotoxic activity of hydroxyphenylpyrazoles as a class of compounds by itself.

Furthermore, it should be noted that albeit the performance of the complex on these cell lines was slightly worse than that of the free 3,5-diarylpyrazole ligand, the complexation with Ru(II) is expected to lower the overall toxicity of the pyrazole ligand. Thus, additional studies investigating the effect on healthy cells are in need. The studies may also be expanded to include a larger variety of cancer cell lines. These results inspired us to develop novel 3(5)-(2-hydroxyphenyl)-4-styryl-1*H*-pyrazoles, both in the free form and coordinated with Ru(II)([9]aneS₃), to learn more about their antitumor potential using the AGS cancer cell line.

Chapter 2

Glycosylation of (*E*)-3(5)-(2-hydroxyphenyl)-4-styryl-
1*H*-pyrazoles

The (*E*)-3(5)-(2-hydroxyphenyl)-4-styryl-1*H*-pyrazoles were prepared from (*E*)-3-styryl-4*H*-chromen-4-ones, as reported by Silva *et al* (details in sub-chapter 2.2.2.).⁸⁷ The glycosylation of (*E*)-3(5)-(2-hydroxyphenyl)-4-styryl-1*H*-pyrazoles was performed by the Koenigs-Knorr method described in the literature⁸⁸ (consult sub-chapter 2.2.3.), affording novel glycosylated pyrazole derivatives.

2.1. Nomenclature adopted for the synthesized compounds

The adopted nomenclature for the (*E*)-3(5)-(2-hydroxyphenyl)-4-styryl-1*H*-pyrazoles glycosylated products and its precursors may be consulted in the next sub-chapters. With exception of the 3-styryl-4*H*-chromen-4-ones, the nomenclature adopted does not follow the IUPAC rules. To simplify, starting from that point the numbering of the presented compounds will start from number 1.

2.1.1. (*E*)-3-Styryl-4*H*-chromen-4-ones

The nomenclature and numbering system adopted for the (*E*)-3-styryl-4*H*-chromen-4-ones **3a-d** follows the recommendations of IUPAC⁸⁹ and the attributed numbering is represented in the Figure 2.1. The styryl group at position 3 may be non-substituted $R^1 = R^2 = H$, or substituted at *ortho*- or *para*- positions of the phenyl ring ($R^1 = CF_3$ or $R^2 = Cl$, OCH_3). The “(*E*)” is used to indicate the stereochemistry of the double bond between carbons α and β . Thus, these compounds will be named as (*E*)-3-(2-/4-Rstyryl)-4*H*-chromen-4-ones **3a-d**, where R is the substituent present in the aromatic ring of the styryl group.

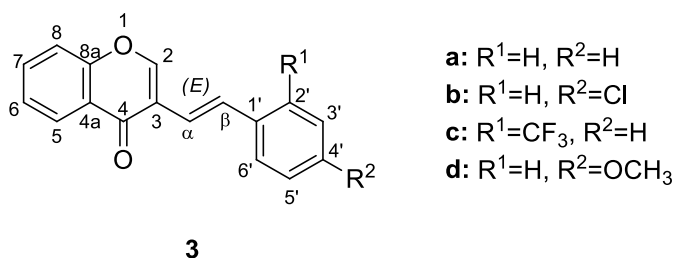
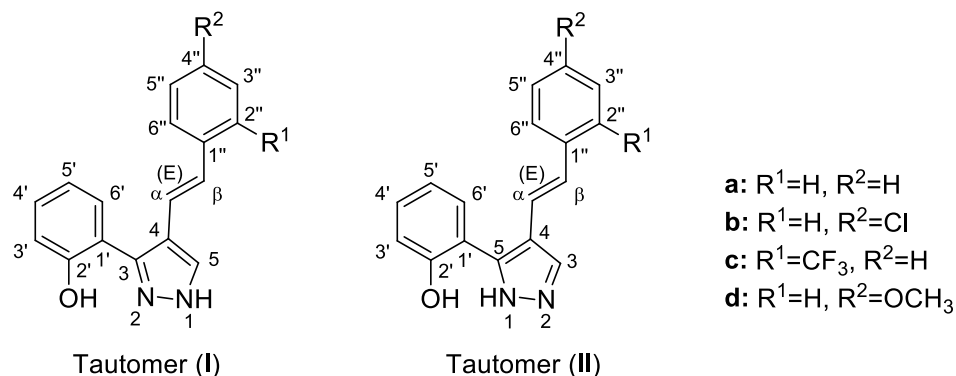


Figure 2.1 – Structure and numbering system of (*E*)-3-(2-/4-Rstyryl)-4*H*-chromen-4-ones **3a-d**.

2.1.2. (*E*)-3(5)-(2-Hydroxyphenyl)-4-styryl-1*H*-pyrazoles

To facilitate the structural characterization of pyrazoles **4a-d** (see Figure 2.2) by comparison with data from the literature, the name given to these compounds does not follow the IUPAC rules. Instead the nomenclature adopted considers the pyrazole ring as the main group which is numbered starting by the NH, while the groups at positions 3 and 4, respectively, are considered as substituents. The hydrogen at N1 position of tautomer **I** (Figure 2.2) can move to N2 forming the tautomer **II** of the pyrazole. This effect, known as prototropy, occurs in pyrazoles which are non-substituted at N1. Therefore, the position 3 is indicated as 3(5) considering the possibility of having one or another pyrazole tautomer. These compounds will be named as (*E*)-3(5)-(2-hydroxyphenyl)-4-(2-/4-Rstyryl)-1*H*-pyrazoles **4a-d**.



4

Figure 2.2 – Structure and numbering system of (*E*)-3(5)-(2-hydroxyphenyl)-4-(2-/4-Rstyryl)-1*H*-pyrazoles **4a-d**.

2.1.3. Pyrazoles containing sugar moieties at position N1

The nomenclature of the compounds represented in Figure 2.3 does not follow the IUPAC rules to facilitate their structural characterization by comparison with the precursor compounds, the pyrazoles **4a-d**. The pyrazole nucleus is considered the main group which is substituted at positions 1, 3 and 4. The sugar unit incorporated in the structure at position N1 is numbered using <''> (see Figure 2.3). Compounds **5a-d**, that present the sugar moiety linked to the pyrazole through the carbon C-1'''' will be named as, (*E*)-1-[β-D-(2,3,4,6-tetra-*O*-acetylglycose-1-yl)]-3-(2-hydroxyphenyl)-4-(2-/4-Rstyryl)-1*H*-pyrazole, while compounds **6a-d** will be named as 1-[(2*R*,3*aR*,5*R*,6*S*,7*S*,7*aR*)-6,7-diacetoxy-5-

acetoxymethyl-2-methyltetrahydro-5*H*-[1,3]dioxolo[4,5-*b*]pyran-2-yl)-(*E*)-3-(2-hydroxyphenyl)-4-(2-/4-Rstyryl)-1*H*-pyrazole.

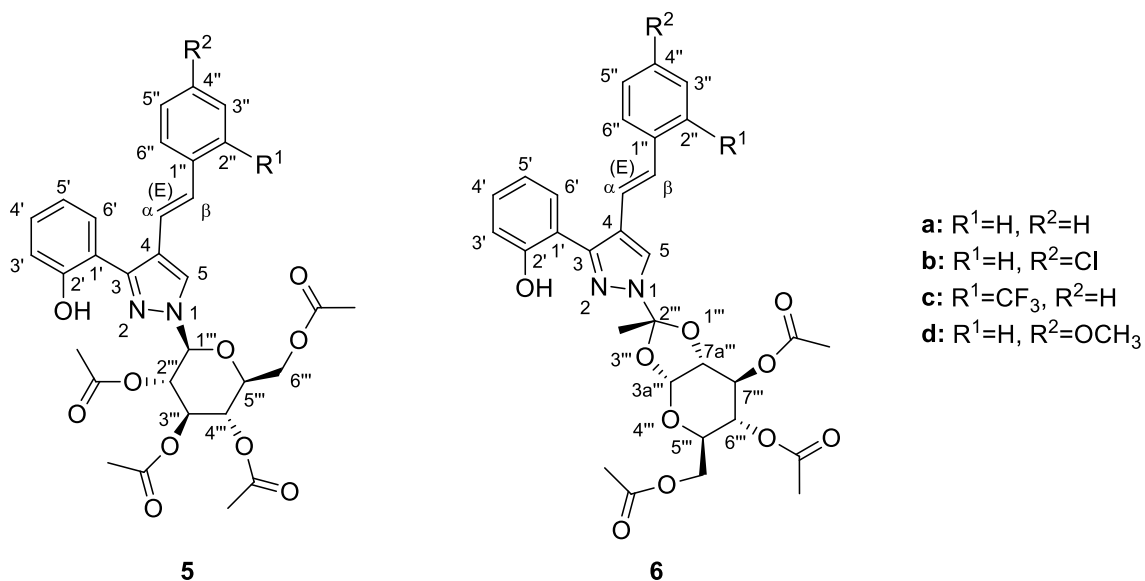


Figure 2.3 – Structure and numbering system of (*E*)-1-[β-D-(2,3,4,6-tetra-*O*-acetylglycose-1-yl)]-3-(2-hydroxyphenyl)-4-(2-/4-Rstyryl)-1*H*-pyrazoles **5a-d**, and 1-[(2*R*,3*aR*,5*R*,6*S*,7*S*,7*aR*)-6,7-diacetoxy-5-acetoxymethyl-2-methyltetrahydro-5*H*-[1,3]dioxolo[4,5-*b*]pyran-2-yl)-(E)-3-(2-hydroxyphenyl)-4-(2-/4-Rstyryl)-1*H*-pyrazole **6a-d**.

The nomenclature of compounds **7a-d** and **8a,b**, represented in Figure 2.4, follows the same rules as those above mentioned for the pyrazole derivatives **5a-d** from which **7a-d** were obtained and for **6a-d** from which **8a,b** were obtained upon the cleavage of the acetyl groups of the sugar moiety.

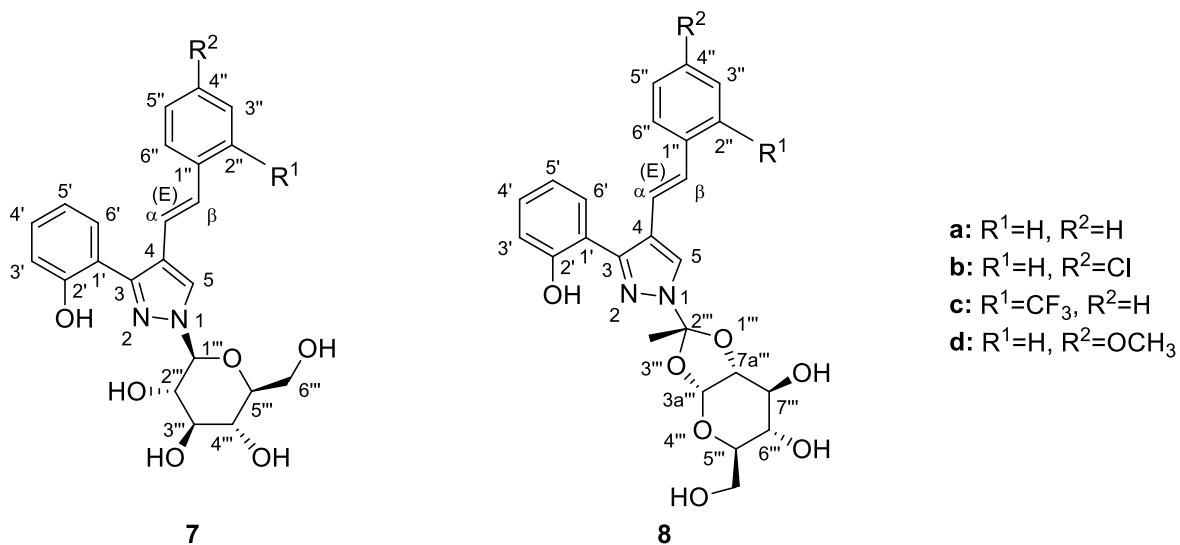


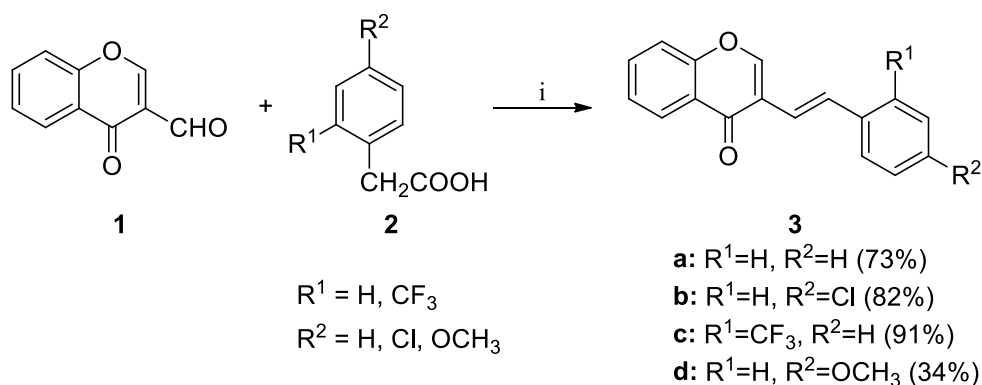
Figure 2.4 – Structure and numbering system of (*E*)-1-[β-D-(glycose-1-yl)]-3-(2-hydroxyphenyl)-4-(2-/4-Rstyryl)-1*H*-pyrazoles **7a-d** and 1-[(2*R*,3*aR*,5*R*,6*S*,7*S*,7*aR*)-6,7-dihydroxy-5-hydroxymethyl-2-methyltetrahydro-5*H*-[1,3]dioxolo[4,5-*b*]pyran-2-yl]-(*E*)-3-(2-hydroxyphenyl)-4-(2-/4-Rstyryl)-1*H*-pyrazoles **8a,b**.

2.2. Synthesis

The methods adopted for the synthesis of the glycosylated compounds and their precursors are briefly described. For the detailed experimental protocols on the synthesis of these compounds, please refer to the chapter 5.

2.2.1. Synthesis of (*E*)-3-styryl-4*H*-chromen-4-ones

The novel (*E*)-3-(4-methoxystyryl)-4*H*-chromen-4-one (**3d**) and the already reported (*E*)-3-styryl-4*H*-chromen-4-ones **3a** and **3b**, are obtained through a Knoevenagel-type condensation followed by *in situ* decarboxylation of 4-oxo-4*H*-chromene-3-carbaldehyde **1** with the appropriate phenylacetic acids in dry pyridine, in the presence of potassium *tert*-butoxide as a base, according to the procedure reported by Silva *et al* (Scheme 2.1).^{90,91} The (*E*)-3-styryl-4*H*-chromen-4-one **3c** was already available in the laboratory and was previously synthesized following the same procedure. The mechanism of this reaction is already described in the literature.⁹¹ The (*E*)-3-styryl-4*H*-chromen-4-ones **3a**, **3b** and **3c** were obtained in very good yields (73%, 82% and 91%, respectively). The yield of **3d** (34%) was lower probably because the pyridine used in the reaction was not freshly dried.



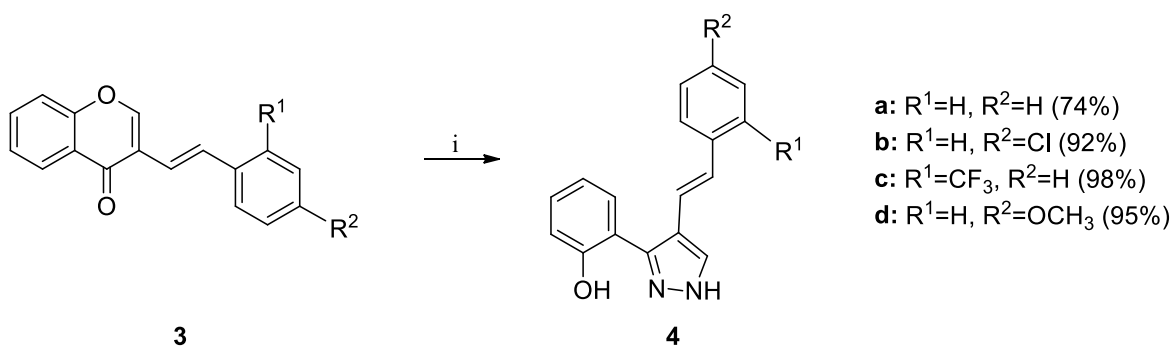
(i) Reagents and conditions: **2** (5.0 equiv.), *tert*-BuOK (1.5 equiv.), dry pyridine, 120 °C, 24h.

Scheme 2.1 – Synthesis of (*E*)-3-styryl-4*H*-chromen-4-ones **3a-d**.

2.2.2. Synthesis of (*E*)-3(5)-(2-hydroxyphenyl)-4-styryl-1*H*-pyrazoles

The new (*E*)-3(5)-(2-hydroxyphenyl)-4-(4-methoxystyryl)-1*H*-pyrazole (**4d**) and the ones already reported, **4a** and **4b**, were prepared from the appropriate (*E*)-3-styryl-4*H*-chromen-4-ones by treatment with hydrazine hydrate in methanol at room temperature,

following the procedure reported by Silva *et al* (Scheme 2.2).⁸⁷ Under such conditions, the expected (*E*)-3(5)-(2-hydroxyphenyl)-4-styryl-1*H*-pyrazoles **4a**, **4b** and **4d** were obtained in very good yields (74-98%). The not yet reported (*E*)-3(5)-(2-hydroxyphenyl)-4-(2-trifluoromethylstyryl)-styryl-1*H*-pyrazole (**4c**) was already available in the laboratory; it was synthesized in very good yield (98%) following the same procedure.



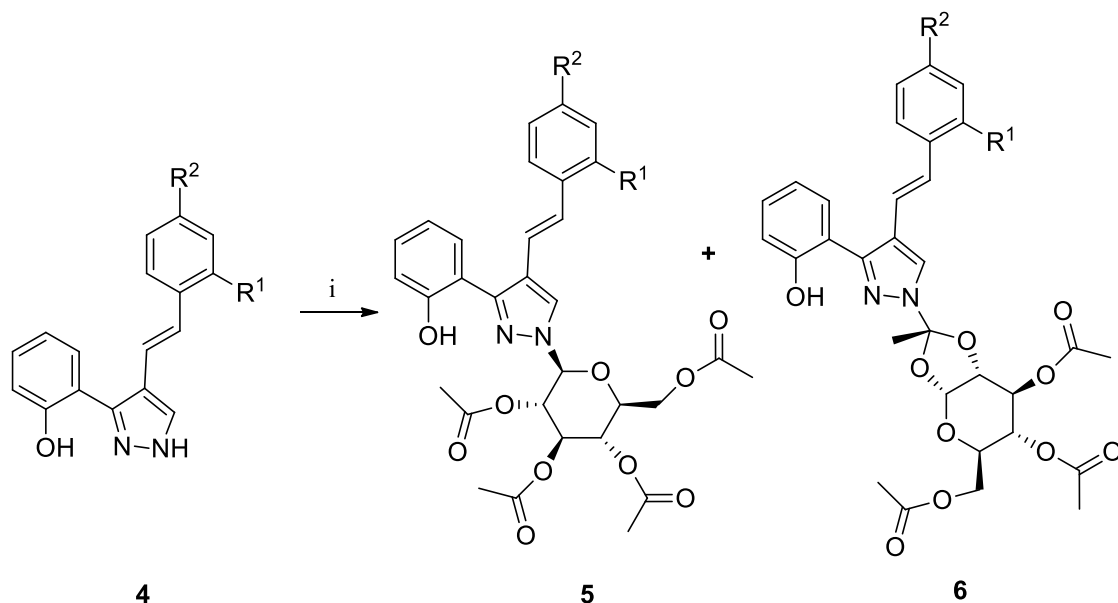
(i) Reagents and conditions: NH₂NH₂·H₂O (2 equiv.), MeOH, r.t., 2 h.

Scheme 2.2 – Synthesis of (*E*)-3(5)-(2-hydroxyphenyl)-4-styryl-1*H*-pyrazoles **4a-d**.

2.2.3. Novel glycosylated (*E*)-3(5)-(2-hydroxyphenyl)-4-styryl-1*H*-pyrazoles obtained by Koenigs-Knorr method

In a first approach, the glycosylation reaction of (*E*)-4-(4-chlorostyryl)-3(5)-(2-hydroxyphenyl)-1*H*-pyrazole (**4b**) with 2,3,4,6-tetra-*O*-acetyl- α -D-glucopyranosyl bromide was performed under molecular sieves (4Å) in dry CH₂Cl₂ using Ag₂CO₃ as a base and AgOTf as promoter following the Koenigs-Knorr method described in the literature.⁸⁸ After purification of the reaction mixture, by thin layer chromatography using CH₂Cl₂:acetone (9:1) as eluent, two *N*-glycosylated products were isolated and characterized by 1D and 2D NMR techniques, as well as by mass spectrometry. The product with lower r.f. corresponds to compound **5b** and the product with higher r.f. to compound **6b** (Scheme 2.3). Using the same protocol, we carried out the glycosylation of the remaining pyrazoles **4a**, **4c** and **4d**, as shown in Scheme 2.3. Different reaction times were tested to perceive the influence of this parameter on the yield of the novel products **5a-d** and **6a-d**. Table 2.1 presents the reaction time and yields of the products isolated in the glycosylation reactions performed in this work. Note that compounds **5d** and **6d**

comprise a mixture of (*E*)- and (*Z*)-isomers and, for this, only their ^1H NMR spectra were collected. These are given in the sub-chapter 5.2.3.



a: $\text{R}^1=\text{H}$, $\text{R}^2=\text{H}$, **b:** $\text{R}^1=\text{H}$, $\text{R}^2=\text{Cl}$, **c:** $\text{R}^1=\text{CF}_3$, $\text{R}^2=\text{H}$, **d:** $\text{R}^1=\text{H}$, $\text{R}^2=\text{OCH}_3$

(i) Reagents and conditions: 2,3,4,6-tetra-*O*-acetyl-D-glucopyranosyl bromide (1.5 equiv.), Ag_2CO_3 (3.0 equiv.), AgOTf (0.15 equiv.), CH_2Cl_2 , r.t.

Scheme 2.3 – Koenigs-Knorr glycosylation of (*E*)-3(5)-(2-hydroxyphenyl)-4-styryl-1*H*-pyrazoles **4a-d**.

This glycosylation reaction requires several days to afford products **5** and **6** in moderate to good yields, as seen in Table 2.1. The yields show that compound **6** is, in most cases, the main reaction product. Yet, the global yield of this reaction seems to be affected by the solvent dryness. In fact, the global yield of the reaction decreases when dichloromethane is not freshly distilled (see entries 1-4, Table 2.1). The storage of dichloromethane in molecular sieves 4Å doesn't remove the water so efficiently as the distillation over calcium hydride. Thus, when the solvent was dried with molecular sieves 4Å (entries 2 and 4, Table 2.1), there were higher traces of water in the reaction mixture, which particularly jeopardized the attained yields for compound **6**. These results may indicate that compound **6** is more susceptible to degradation in the presence of water. Furthermore, the total reaction yield is also affected by the reaction time. To see the effect of the reaction time, the substituent effect and solvent drying procedure must be the same (see entries 5 and 6, Table 2.1). For these experiments, the total yield was higher when the

reaction time was longer. These results indicate that this reaction needs prolonged reaction time to achieve a better yield.

Table 2.1 – Reaction time and yields of the Koenigs-Knorr glycosylation of (*E*)-3(5)-(2-hydroxyphenyl)-4-styryl-1*H*-pyrazoles **4a-d**.

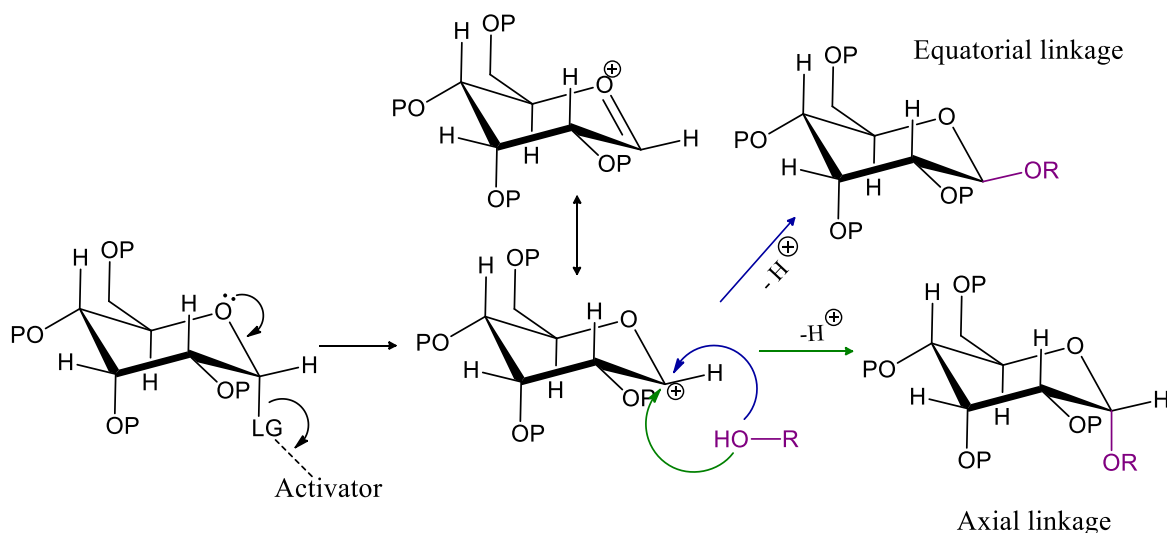
Entry	R ¹	R ²	Reaction time (days)	Yield of 5 (%) ^[a]	Yield of 6 (%) ^[a]	Total yield (%)
1 ^[b]	H	H	7	20	52	72
2 ^[d]	H	H	10	21	39	60
3 ^{[c],[b]}	H	Cl	7	19	50	69
4 ^[d]	H	Cl	10	25	22	47
5 ^[d]	CF ₃	H	7	30	6	36
6 ^[d]	CF ₃	H	10	11	41	52
7 ^[b]	H	OMe	7	12	39	51

[a] Yields of isolated product obtained after purification by thin layer chromatography. [b] Dichloromethane was dried over calcium hydride and kept with molecular sieves 4Å. [c] 17% of starting material was recovered. [d] Dichloromethane was dried with molecular sieves 4Å without prior distillation over calcium hydride.

During a glycosylation reaction there are several factors that may influence the obtained products. Among those factors, stereochemistry, neighboring group participation and the protecting groups employed at the sugar moiety are of interest. Notice that glycosylation is a reaction where a glycosyl donor (a carbohydrate), which behaves as an electrophile, is attached to a hydroxyl or other functional group of a glycosyl acceptor, a nucleophile, forming a glycoside under appropriate reaction conditions.⁹² This reaction requires the presence of an activator or promoter, such as silver triflate (AgOTf). The promoter will aid the departure of the leaving group present in the glycosyl donor (such as the Br group), allowing the formation of a reactive intermediate.⁹³ The resulting electrophilic anomeric carbon of the glycosyl donor then couples with the glycosyl acceptor, forming a glycosidic bond.

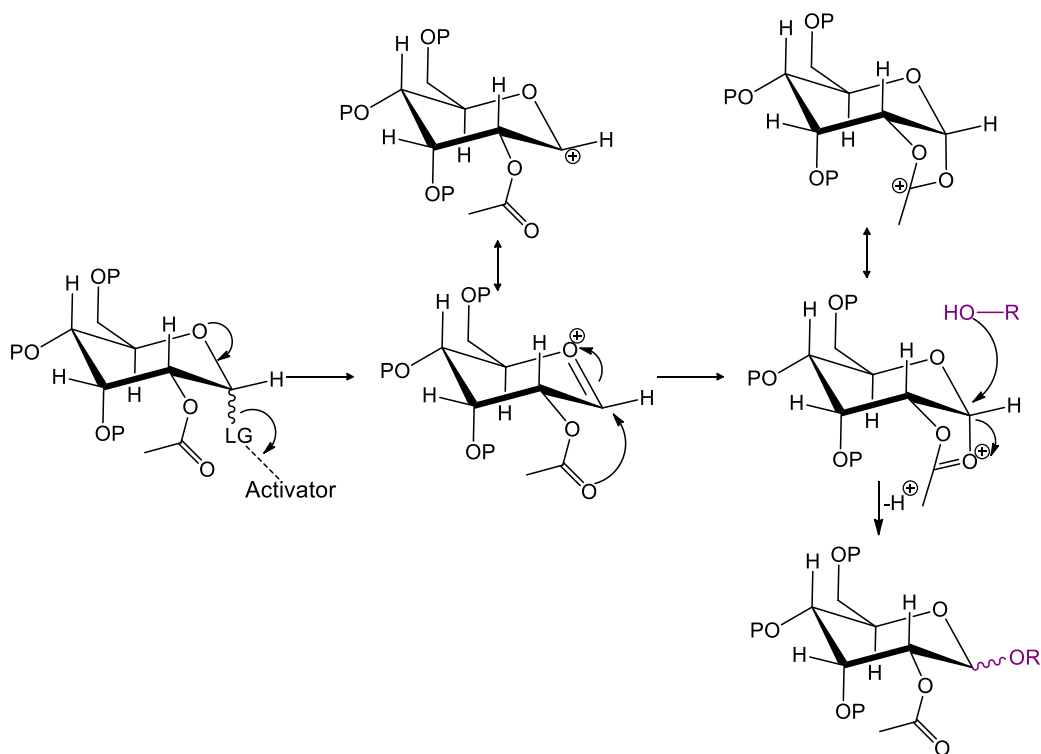
When the glycosyl acceptor attacks the electrophilic anomeric carbon of the glycosyl donor, it may be either from the top or the bottom of the sugar ring.⁹³ Consequently, it's common to obtain a mixture of products, depending on the possibility of having two different stereochemical approaches. The formed linkage may either be axial or

equatorial (*i.e.* α or β , respectively, taking glucose as example). To perceive this, the mechanism of a glycosylation reaction is showed in the Scheme 2.4.



Scheme 2.4 – General mechanism of the glycosylation reaction; herein P stands for Protecting Group and LG stands for Leaving Group. Notice the attack performed by the glycosyl acceptor, represented in purple, to the anomeric carbon of the glycosyl donor from either the top (blue arrow) or the bottom (green arrow). Adapted from the literature.⁹³

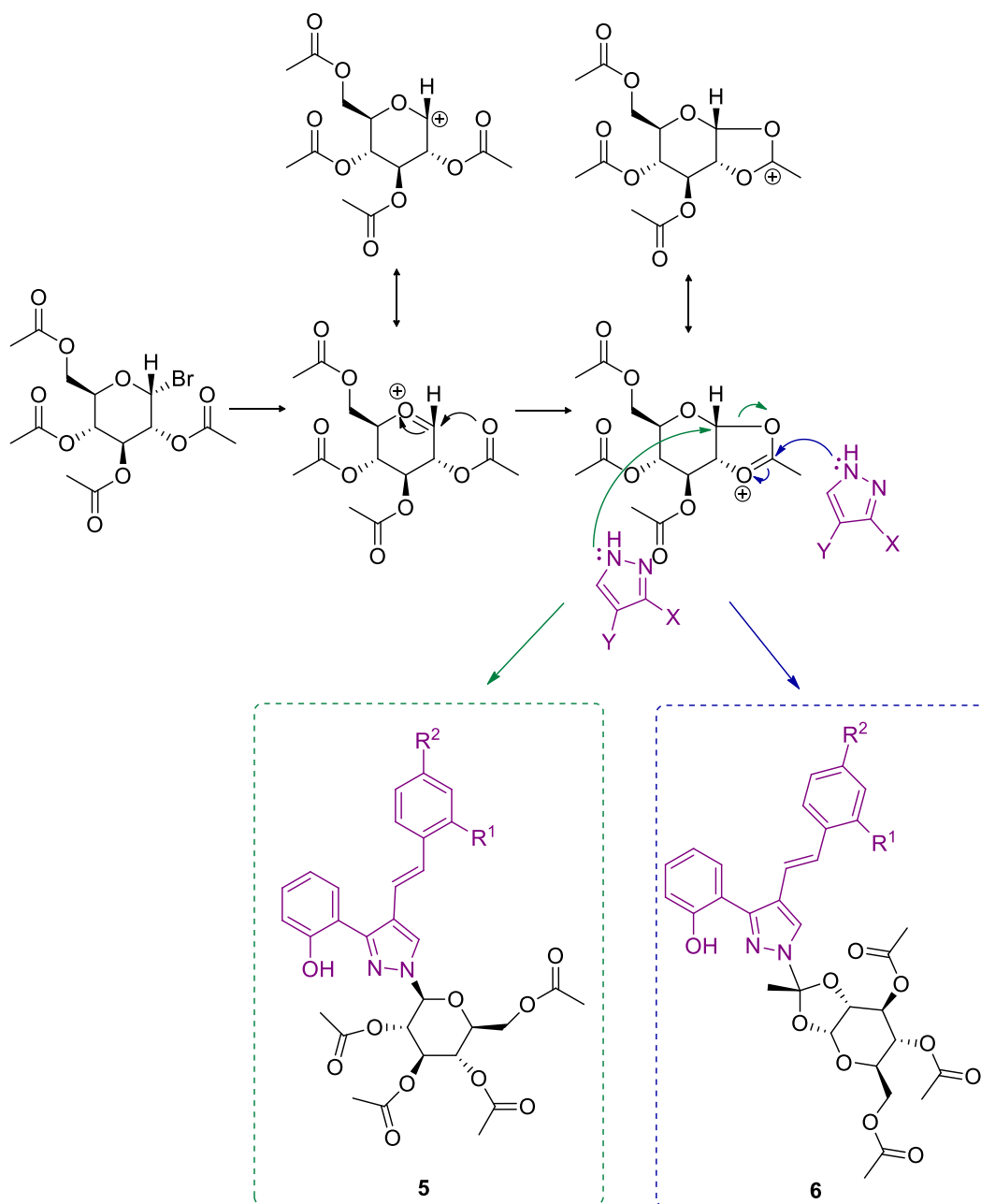
The stereochemistry of the glycosylated product may also be affected by the type of protecting group employed at the C-2 of the glycosyl donor.⁹³ A non-participating group usually allows the nucleophilic attack of the glycosyl acceptor either from the bottom or top surface. This means that a non-participant group often leads to a mixture of α - and β -glycosides. However, when a participating group (such as the acetyl group) is involved in the glycosylation reaction, the nucleophilic attack of the glycosyl acceptor is limited. Consequently, participant groups generally promote the formation of β -glycosides. The occurrence of the neighbour group participation in the glycosylation reaction is depicted in the Scheme 2.5.



Scheme 2.5 – Neighbouring group participation in the glycosylation reaction. The glycosyl acceptor is represented in the purple color.

The effect of the protecting groups is not limited to the stereochemistry. In fact, protecting groups also play a role in the reactivity of the glycosyl donors.⁹⁴ Electron-donating protecting groups, like ether, increase the reactivity of the glycosyl donor. On the other hand, electron-withdrawing protecting groups, such as the acetyl group, are considered deactivating since they lower the reactivity of the sugar donor. Notice that 2,3,4,6-tetra-*O*-acetyl- α -D-glucopyranosyl bromide, the glycosyl donor used in this work, has the acetyl as protecting group; that may be the reason for the need of long reaction times observed in the reactions performed.

The glycosylation reaction mechanisms presented in Schemes 2.4 and 2.5 help to understand the reaction mechanisms that lead to the formation of compounds **5a-d** and **6a-d**. The proposed mechanisms for the formation of compounds **5a-d** and **6a-d** may be consulted in the Scheme 2.6.



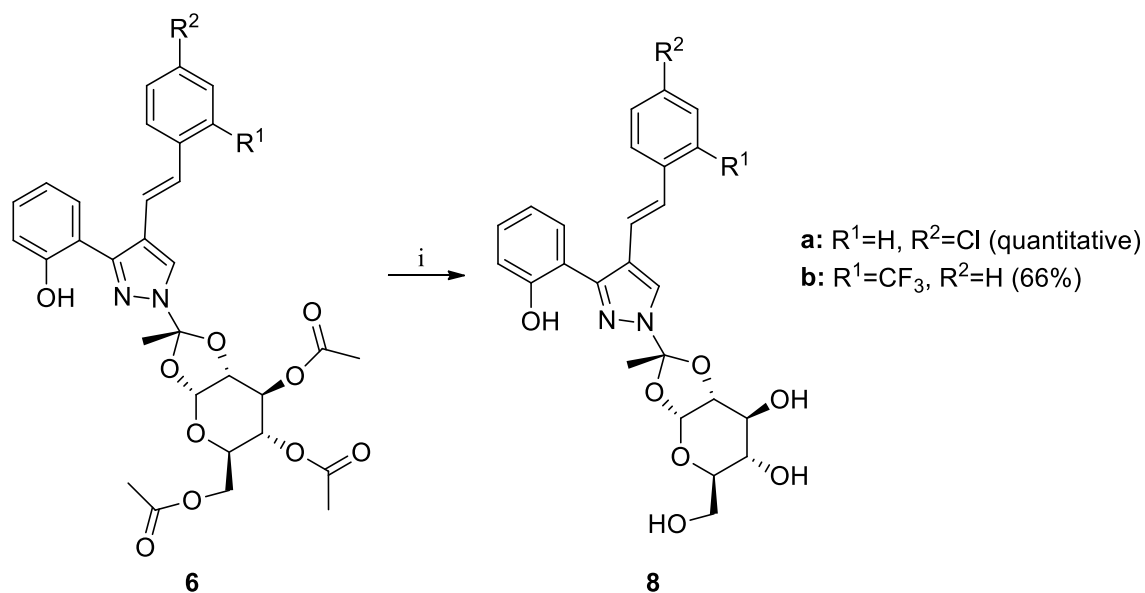
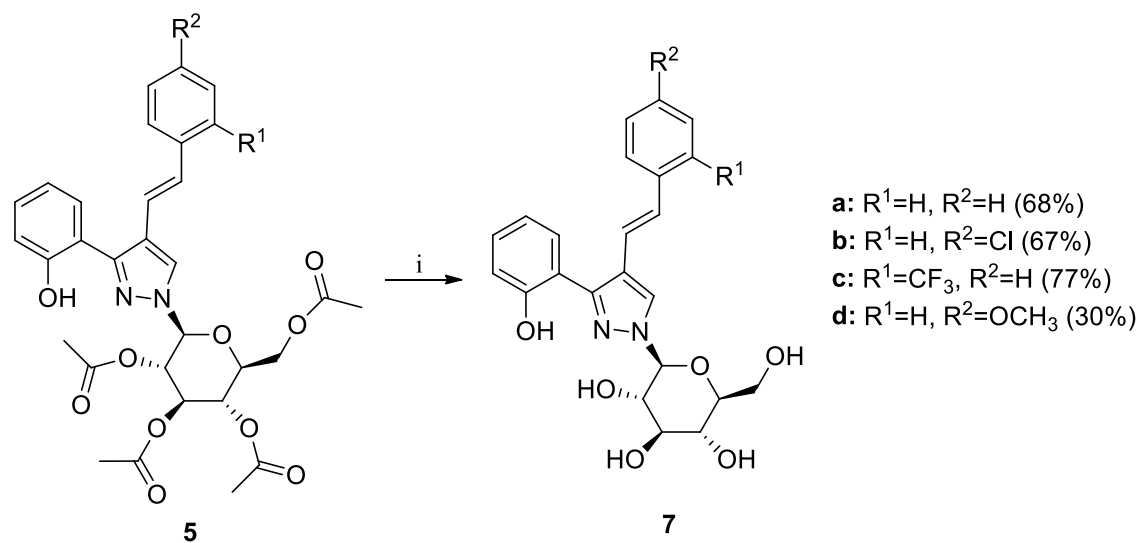
X = 2-hydroxyphenyl; Y = 2-aryl/phenylvinyl

a: R¹=H, R²=H, b: R¹=H, R²=Cl, c: R¹=CF₃, R²=H, d: R¹=H, R²=OCH₃

Scheme 2.6 – Proposed mechanisms for the formation of compounds **5a-d** (represented in green) and **6a-d** (denoted in blue). The pyrazole derivative is represented in purple. To simplify, the sugar moieties of compounds **5a-d** and **6a-d** are represented as planar structures.

2.2.3.1. Removal of the protecting groups of the glycosylated products

The cleavage of the acetyl protecting groups of the new *N*-glycosylated compounds **5a-d** and **6a-d** was performed following the method reported by Pathak *et al*, as seen in Scheme 2.7.⁹⁵ To a solution of the appropriate compound **5a-d** or **6a-d** in methanol was added Amberlite[®] IRA-400(OH) resin as shown in Scheme 2.4. This resin was prepared from Amberlite[®] IRA-400(Cl) resin which was treated with a 1.0 M sodium hydroxide solution, washed with water and methanol, thus exchanging the Cl by an OH group. The reaction mixture was left at 25-30 °C with stirring for 4 hours, except for compound **7b** which reacted for 21 hours to achieve full cleavage of the protecting groups. After that period, the reaction mixture was filtered and the resin was washed with methanol. The solvent was evaporated to dryness under reduced pressure to afford the novel deprotected *N*-glycosylated products **7a-d** and **8a,b**. The reaction was not successful for all derivatives. In fact, the deprotection of compound **5d** leads to a mixture of *cis* and *trans* isomers, due to the isomerization of the double bond of the styryl group. The deprotection of compound **6a** resulted in modifications of the sugar moiety. Finally, the deprotection reaction of compound **6d** was not complete; in the ¹H NMR spectrum of the reaction product it was possible to observe some signals due to the resonance of the acetyl groups of the starting material.



(i) Reagents and conditions: Amberlite-IRA400 (OH), MeOH, r.t., 4h and 21h for compound **7b**

Scheme 2.7 – Cleavage of the acetyl protecting groups.

2.3. Structural characterization of the synthesised compounds

The compounds having the chloro as substituent ($R^2 = \text{Cl}$) are selected as example for structural characterization discussion. The characterization of the (*E*)-3-(4-chlorostyryl)-4*H*-chromen-4-one (**3b**), already reported by Sandulache *et al*, won't be presented here.⁹⁶

2.3.1. (*E*)-3(5)-(2-Hydroxyphenyl)-4-styryl-1*H*-pyrazoles

The structural characterization of (*E*)-3(5)-(2-hydroxyphenyl)-4-styryl-1*H*-pyrazoles **4a-d** will not be discussed in detail as it is published by Silva *et al*,⁸⁷ except for compound **4b** which was selected as an example, and for the novel compound **4d** whose full characterization may be consulted in the sub-chapter 5.2.2.

The ¹H NMR spectrum of (*E*)-4-(4-chlorostyryl)-3(5)-(2-hydroxyphenyl)-1*H*-pyrazole (**4b**) illustrates the various typical signals of (*E*)-3(5)-(2-hydroxyphenyl)-4-styryl-1*H*-pyrazoles (see Figure 2.5).

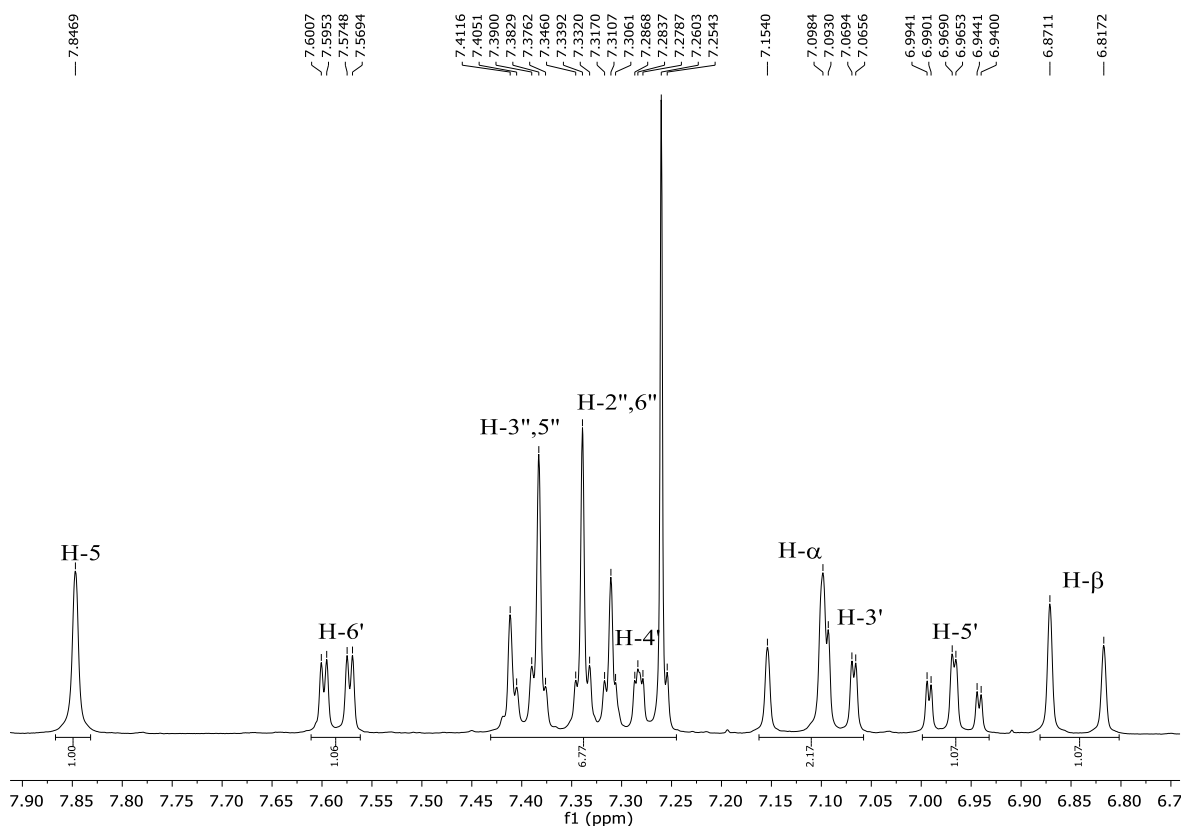


Figure 2.5 – Expansion of the ¹H NMR spectrum of (*E*)-4-(4-chlorostyryl)-3(5)-(2-hydroxyphenyl)-1*H*-pyrazole (**4b**) (CDCl₃, 300.13 MHz).

The singlet at δ 7.85 ppm, due to the resonance of H-5, and the doublets at δ 7.13 ppm and δ 6.84 ppm corresponding to the resonance of protons H- α and H- β are among the characteristic signals of these compounds. The coupling constant between H- α and H- β ($J = 16.4$ Hz) indicates a *trans* configuration of this vinylic system. The resonance of the 2'-OH proton is also a typical signal of these compounds. However, this is a labile proton which in some cases is not observed in the ^1H NMR spectrum, as in this example. There are also two doublets in the aromatic region, at δ 7.32 and 7.39 ppm, respectively, due to the resonance of the protons H-2'',6'' and H-3'',5'' of the *para*-substituted (4-Cl) phenyl ring. The other signals in the aromatic region are two doublets of doublets corresponding to the resonance of protons H-6' at δ 7.58 ppm ($J = 7.6, 1.6$ Hz) and H-3' at 7.08 ppm ($J = 8.4, 1.3$ Hz), a multiplet due to the resonance of H-4' at δ 7.28 – 7.35 ppm and a doublet of triplets due to the resonance of H-5' at δ 6.97 ppm ($J = 7.6, 1.3$ Hz).

Regarding the ^{13}C NMR signals, the spectrum of **4b**, on Figure 2.6, also exhibits the characteristic resonances of this class of compounds. Among them are the signals due to the resonance of the carbons of the pyrazole moiety C-3 (δ 148.0 ppm), C-4 (δ 120.5 ppm) and C-5 (δ 127.7 ppm). These carbon resonances are assigned based in correlations found in the HSQC spectra (H-5 \rightarrow C-5) and in the HMBC spectra (H- α \rightarrow C-3 and C-5, H-5 \rightarrow C-3 and C-4, H-6' \rightarrow C-3). The resonance of C-2' is also typical, appearing at high frequency values (δ 155.6 ppm) since C-2' is linked to the electronegative oxygen atom of the OH group. C- α and C- β are assigned based in the correlations found in the HSQC spectra (H- α \rightarrow C- α , H- β \rightarrow C- β). The most deprotected carbon corresponds to C- β , allowing the unequivocal assignment of the proton and carbon resonances of the vinylic system.

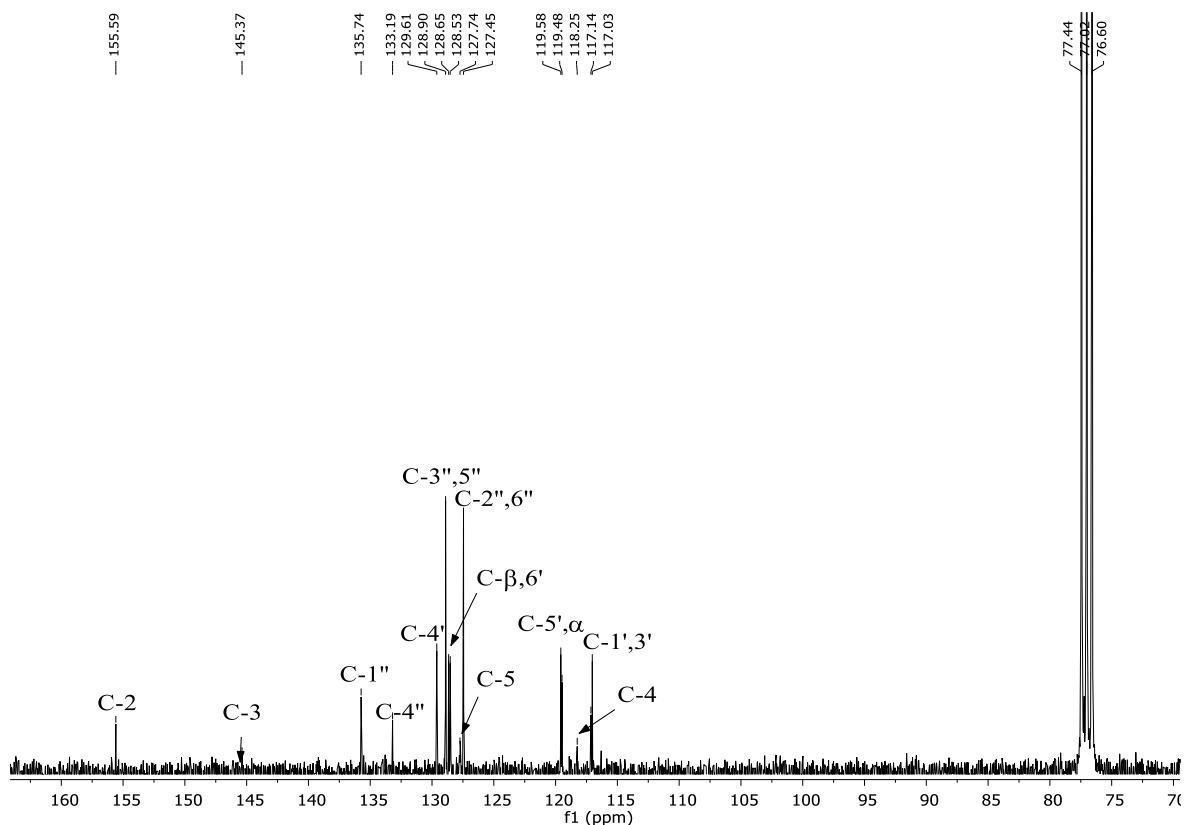


Figure 2.6 – Expansion of the ^{13}C NMR spectrum of (*E*)-4-(4-chlorostyryl)-3(5)-(2-hydroxyphenyl)-1*H*-pyrazole (**4b**) (CDCl_3 , 75.47 MHz).

2.3.2. (*E*)-1-[β -D-(2,3,4,6-Tetra-*O*-acetylglycose-1-yl)]-3-(2-hydroxyphenyl)-4-styryl-1*H*-pyrazoles

The structure of the novel (*E*)-1-[β -D-(2,3,4,6-tetra-*O*-acetylglycose-1-yl)]-3-(2-hydroxyphenyl)-4-styryl-1*H*-pyrazoles **5a-d** was elucidated based on 1D (^1H and ^{13}C) and 2D (HSQC, HMBC, COSY and NOESY) NMR spectroscopic experiments. The structure of compounds **5a-d** was also confirmed by comparing their NMR spectra with those of the corresponding (*E*)-3(5)-(2-hydroxyphenyl)-4-styryl-1*H*-pyrazole precursor. The most characteristic signals in the ^1H NMR of compounds **5** appear in the aliphatic region and are due to the sugar moiety protons (H-1'''-H-6''') and to the acetyl protecting groups. The ^1H NMR spectrum example of (*E*)-1-[β -D-(2,3,4,6-tetra-*O*-acetylglycose-1-yl)]-4-(4-chlorostyryl)-3-(2-hydroxyphenyl)-1*H*-pyrazole (**5b**), is given in the Figure 2.7.

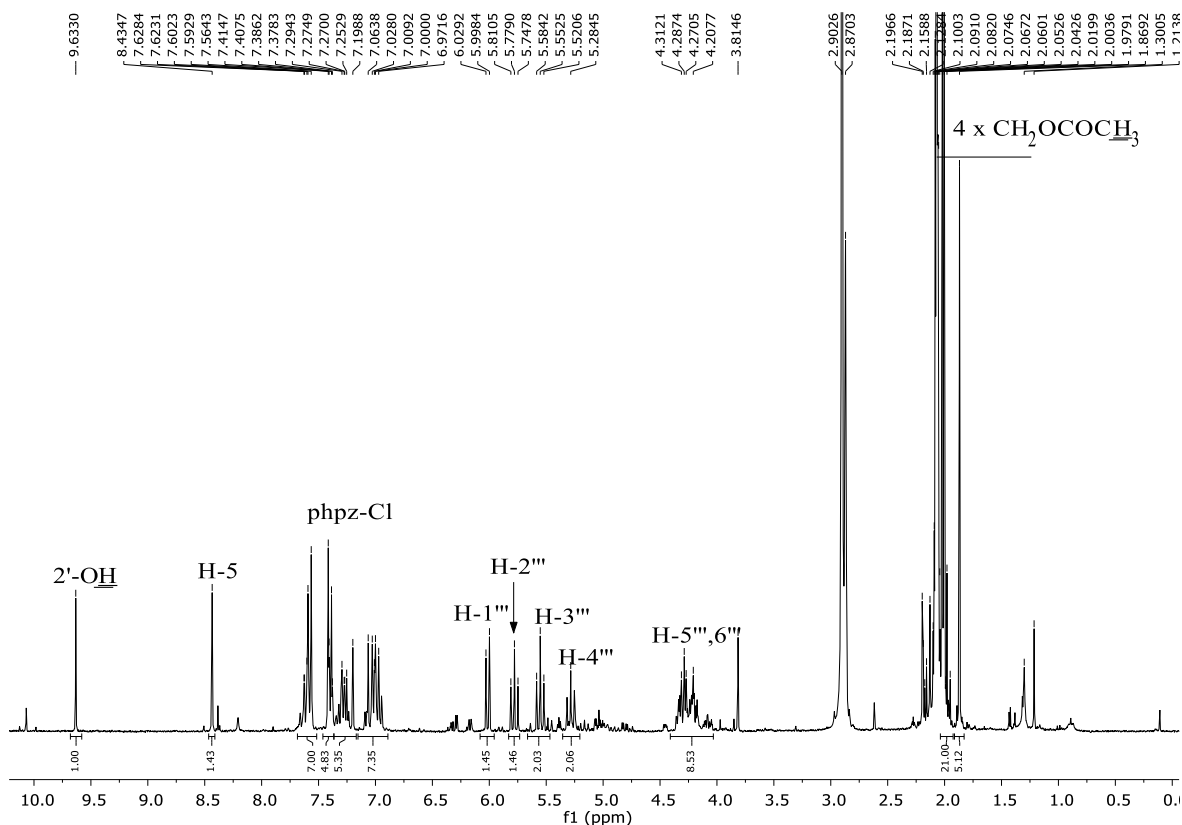


Figure 2.7 – ^1H NMR spectrum of (*E*)-1-[β -D-(2,3,4,6-tetra-*O*-acetylglucose-1-yl)]-4-(4-chlorostyryl)-3-(2-hydroxyphenyl)-1*H*-pyrazole (**5b**) [$(\text{CD}_3)_2\text{CO}$, 300.13 MHz].[‡]

The resonance of H-1''', H-2''', H-3''', H-4''', H-5''' and H-6''' and of the protons of the acetyl protecting groups appear at very similar chemical shift values for all the compounds **5a-d**, as seen in Table 2.2. The resonances of the sugar moiety protons were attributed based on the COSY spectra. Typically, there's a doublet due to the resonance of the anomeric proton H-1''' at high frequency values, δ 6.00 – 6.03 ppm, as a result of the deshielding effect of the electronegative atoms, with a coupling constant $J = 9.5$ Hz for all the derivatives. The value of this coupling constant confirmed the β -anomeric form of D-glucose in compounds **5**. There are three triplets corresponding to the resonance of protons H-2''' (δ 5.78 – 5.83 ppm), H-3''' (δ 5.55 – 5.56 ppm), and H-4''' (δ 5.28 – 5.29 ppm), all having a coupling constant of $J = 9.5$ Hz in compounds **5a-d**. The multiplet in the interval of δ 3.81 – 4.36 ppm is due to the resonance of protons H-5''' and H-6'''. Another characteristic of compounds **5a-d** is the presence of four singlets (δ 1.87 –

[‡] The abbreviation “Phpz-Cl” presented in the majority of the spectra refers to the proton or carbon resonance signals of the pyrazole moiety.

2.10 ppm) corresponding to the resonance of the methyl groups of the acetyl protecting groups. The signals due to the resonance of the protons of the pyrazole scaffold (see subchapter 2.3.1) are also observed.

The most characteristic signals in the ^{13}C NMR spectra of compounds **5a-d** are ascribed to the resonances of the sugar moiety carbons. The ^{13}C NMR spectrum of (*E*)-1-[β -D-(2,3,4,6-tetra-*O*-acetylglycose-1-yl)]-4-(4-chlorostyryl)-3-(2-hydroxyphenyl)-1*H*-pyrazole (**5b**) is given as example in Figure 2.8. The carbon resonances of both C-1''' and C-5''' appear at higher chemical shifts (δ 87.3 and 75.0 ppm, respectively) than C-2''' (δ 71.0 – 71.1 ppm), C-3''' (δ 73.7 ppm), C-4''' (δ 68.4 – 68.8 ppm) and C-6''' (δ 62.7 ppm). Since C-1''' and C-5''' are linked to two electronegative atoms, they are more deprotected than carbons C-2''' to C-6'''. The most protected carbons are $-\text{COCH}_3$, appearing at δ 20.2 – 20.6 ppm. The carbon resonances of the four protecting carbonyl groups ($-\text{COCH}_3$) are highly deshielded, appearing at δ 169.4 – 170.7 ppm. The fully detailed ^{13}C NMR chemical shifts of compounds **5a-d** are presented in the experimental section – chapter 5.

Table 2.2 – Chemical shifts (ppm, relative to TMS) and coupling constants (*J*, Hz) of ¹H NMR spectra of (*E*)-1-[β-D-(2,3,4,6-tetra-*O*-acetylglycose-1-yl)]-3-(2-hydroxyphenyl)-4-styryl-1*H*-pyrazoles **5a-d**.

Compound Signal	5a	5b	5c	5d ^[a]
H-5	8.43, s	8.43, s	8.52, s	8.37, s
2'-OH	9.68, s	9.63, s	9.53, s	9.74, s
H-3'	7.02, dd <i>J</i> 7.7, 1.0	7.00-7.09, m	7.02, dd <i>J</i> 8.0, 1.1	6.98-7.02, m
H-4'	7.27-7.31, m	7.29, ddd <i>J</i> 7.7, 7.9, 1.6	7.30, ddd <i>J</i> 8.0, 7.6, 1.6	7.26-7.30, m
H-5'	6.98, ddd <i>J</i> 7.5, 7.6, 1.0	6.97, t <i>J</i> 7.9	6.97, dt <i>J</i> 7.6, 1.1	6.94-6.98, m
H-6'	7.64, dd <i>J</i> 7.6, 1.6	7.63, dd <i>J</i> 7.9, 1.6	7.59, dd <i>J</i> 7.6, 1.6	7.65, dd <i>J</i> 7.8, 1.6
H-2''	7.56, d <i>J</i> 7.5	7.58, d <i>J</i> 8.2	–	7.50, d <i>J</i> 8.7
H-3''	7.38, t <i>J</i> 7.5	7.40, d <i>J</i> 8.2	7.75, d <i>J</i> 7.8	6.95, d <i>J</i> 8.7
H-4''	7.27-7.31, m	–	7.50, t <i>J</i> 7.8	–
H-5''	7.38, t <i>J</i> 7.5	7.40, d <i>J</i> 8.2	7.68, t <i>J</i> 7.8	6.95, d <i>J</i> 8.7
H-6''	7.56, d <i>J</i> 7.5	7.58, d <i>J</i> 8.2	7.96, d <i>J</i> 7.8	7.50, d <i>J</i> 8.7
H-α	7.21, d <i>J</i> 16.3	7.23, d <i>J</i> 16.3	7.25, d <i>J</i> 16.0	6.98, d ^[b] <i>J</i> 16.2
H-β	7.05, d <i>J</i> 16.3	7.04, d <i>J</i> 16.3	7.32, d <i>J</i> 16.0	7.05, d ^[b] <i>J</i> 16.2
H-1'''	6.02, d <i>J</i> 9.5	6.01, d <i>J</i> 9.5	6.03, d <i>J</i> 9.5	6.00, d <i>J</i> 9.5
H-2'''	5.79, t <i>J</i> 9.5	5.78, t <i>J</i> 9.5	5.83, t <i>J</i> 9.5	5.78, t <i>J</i> 9.5
H-3'''	5.56, t <i>J</i> 9.5	5.55, t <i>J</i> 9.5	5.55, t <i>J</i> 9.5	5.55, t <i>J</i> 9.5
H-4'''	5.29, t <i>J</i> 9.5	5.28, t <i>J</i> 9.5	5.29, t <i>J</i> 9.5	5.29, t <i>J</i> 9.5
H-5'''	3.81-4.34, m	4.16-4.36, m	4.19-4.34, m	4.18-4.34, m
6'''-CH₂OCOCH₃	3.81-4.34, m	4.16-4.36, m	4.19-4.34, m	4.18-4.34, m
-COCH₃	1.98, s	1.87, s	1.88, s	1.87, s
	2.01, s	2.00, s	1.98-2.10, m	2.00, s
	2.04-2.10, m	2.02, s		2.02, s
		2.04-2.07, m		2.04-2.07, m

[a] Compound **5d** is a mixture of *cis* and *trans* isomers. In this table, only the proton signals correspondent to the *trans* isomer are considered since it is the most abundant isomer. The ¹H NMR data may be consulted in the sub-chapter 5.2.3. [b] Protons H-α and H-β are indistinguishable in this case.

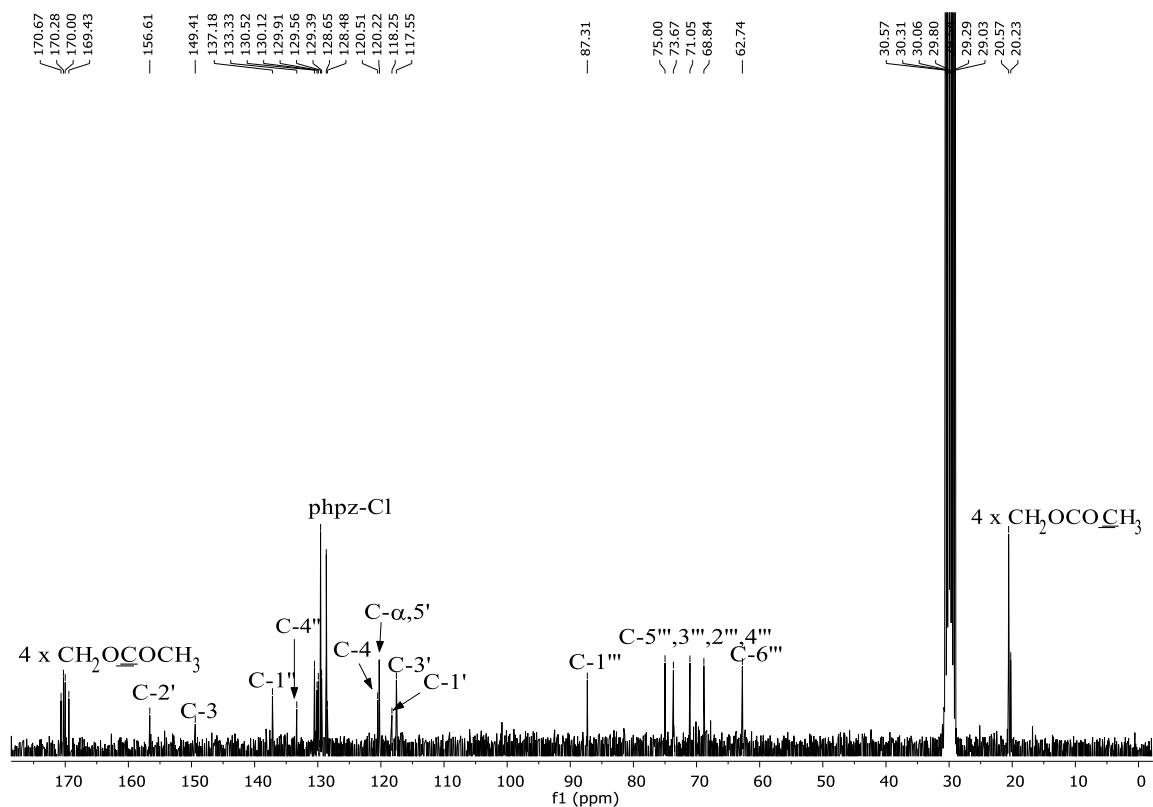
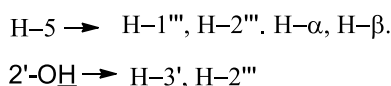
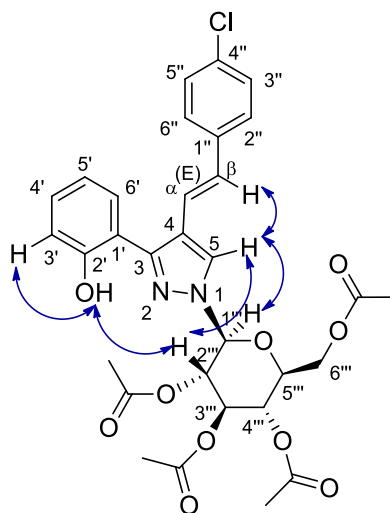


Figure 2.8 – ^{13}C NMR spectrum (*E*)-1-[β -D-(2,3,4,6-tetra-*O*-acetylglucose-1-yl)]-4-(4-chlorostyryl)-3-(2-hydroxyphenyl)-1*H*-pyrazole (**5b**) [$(\text{CD}_3)_2\text{CO}$, 75.47 MHz].

1D and 2D NMR experiments allowed the assignment of the proton and carbon resonances of compounds **5a-d** and revealed the nature of the formed glycosidic bond. Theoretically, both *O*-glycosylated and *N*-glycosylated products could have been obtained from the glycosylation reaction performed in this work (review sub-chapter 2.2.3.). Since compounds **5a-d** present the resonance of the 2'-OH proton in the ^1H NMR (at δ 9.53 – 9.74 ppm, see Table 2.2), it's possible to infer that compounds **5a-d** are *N*-glycosylated. Also, the presence of the resonance of 2'-OH proton at δ 9.53 – 9.74 ppm is indicative of a hydrogen bond between the 2'-OH and the N2 of the pyrazole nucleus. This non-covalent bond may cause hindrance to *O*-glycosylation. The NOESY correlations observed for compound **5b** (Scheme 2.8) are used to exemplify *N*-glycosylation in this class of compounds. Indeed, the NOESY spectrum of compound **5b** shows a correlation between 2'-OH \rightarrow H-3' and H-2'''. In the case of *O*-glycosylation, the 2'-OH proton would have been removed and the mentioned correlations would not be observed, that is the presence of these correlations is intrinsic evidence that compound **5b** is *N*-glycosylated. This conclusion is further supported by the correlations H-5 \rightarrow H-1''' and H-2'''. The

correlation found in the HMBC spectrum of compound **5b** (H-1''' → C-5), also proves the linkage of the sugar moiety to the N1 position of the pyrazole ring. Since all compounds **5** present the resonance of the 2'-OH proton in the ¹H NMR (δ 9.53 – 9.74 ppm, see Table 2.2), it's possible to confirm that compounds **5a-d** are *N*-glycosylated.



Scheme 2.8 – Main correlations (blue arrows) observed in the NOESY spectra of compound **5b**.

2.3.3. 1-[(2*R*,3*aR*,5*R*,6*S*,7*S*,7*aR*)-6,7-diacetoxy-5-acetoxymethyl-2-methyltetrahydro-5*H*-[1,3]dioxolo[4,5-*b*]pyran-2-yl]-(*E*)-3-(2-hydroxyphenyl)-4-styryl-1*H*-pyrazoles

The structure of the novel compounds **6a-d** was determined based on 1D (¹H and ¹³C) and 2D (HSQC, HMBC and NOESY) NMR experiments. The most characteristic signals in the ¹H NMR spectra of compounds **6** are due to the sugar moiety (as example see the ¹H NMR spectrum of 1-[(2*R*,3*aR*,5*R*,6*S*,7*S*,7*aR*)-6,7-diacetoxy-5-acetoxymethyl-2-methyltetrahydro-5*H*-[1,3]dioxolo[4,5-*b*]pyran-2-yl]-(*E*)-4-(4-chlorostyryl)-3-(2-hydroxyphenyl)-1*H*-pyrazole (**6b**) in the Figure 2.9). Typically, the ¹H NMR spectra of compounds **6a-d** presents a doublet due to the resonance of proton H-3a''' at δ 5.75 – 6.18 ppm and two doublet of doublets of doublets corresponding to H-6''' (δ 4.89 – 4.99 ppm) and H-5''' (δ 4.42 – 4.47 ppm) proton resonances (see Table 2.3). A triplet corresponding

to the H-7''' resonance is usually detected at δ 5.14 – 5.26 ppm with a coupling constant around $J = 2.3 - 2.9$ Hz. There's also a multiplet due to the resonance of 5'''-CH₂OCOCH₃ at δ 4.24 – 4.33 ppm and a triplet corresponding to the proton H-7a''' at δ 4.21 – 4.24 ppm. Also, the highly shielded proton resonance due to 2'''-CH₃ (δ 2.19 ppm) is an evidence that confirms the structure proposed for compounds **6a-d**. The remaining typical signals are due to the resonance of -COCH₃ protons. In most cases there is a multiplet at δ 2.05 – 2.10 ppm due to the resonance of two -COCH₃ groups and one broad singlet at δ 2.13 ppm due to the resonance of three protons of one -COCH₃ group. Notice that compounds **6a-d** only present three protecting groups when compared to compounds **5a-d** (compare Figure 2.7 and 2.9).

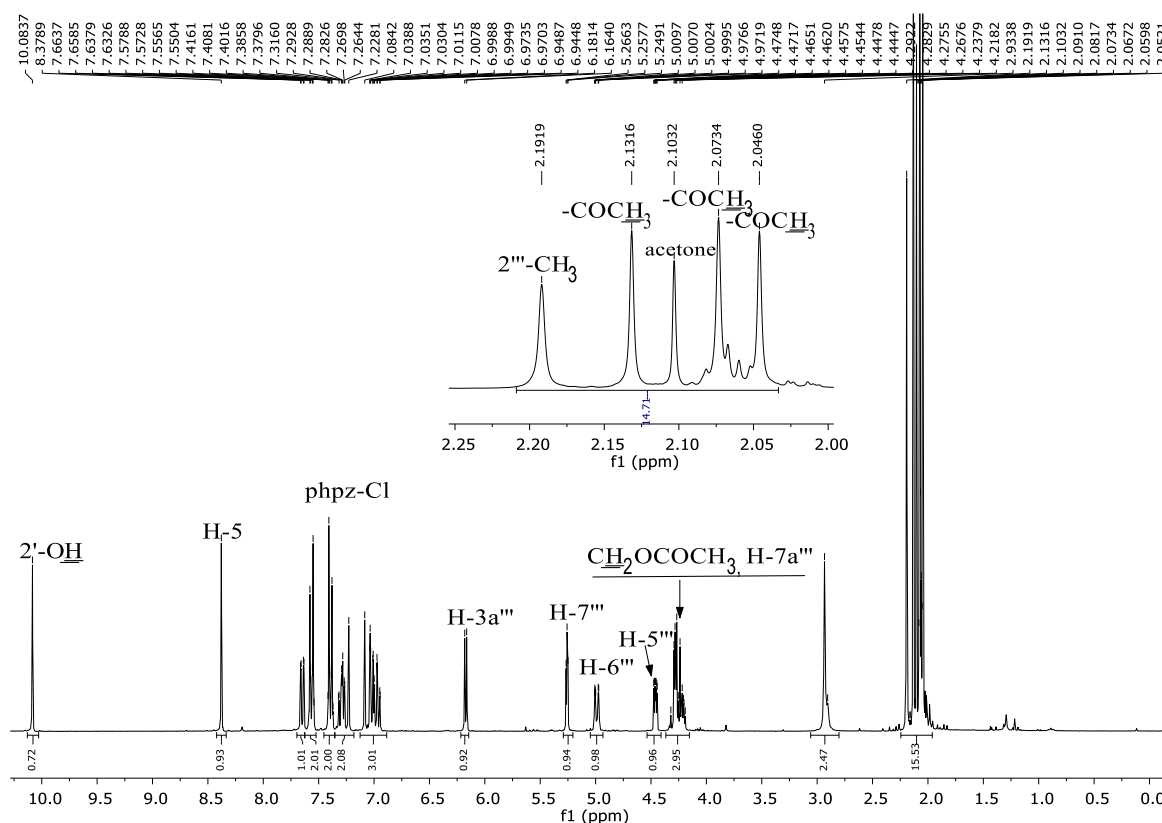


Figure 2.9 – ¹H NMR spectrum of 1-[(2*R*,3*aR*,5*R*,6*S*,7*S*,7*aR*)-6,7-diacetoxy-5-acetoxymethyl-2-methyltetrahydro-5*H*-[1,3]dioxolo[4,5-*b*]pyran-2-yl]-(*E*)-4-(4-chlorostyryl)-3-(2-hydroxyphenyl)-1*H*-pyrazole (**6b**) [(CD₃)₂CO, 300.13 MHz]. An expansion of the aliphatic region, from δ 2.0 – 2.3 ppm, was presented to facilitate the analysis of the spectrum.

Table 2.3 – Chemical shifts (ppm, relative to TMS) and coupling constants (*J*, Hz) of ¹H NMR of 1-[(2*R*,3*aR*,5*R*,6*S*,7*S*,7*aR*)-6,7-diacetoxy-5-acetoxymethyl-2-methyltetrahydro-5*H*-[1,3]dioxolo[4,5-*b*]pyran-2-yl]-(*E*)-3-(2-hydroxyphenyl)-4-styryl-1*H*-pyrazoles **6a-d**.

Compound Signal	6a	6b	6c	6d ^[a]
H-5	8.37, s	8.38, s	8.43, s	8.16, s
2'-OH	10.12, s	10.08, s	–	9.74, s
H-3'	7.02, dd <i>J</i> 7.8, 1.1	7.02, dd <i>J</i> 8.0, 1.1	7.02, dd <i>J</i> 8.2, 1.2	6.93-7.01, m
H-4'	7.27-7.32, m	7.29, ddd <i>J</i> 8.0, 7.6, 1.6	7.28-7.34, m	7.25, ddd <i>J</i> 8.2, 7.7, 1.5
H-5'	6.96-6.98, m	6.97, ddd <i>J</i> 7.7, 7.6, 1.1	6.96, dt <i>J</i> 7.6, 1.2	6.93-7.01, m
H-6'	7.67, dd <i>J</i> 7.8, 1.6	7.65, dd <i>J</i> 7.7, 1.6	7.61, dd <i>J</i> 7.6, 1.6	7.69, d <i>J</i> 7.5
H-2''	7.55, d <i>J</i> 7.4	7.56, d <i>J</i> 8.6	–	7.50, d <i>J</i> 8.7
H-3''	7.38, t <i>J</i> 7.4	7.39, d <i>J</i> 8.6	7.75, d <i>J</i> 7.8	6.95, d <i>J</i> 8.7
H-4''	7.27-7.32, m	–	7.50, t <i>J</i> 7.8	–
H-5''	7.38, t <i>J</i> 7.4	7.39, d <i>J</i> 8.6	7.68, t <i>J</i> 7.8	6.95, d <i>J</i> 8.7
H-6''	7.55, d <i>J</i> 7.4	7.56, d <i>J</i> 8.6	7.93, d <i>J</i> 7.8	7.50, d <i>J</i> 8.7
H-α	7.24, d <i>J</i> 16.5	7.26, d <i>J</i> 16.2	7.26, d <i>J</i> 16.0	7.15, d ^[b] <i>J</i> 16.2
H-β	7.07, d <i>J</i> 16.5	7.05, d <i>J</i> 16.2	7.28-7.34, m	6.96, d ^[b] <i>J</i> 16.2
2'''-CH₃	2.19, s	2.19, s	2.19, s	– ^[c]
H-3a'''	6.18, d <i>J</i> 5.2	6.17, d <i>J</i> 5.2	6.16, d <i>J</i> 5.2	5.75, d <i>J</i> 5.4
H-5'''	4.46, ddd <i>J</i> 5.2, 2.8, 0.9	4.46, ddd <i>J</i> 5.2, 2.8, 0.9	4.47, ddd <i>J</i> 5.2, 2.3, 0.8	4.42, ddd <i>J</i> 5.4, 3.1, 0.8
H-6'''	4.97, ddd <i>J</i> 9.1, 1.8, 0.9	4.99, ddd <i>J</i> 9.8, 2.0, 0.9	4.98, ddd <i>J</i> 8.5, 2.0, 0.8	4.89, ddd <i>J</i> 9.6, 3.1, 0.8
H-7'''	5.25, t <i>J</i> 2.8	5.26, t <i>J</i> 2.8	5.25, t <i>J</i> 2.3	5.14, t <i>J</i> 2.9
H-7a'''	4.23, t <i>J</i> 5.2	4.24, t <i>J</i> 5.2	4.21, t <i>J</i> 5.2	– ^[c]
5'''-CH₂OCOCH₃	4.26-4.31, m	4.25-4.33, m	4.25-4.31, m	4.24-4.31, m
-COCH₃	2.05-2.10, m	2.05-2.07, m	2.05-2.07, m	– ^[c]
	2.13, br s	2.13, br s	2.13, br s	

[a] Compound **6d** is a mixture of *cis* and *trans* isomers. This table only contemplates the proton signals correspondent to the *trans* isomer. The full ¹H NMR data may be consulted in the sub-chapter 5.2.3. [b] Protons H-α and H-β are indistinguishable in the ¹H NMR spectrum. [c] It was not possible to identify the signals due to the resonance of these protons.

Regarding the ^{13}C NMR spectra of compounds **6a-d**, the most characteristic signals are due to the carbon resonances of the sugar moiety [as example see the ^{13}C NMR spectrum of 1-[(2*R*,3*aR*,5*R*,6*S*,7*S*,7*aR*)-6,7-diacetoxy-5-acetoxymethyl-2-methyltetrahydro-5*H*-[1,3]dioxolo[4,5-*b*]pyran-2-yl]-(*E*)-4-(4-chlorostyryl)-3-(2-hydroxyphenyl)-1*H*-pyrazole (**6b**) (Figure 2.10)].

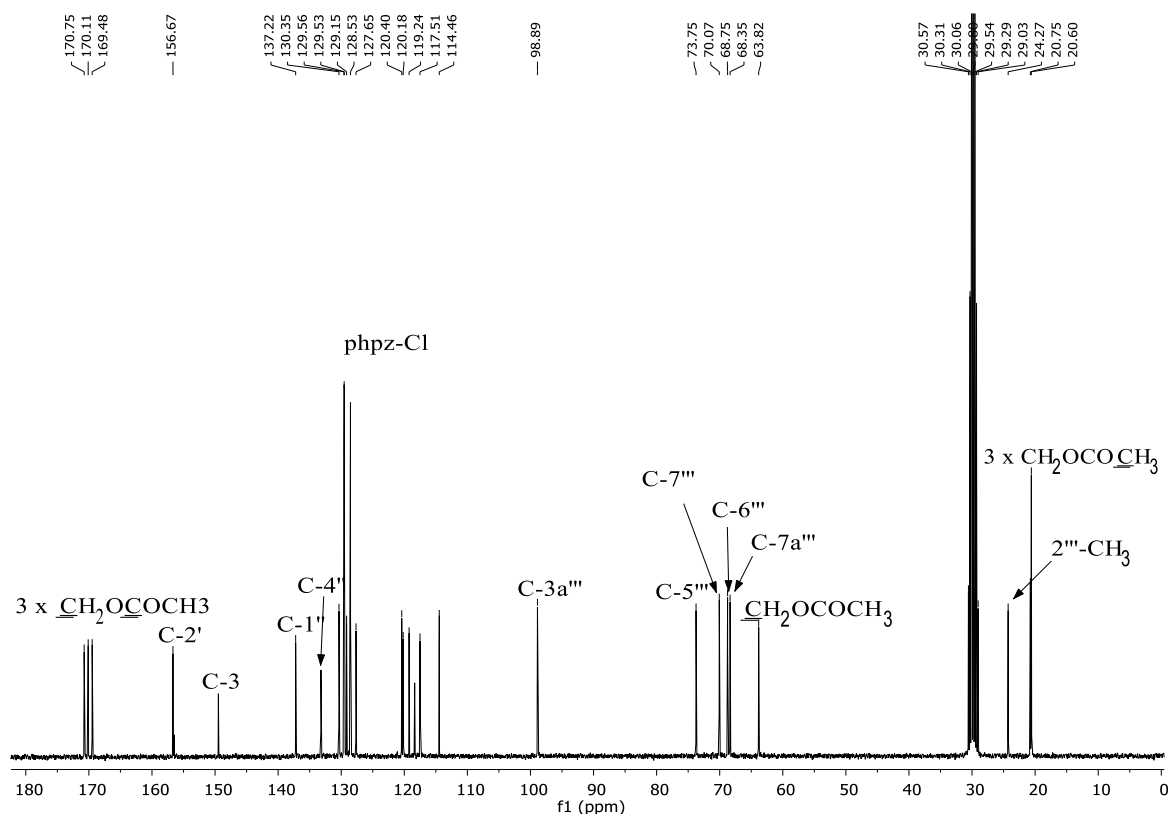
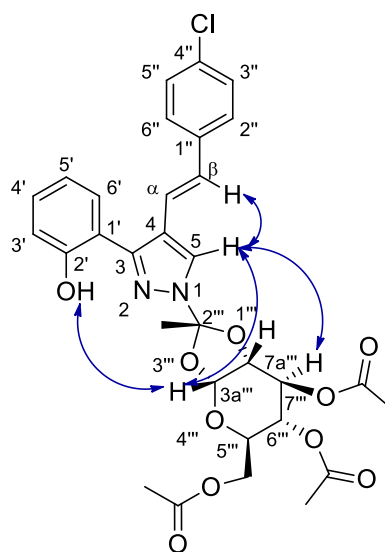


Figure 2.10 – ^{13}C NMR spectrum of 1-[(2*R*,3*aR*,5*R*,6*S*,7*S*,7*aR*)-6,7-diacetoxy-5-acetoxymethyl-2-methyltetrahydro-5*H*-[1,3]dioxolo[4,5-*b*]pyran-2-yl]-(*E*)-4-(4-chlorostyryl)-3-(2-hydroxyphenyl)-1*H*-pyrazole (**6b**) [(CD_3) $_2\text{CO}$, 75.47 MHz].

The most relevant carbon resonances corresponding to the sugar moiety are: C-3*a'''* (δ 98.9 ppm), C-5''' (δ 73.8 ppm), C-7''' (δ 70.1 ppm), C-6''' (δ 68.8 ppm), C-7*a'''* (δ 68.4 ppm), and 5'''- $\text{CH}_2\text{OCOCH}_3$ (δ 63.8 – 63.9 ppm). Notice that most of these carbon resonances appear at the same chemical shift for all derivatives **6a-d**. The resonance of C-3*a'''* appears at high frequency values since it is bounded to two oxygen atoms. Additionally, in the ^{13}C NMR spectra of compounds **6** is also usual to observe the resonances of C-2''' and 2'''- CH_3 at δ 114.5 – 114.6 ppm and δ 24.3 – 24.4 ppm, respectively. Finally, concerning the resonance of the carbons of the acetyl protecting

groups, they usually appear at δ 169.5 – 170.8 ppm for $-\underline{\text{C}}\text{OCH}_3$ and at δ 20.6 – 20.8 ppm for $-\text{CO}\underline{\text{C}}\text{H}_3$.

The 1D and 2D NMR data also demonstrated that compounds **6** are *N*-glycosylated. The NOESY correlations which reinforced the nature of the glycosidic bond will be presented in the Scheme 2.9, taking compound **6b** as example. The following correlations $2'\text{-OH} \rightarrow \text{H-3}'$ and $\text{H-3a}'''' \rightarrow \text{H-3}'$ unequivocally prove the nature of the glycosidic bond. The *N*-glycosylation is also supported by the correlation $\text{H-5} \rightarrow \text{H-3a}''''$ and $\text{H-7}''''$. Nevertheless, the presence in the ^1H NMR spectra of the signal due to the resonance of $2'\text{-OH}$ is enough to prove that the *O*-glycosylation didn't occur. The signal due to the resonance of $2'\text{-OH}$ is present in all compounds **6** at δ 9.74 – 10.12 ppm, see Table 2.3, except for compound **6c**. Still, in the NOESY spectrum of compound **6c** (not shown) it's possible to see the correlation $\text{H-5} \rightarrow \text{H-3a}''''$, which ensures that compound **6c** is *N*-glycosylated at N1 position of the pyrazole moiety. Once again, the chemical shifts of the $2'\text{-OH}$ proton (δ 9.74 – 10.12 ppm) indicate the presence of a hydrogen bond between the $2'\text{-OH}$ and the N2 atom. Since all the compounds obtained in the glycosylation of the pyrazoles **4a-d** were *N*-glycosylated, we may infer that probably due to the steric hindrance and to the existence of an intramolecular hydrogen bond between $2'\text{-OH}$ and N2 the *O*-glycosylation is more difficult to occur than the *N*-glycosylation. The stereochemistry of $\text{H-3a}''''$ and $\text{H-7a}''''$ was attributed based on the correlation observed in the NOESY spectra $\text{H-3a}'''' \rightarrow \text{H-7a}''''$, thus indicating a *cis* configuration of these two protons.



H-5 → H-3a''', H-7''', H-α, H-β

2'-OH → H-3a''', H-3'

Scheme 2.9 – Main correlations (blue arrows) observed in the NOESY spectra of compound **6b**.

2.3.4. (*E*)-1-[β-D-(glycose-1-yl)]-3-(2-hydroxyphenyl)-4-styryl-1*H*-pyrazoles

The structure of compounds **7** was established based on 1D (^1H and ^{13}C) and 2D (HSQC, HMBC, COSY and NOESY) NMR experiments. The compounds result from cleavage of the acetyl protecting groups of compounds **5a-d**, and for this the main difference in the ^1H NMR spectra of compounds **7** is the absence in the aliphatic region of the spectra of the signals ascribed to the protons of the protecting groups of the sugar moiety. As example, the ^1H NMR spectrum of (*E*)-4-(4-chlorostyryl)-1-[β-D-(glycose-1-yl)]-3-(2-hydroxyphenyl)-1*H*-pyrazole (**7b**) is given in the Figure 2.11. Also noteworthy is the presence of two doublet of doublets due to the resonance of 6''''-CH₂OH protons. The resonance of one of these protons appears at δ 3.72 – 3.73 ppm with $J = 11.9 - 12.0$, 4.8 – 5.3 Hz and the resonance due to the other proton appears at δ 3.89 ppm with $J = 11.9 - 12.0$, 1.8 – 2.2 Hz, except for compound **7d**, as seen in the Table 2.4. Since C-5'''' is a chiral center, 6''''-CH₂OH protons are diastereotopic with different chemical environment and they give separate signals. The typical signals of compounds **5** and **7** may be the same, but their chemical shift is not. The signals due to the resonance of the protons of sugar moiety of compounds **7**, are observed in their ^1H NMR spectra in the following descending order (from the highest to the lowest chemical shift): H-1'''' (δ 5.28 – 5.47 ppm), H-2'''' (δ

3.91 – 4.09 ppm), 6'''-CH₂OH protons (as already mentioned), H-3''' (δ 3.63 – 3.69 ppm), H-5''' (δ 3.47 – 3.63 ppm) and H-4''' (δ 3.42 – 3.58 ppm).

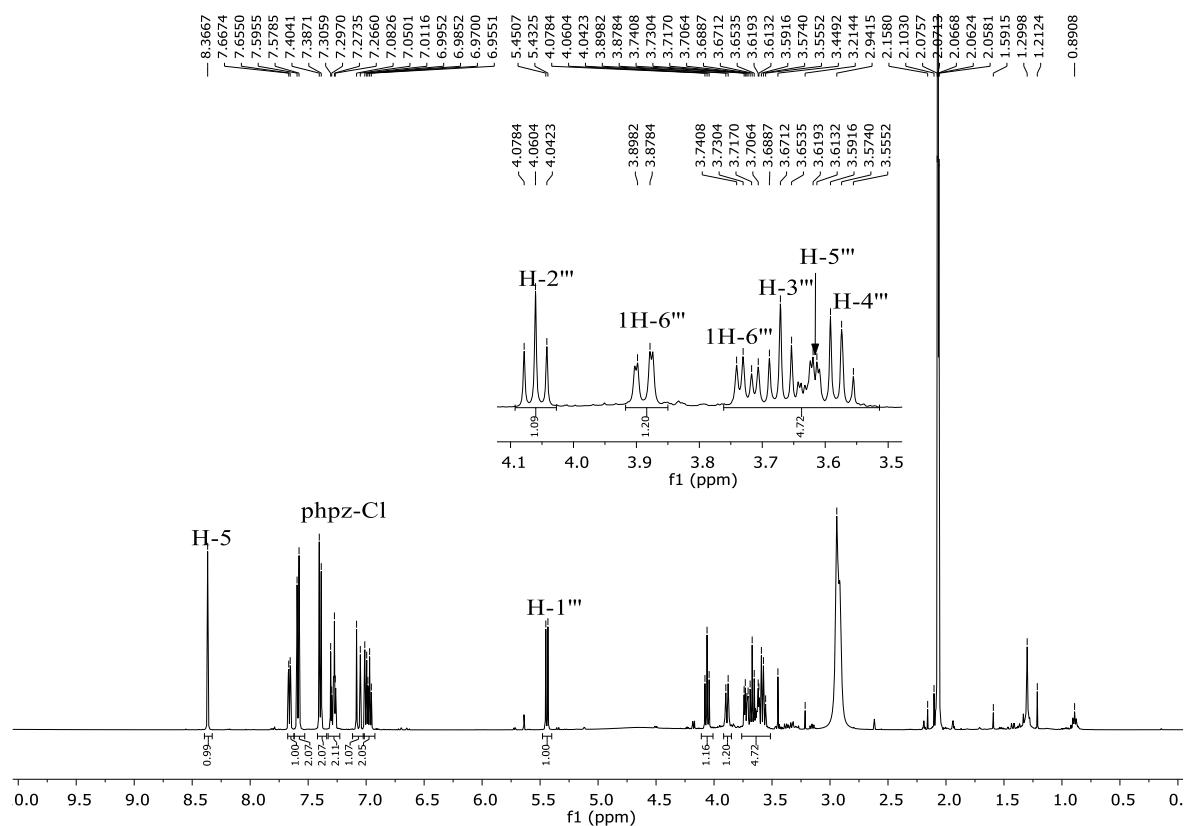


Figure 2.11 – ¹H NMR spectrum of (*E*)-4-(4-chlorostyryl)-1-[β-D-(glycose-1-yl)]-3-(2-hydroxyphenyl)-1*H*-pyrazole (**7b**) [(CD₃)₂CO, 500.16 MHz] and expansion showing the signals of the sugar moiety at δ 3.5 – 4.1 ppm.

Table 2.4 – Chemical shifts (ppm, relative to TMS) and coupling constants (*J*, Hz) of ¹H NMR of (*E*)-1-[β-D-(glycose-1-yl)]-3-(2-hydroxyphenyl)-4-styryl-1*H*-pyrazoles **7a-d**.

Compound Signal	7a	7b	7c	7d ^[a]
H-5	8.35, s	8.37, s	8.45, s	8.15, s
2'-OH	–	–	–	–
H-3'	7.00, dd <i>J</i> 8.4	7.00, dd <i>J</i> 7.8, 1.0	7.01, dd <i>J</i> 8.0, 1.0	6.82-6.86, m
H-4'	7.25-7.29, m	7.26-7.30, m	7.28, dt <i>J</i> 8.0, 7.6, 1.7	7.12, dt <i>J</i> 7.8, 1.6
H-5'	6.98, t <i>J</i> 7.6	6.97, ddd <i>J</i> 7.8, 7.5, 1.0	6.97, dt <i>J</i> 7.6, 1.0	6.82-6.86, m
H-6'	7.68, dd <i>J</i> 7.6, 1.2	7.67, dd <i>J</i> 7.8, 1.5	7.65, dd <i>J</i> 7.6, 1.7	7.54, dd <i>J</i> 7.8, 1.6
H-2''	7.56, d <i>J</i> 7.6	7.59, d <i>J</i> 8.5	–	7.36, d <i>J</i> 8.7
H-3''	7.38, t <i>J</i> 7.6	7.40, d <i>J</i> 8.5	7.75, d <i>J</i> 7.8	6.81, d <i>J</i> 8.7
H-4''	7.25-7.29, m	–	7.50, t <i>J</i> 7.8	–
H-5''	7.38, t <i>J</i> 7.6	7.40, d <i>J</i> 8.5	7.68, t <i>J</i> 7.8	6.81, d <i>J</i> 8.7
H-6''	7.56, d <i>J</i> 7.6	7.59, d <i>J</i> 8.5	7.97, d <i>J</i> 7.8	7.36, d <i>J</i> 8.7
H-α	7.25-7.29, m	7.29, d <i>J</i> 16.3	7.30-7.33, m	6.98, d <i>J</i> 16.4 ^[b]
H-β	7.07, d <i>J</i> 16.2	7.07, d <i>J</i> 16.3	7.30-7.33, m	6.86, d <i>J</i> 16.4 ^[b]
H-1'''	5.44, d <i>J</i> 9.3	5.44, d <i>J</i> 9.1	5.47, d <i>J</i> 9.1	5.28, d <i>J</i> 8.9
H-2'''	4.07, t <i>J</i> 9.3	4.06, t <i>J</i> 9.1	4.09, t <i>J</i> 9.1	3.91, t <i>J</i> 8.9
H-3'''	3.67, t <i>J</i> 9.3	3.67, t <i>J</i> 9.1	3.66, t <i>J</i> 9.1	3.63-3.69, m
H-4'''	3.58, t <i>J</i> 9.3	3.57, t <i>J</i> 9.1	3.56, t <i>J</i> 9.1	3.42, t <i>J</i> 8.9
H-5'''	3.63, ddd <i>J</i> 9.3, 4.8, 1.8	3.63, ddd <i>J</i> 9.1, 5.3, 2.2	3.62, ddd <i>J</i> 9.1, 5.3, 2.0	3.47-3.61, m
6'''-CH₂OH	3.73, dd <i>J</i> 11.9, 4.8	3.72, dd <i>J</i> 12.0, 5.3	3.72, dd <i>J</i> 12.0, 5.3	3.69-3.79, m
6'''-CH₂OH	3.89, dd <i>J</i> 11.9, 1.8	3.89, dd <i>J</i> 12.0, 2.2	3.89, dd <i>J</i> 12.0, 2.0	3.69-3.79, m

Compound **7d** is a mixture of *cis* and *trans* isomers. This table only presents the proton signals correspondent to the *trans* isomer. The full ¹H NMR data may be consulted in the sub-chapter 5.2.3. [b] Protons H-α and H-β are indistinguishable in the ¹H NMR spectrum.

The ^{13}C NMR spectra of compounds **7a-d** also confirms the removal of the protecting groups as no signals of these carbons are present. The example spectrum of compound **7b** is presented in the Figure 2.12. Besides this feature, there are no other significant changes in the ^{13}C NMR spectra. The 6'''-CH₂OH protons were assigned as diastereotopic through the HSQC correlations. The two distinct proton resonances corresponding to 6'''-CH₂OH protons were both correlated to the C-6''' in the HSQC spectrum, which allowed their unequivocal identification.

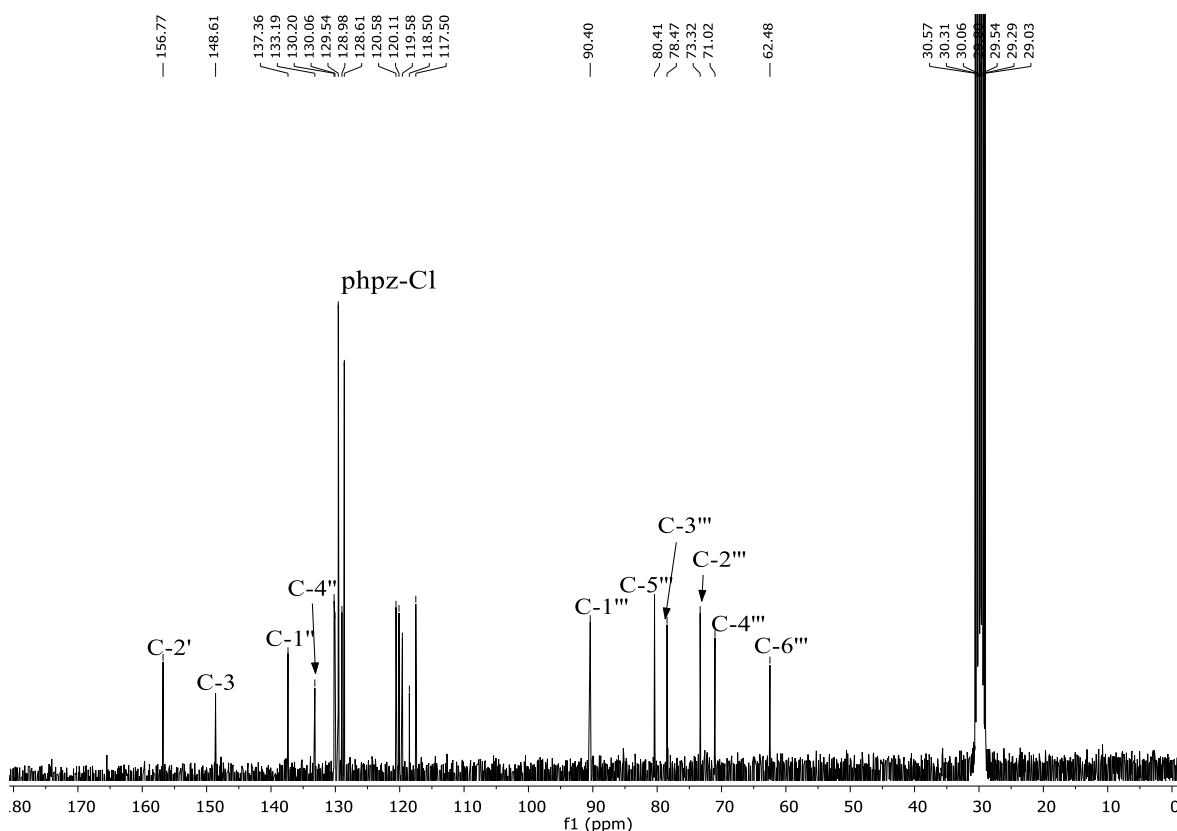


Figure 2.12 – ^{13}C NMR spectrum of (*E*)-4-(4-chlorostyryl)-1-[β -D-(glycose-1-yl)]-3-(2-hydroxyphenyl)-1*H*-pyrazole (**7b**) [(CD₃)₂CO, 75.47 MHz].

2.3.5. 1-[(2*R*,3*aR*,5*R*,6*S*,7*S*,7*aR*)-6,7-dihydroxy-5-hydroxymethyl-2-methyltetrahydro-5*H*-[1,3]dioxolo[4,5-*b*]pyran-2-yl]-(*E*)-3-(2-hydroxyphenyl)-4-styryl-1*H*-pyrazoles

The structure of compounds **8a,b** was determined based on 1D (^1H and ^{13}C) and 2D (HMBC, HSQC and NOESY) NMR experiments. Compounds **8a,b** were obtained from compound **6a** and compound **6c** by cleavage of the acetyl protecting groups. Thus the main

characteristic in the ^1H NMR spectra of compounds **8a,b** is the absence of the signals due to the resonance of the protons of the acetyl protecting groups, in the aliphatic region of the spectra (see as example, the spectrum of (*E*)-4-(4-chlorostyryl)-1-[(2*R*,3*aR*,5*R*,6*S*,7*S*,7*aR*)-6,7-dihydroxy-5-hydroxymethyl-2-methyltetrahydro-5*H*-[1,3]dioxolo[4,5-*b*]pyran-2-yl]-3-(2-hydroxyphenyl)-1*H*-pyrazole (**8b**) in the Figure 2.13).

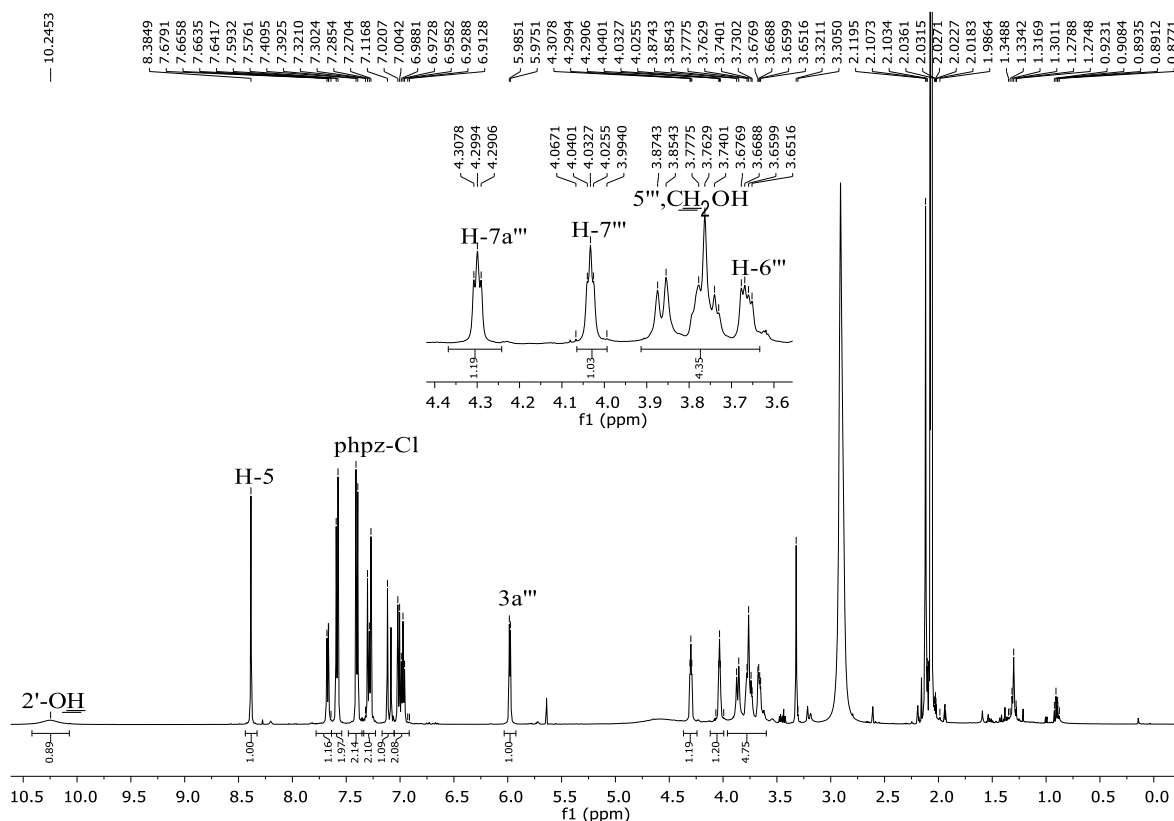


Figure 2.13 – ^1H NMR spectrum of (*E*)-4-(4-chlorostyryl)-1-[(2*R*,3*aR*,5*R*,6*S*,7*S*,7*aR*)-6,7-dihydroxy-5-hydroxymethyl-2-methyltetrahydro-5*H*-[1,3]dioxolo[4,5-*b*]pyran-2-yl]-3-(2-hydroxyphenyl)-1*H*-pyrazole (**8b**) [(CD_3) $_2$ CO, 500.16 MHz].

Regarding the other signals there are some changes when compared to compounds **6a-d**. The signals due to the resonance of protons of the sugar appear at different chemical shifts when comparing compounds **6a-d** and **8a,b** (see Table 2.5). In the case of compounds **8a-d** the signals appear in the following order (from the highest to the lowest chemical shift): H-3a''' (δ 5.97 – 5.98 ppm), H-7a''' (δ 4.30 – 4.31 ppm), H-7''' (δ 4.03 ppm), H-5''' (δ 3.73 – 3.78 ppm), 5'''-CH $_2$ OH (δ 3.86 ppm), 5'''-CH $_2$ OH (δ 3.73 – 3.78 ppm) and H-6''' (δ 3.66 ppm), as seen in the Table 2.5. Notice that protons 5'''-CH $_2$ OH are diastereotopic and therefore appear at different chemical shifts.

Table 2.5 – Chemical shifts (ppm, relative to TMS) and coupling constants (*J*, Hz) of ¹H NMR of 1-[(2*R*,3*aR*,5*R*,6*S*,7*S*,7*aR*)-6,7-dihydroxy-5-hydroxymethyl-2-methyltetrahydro-5*H*-[1,3]dioxolo[4,5-*b*]pyran-2-yl]-(*E*)-3-(2-hydroxyphenyl)-4-styryl-1*H*-pyrazoles **8a,b**.

Signal	Compound	
	8a	8b
H-5	8.38, s	8.43, s
2'-OH	10.25, br s	–
H-3'	7.01, d <i>J</i> 8.3	7.02, dd <i>J</i> 8.2, 1.1
H-4'	7.27-7.30, m	7.27-7.37, m
H-5'	6.97, t <i>J</i> 7.6	6.96, ddd <i>J</i> 7.5, 7.7, 1.1
H-6'	7.67, dd <i>J</i> 7.6, 1.1	7.64, dd <i>J</i> 7.7, 1.6
H-2''	7.58, d <i>J</i> 8.5	–
H-3''	7.40, d <i>J</i> 8.5	7.75, d <i>J</i> 7.8
H-4''	–	7.50, t <i>J</i> 7.8
H-5''	7.40, d <i>J</i> 8.5	7.68, t <i>J</i> 7.8
H-6''	7.58, d <i>J</i> 8.5	7.95, d <i>J</i> 7.8
H-α	7.29, d <i>J</i> 16.1	7.31, d <i>J</i> 16.0
H-β	7.10, d <i>J</i> 16.1	7.30, d <i>J</i> 16.0
2'''-CH₃	2.19, s	2.13, s
H-3a'''	5.98, d <i>J</i> 4.6	5.97, d <i>J</i> 4.8
H-5'''	3.73-3.78, m	3.78, dd <i>J</i> 5.6, 2.3
H-6'''	3.66, dd <i>J</i> 8.5, 3.9	3.66, dd <i>J</i> 8.9, 4.4
H-7'''	4.03, t <i>J</i> 3.9	4.03, t <i>J</i> 4.4
H-7a'''	4.30, t <i>J</i> 4.6	4.31, t 4.8 Hz
5'''-CH₂OH	3.86, d, <i>J</i> 10.0	3.86, dd <i>J</i> 11.2, 2.3
5'''-CH₂OH	3.73-3.78, m	3.73, t <i>J</i> 5.6

The ^{13}C NMR data confirms the removal of the protecting groups. As example, see the spectrum of (*E*)-4-(4-chlorostyryl)-1-[(2*R*,3*aR*,5*R*,6*S*,7*S*,7*aR*)-6,7-dihydroxy-5-hydroxymethyl-2-methyltetrahydro-5*H*-[1,3]dioxolo[4,5-*b*]pyran-2-yl]-3-(2-hydroxyphenyl)-1*H*-pyrazole (**8b**) in the Figure 2.14. Additionally, it's possible to perceive that the signals due to the carbon resonances of the sugar moiety are different when compared to compounds **6a-d**. These signals appear in the spectra of compounds **8a,b** from the highest to the lowest chemical shift as: C-3a''' (δ 99.5 – 99.6 ppm), C-7a''' (δ 78.2 – 78.3 ppm), C-5''' (δ 74.9 ppm), C-7''' (δ 73.7 – 73.8 ppm), C-6''' (δ 70.4 ppm) and 5'''-CH₂OH (δ 63.0 ppm). There are no other significant changes in the ^{13}C NMR spectra of compounds **8a,b** when compared to those of compounds **6a-d**.

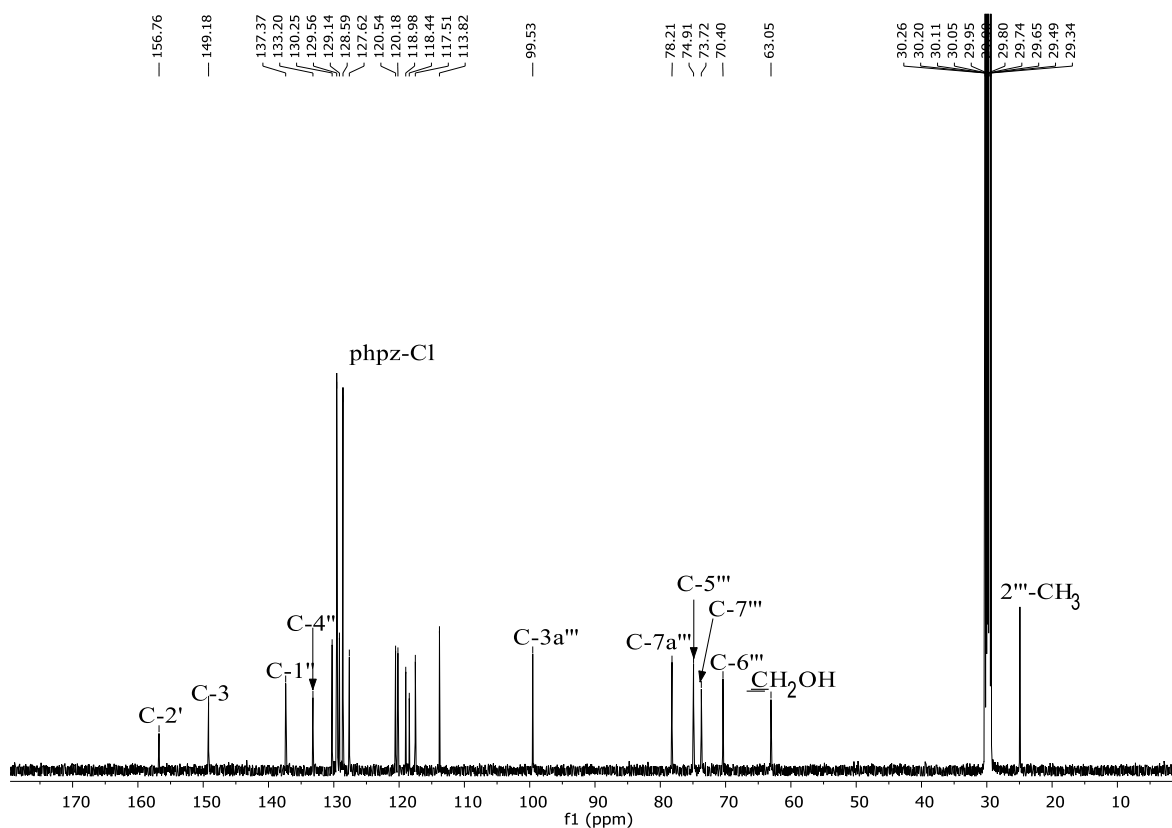


Figure 2.14 – ^{13}C NMR spectrum of (*E*)-4-(4-chlorostyryl)-1-[(2*R*,3*aR*,5*R*,6*S*,7*S*,7*aR*)-6,7-dihydroxy-5-hydroxymethyl-2-methyltetrahydro-5*H*-[1,3]dioxolo[4,5-*b*]pyran-2-yl]-3-(2-hydroxyphenyl)-1*H*-pyrazole (**8b**) [(CD₃)₂CO, 75.47 MHz].

Chapter 3

Synthesis of ruthenium complexes with pyrazoles

3.1. Nomenclature adopted for the ruthenium-pyrazole complexes

The nomenclature adopted for the novel complexes $[\text{Ru}([\text{9}]\text{aneS}_3)((E)\text{-3(5)-(2-hydroxyphenyl)-4-(2-/4-Rstyryl)-1H-pyrazole})(\text{DMSO})\text{Cl}]\text{Cl}$ does not follow the IUPAC rules. The structure of these compounds and the respective carbon numbering system may be consulted in the Figure 3.1. The nomenclature and numbering system for the pyrazole scaffold follows the rationale described in the sub-chapter 2.1.2.

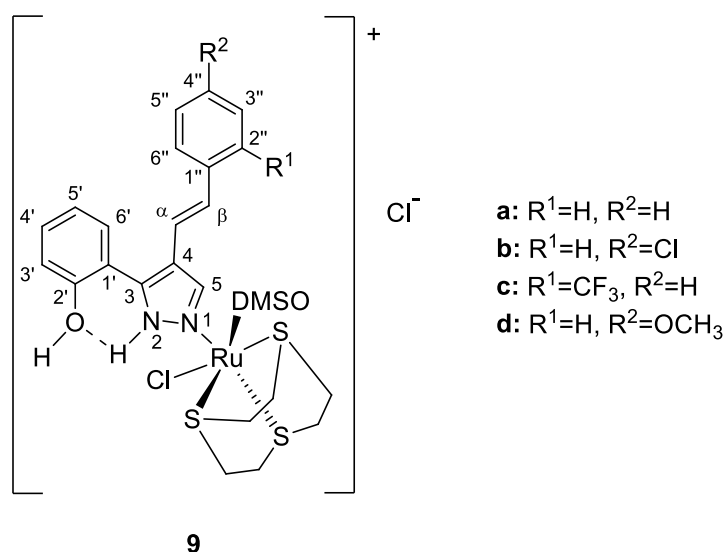
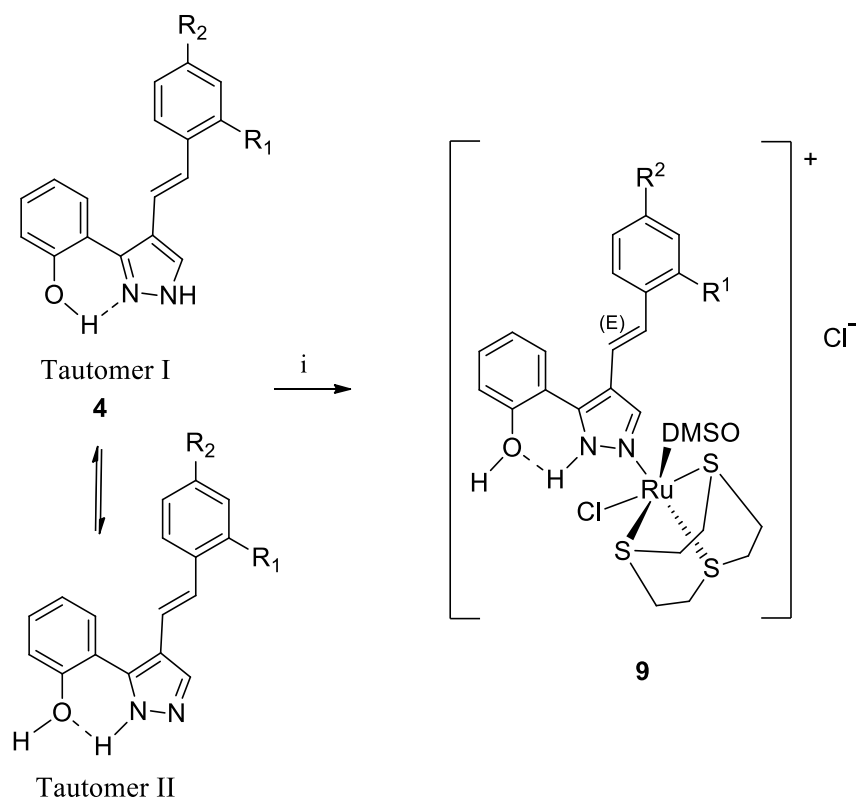


Figure 3.1 – Structure and atom numbering for the complexes with the general formula $[\text{Ru}([\text{9}]\text{aneS}_3)((E)\text{-3(5)-(2-hydroxyphenyl)-4-(2-/4-R-styryl)-1H-pyrazole})(\text{DMSO})\text{Cl}]\text{Cl}$. The stereochemistry presented here is merely representative.

3.2. Preparation of the complexes

The complexes were obtained by adapting the procedure of Marques *et al* (see Scheme 3.1).²⁰ Briefly, the precursor $\text{Ru}([\text{9}]\text{aneS}_3)(\text{DMSO})\text{Cl}_2$ is allowed to react with the compounds **4a-4d** in refluxing methanol, under a nitrogen atmosphere, for 18h.



a: R¹=H, R²=H (30%); **b:** R¹=H, R²=Cl (72%); **c:** R¹=CF₃, R²=H (51%); **d:** R¹=H, R²=OCH₃

(i) Reagents and conditions: Ru([9]aneS₃)(DMSO)Cl₂ (0.8 equiv.), MeOH, 60 °C, 18h.

Scheme 3.1 – Complexation of the free pyrazole derivatives **4a-d** with Ru([9]aneS₃)(DMSO)Cl₂. The prototropy effect in **4a-d** is also depicted. The stereochemistry presented here is merely representative.

3.3. Structural characterization of the ruthenium-pyrazole complexes

The structural characterization of the family of complexes **9** was performed by NMR, namely 1D (¹H and ¹³C) and 2D (HMBC, HSQC and NOESY) techniques, infrared, mass spectrometry and elemental analysis. Typically, the spectra of the complexes present a set of signals ascribed to the resonance of the protons of the macrocycle, [9]aneS₃, as well as those of the corresponding pyrazole ligand and of DMSO, that remained in the coordination sphere. As an example, the spectrum of the complex [Ru([9]aneS₃)(*E*)-4-(4-chlorostyryl)-3(5)-(2-hydroxyphenyl)-1*H*-pyrazole)(DMSO)Cl]Cl (**9b**) is presented in the Figure 3.2. Some protons present two signals, indicating the presence of non-equivalent stereochemistry around the ruthenium coordination sphere. This is observed for the signals corresponding of the NH, 2'-OH and H-5 protons. Note also that the intensities of the

mentioned signals are different, indicating that one of the species is predominant over the other. The NH , $2'\text{-OH}$ and H-5 signals at δ 12.90 – 13.09, 10.80 – 10.90 and 8.26 – 8.30 ppm, respectively, are attributed to the most abundant ruthenium complex (see Table 3.1). Therefore, the NH , $2'\text{-OH}$, H-5 resonance signals at δ 12.85 – 13.10, 10.58 – 10.65 and 8.24 – 8.34 ppm, respectively, are attributed to the less abundant ruthenium complex. Herein only the signals of the most abundant species will be presented, for simplicity of the discussion. The remaining data and its attribution can be consulted in the sub-chapter 5.2.5.

For the protons of the pyrazole ligand, it is possible to determine a coupling constant between H- α and H- β ranging between $J = 15.8 - 16.3$ Hz, thus indicating that the vinylic system retained the *trans* configuration. Regarding the typical resonance signals of the [9]aneS₃ macrocycle, they appear as a multiplet at δ 2.57 – 2.88 ppm. The integration of the ¹H NMR signals of [9]aneS₃ tallies well with the expected 12 protons. Next to the [9]aneS₃ resonances there is a multiplet at δ 2.88 – 3.14 ppm corresponding to six DMSO proton resonances.

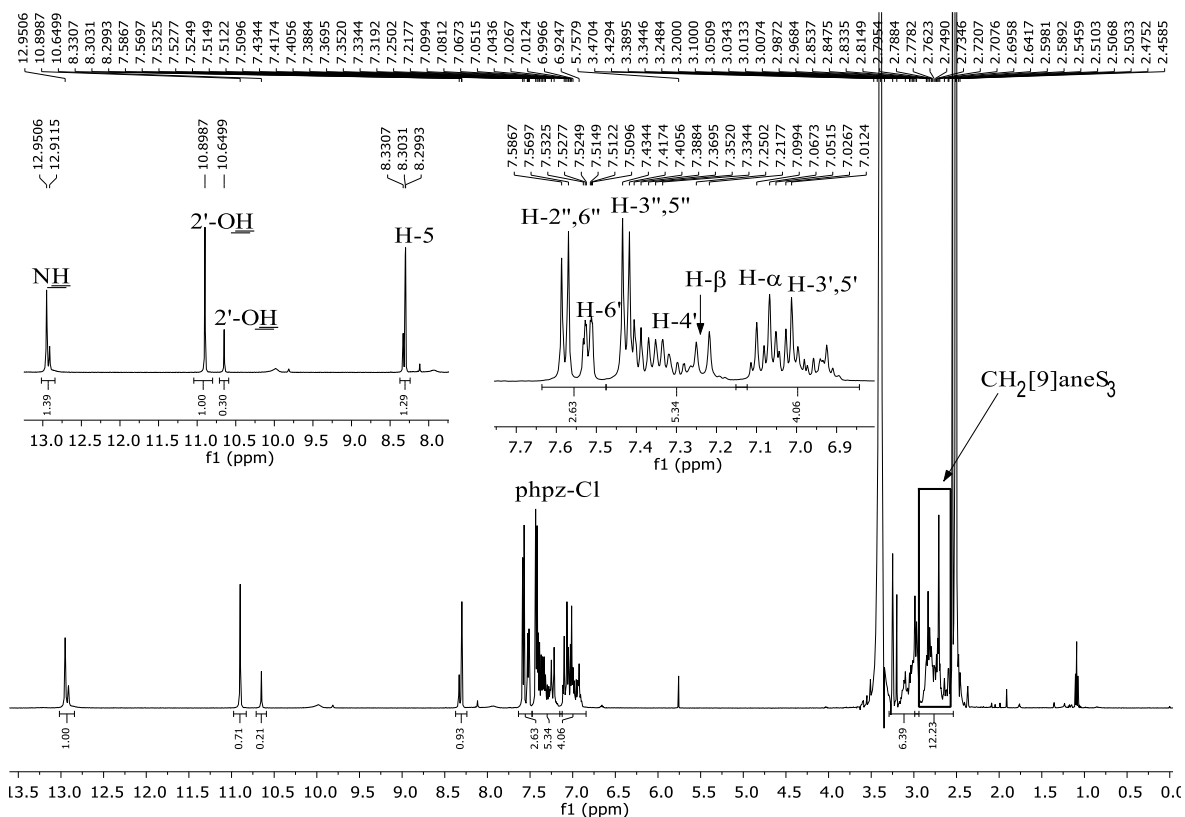


Figure 3.2 – ¹H NMR spectrum of [Ru([9]aneS₃)(*E*)-4-(4-chlorostyryl)-3(5)-(2-hydroxyphenyl)-1H-pyrazole)(DMSO)Cl]Cl (**9b**) (DMSO-D₆, 500.16 MHz).

Table 3.1 – Chemical shifts (ppm, relative to TMS) and coupling constants (J , Hz) of ^1H NMR of $[\text{Ru}(\text{[9]aneS}_3)((E)\text{-3(5)-(2-hydroxyphenyl)-4-styryl-1H-pyrazole})(\text{DMSO})\text{Cl}]\text{Cl}$ **9a-d**. Only the most abundant signals are presented here.

Compound Signal	9a	9b	9c	9d
NH	12.93, s	12.95, s	13.09, s	12.90, s
2'-OH	10.90, s	10.90, s	10.80, s	10.90, s
H-5	8.29, d J 2.0	8.30, d J 1.9	8.30, d J 1.9	8.26, d J 1.9
H-3'	7.07-7.08, m	7.04-7.11, m	7.06-7.07, m	7.06, d J 7.9
H-4'	7.19-7.31, m	7.26-7.41, m	7.30-7.36, m	7.32, ddd J 7.9, 7.8, 1.3
H-5'	7.00-7.05, m	7.01, t J 7.6	6.98, t J 7.5	6.99-7.05, m
H-6'	7.52, dd J 7.8, 1.6	7.51, dd J 7.6, 1.4	7.46, d J 7.5	7.53, dd J 7.8, 1.3
H-2''	7.55, d J 7.6	7.57, d J 8.5	–	7.49, d J 8.8
H-3''	7.38, t J 7.6	7.43, d J 8.5	7.73, d J 7.7	6.95, d J 8.8
H-4''	7.19-7.31, m	–	7.49, t J 7.7	–
H-5''	7.38, t J 7.6	7.43, d J 8.5	7.67, t J 7.7	6.95, d J 8.8
H-6''	7.55, d J 7.6	7.58, d J 8.5	7.89, d J 7.7	7.49, d J 8.8
H-α	7.03, d J 16.2	7.08, d J 16.2	7.10, d J 15.8	6.84, d J 16.3
H-β	7.10, d J 16.2	7.23, d J 16.2	7.03, d J 15.8	7.17, d J 16.3
Ru[9]aneS₃	2.57-2.85, m	2.59-2.88, m	2.59-2.86, m	2.59-2.87, m
Ru-DMSO	2.95-3.06, m	2.91-3.10, m	2.88-3.04, m	2.95-3.14, m

The ^{13}C NMR spectra of the complexes also presents resonances in two well defined regions: δ 30.1 – 35.2 ppm for the [9]aneS₃ carbon resonances and δ 114.0 – 158.9 ppm for the pyrazole ligand resonances. An example is the spectrum of complex **9b** depicted in the Figure 3.3. Some carbon atoms also give rise to two signals (same as observed for the proton resonances), which is attributed to the presence of two non-equivalent geometries.

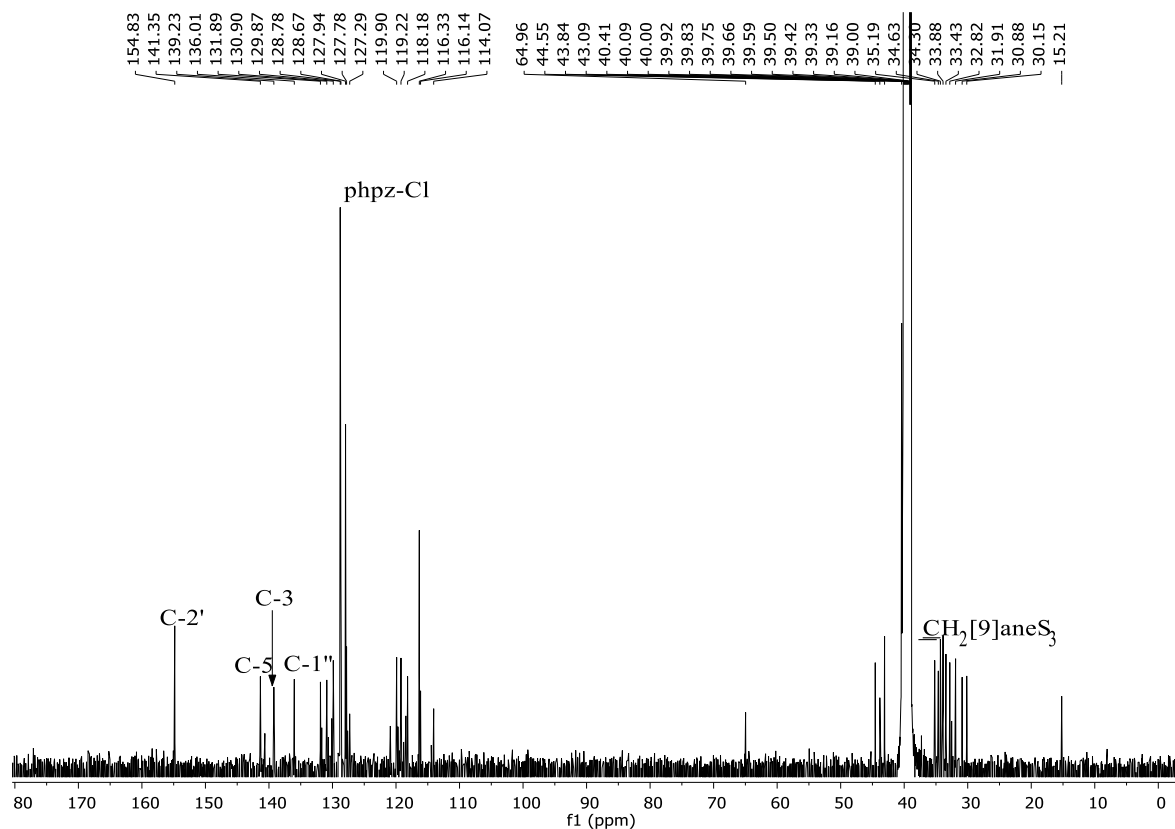


Figure 3.3 – ^{13}C NMR spectrum (DMSO- D_6 , 500.16 MHz) of $[\text{Ru}([\text{9}] \text{aneS}_3)((E)\text{-4-(4-chlorostyryl)-3(5)-(2-hydroxyphenyl)-1H-pyrazole)(DMSO)Cl]Cl$ (**9b**).

The NOESY correlation $2'\text{-OH} \rightarrow \text{NH}$ allows inferring the *N*-coordination of compounds **4** to the ruthenium centre. This correlation implies that the ligand coordination occurred at the N1 of the pyrazole ring (as depicted in Scheme 3.1). Had the coordination taken place at the adjacent N, this correlation would not be visible, because, to avoid steric hindrance, the phenol ring would rotate to have the $2'\text{-OH}$ away from the pyrazole and thus it would not be able to correlate with NH . This correlation is also indicative of the coordination of compounds **4a-d** to the ruthenium centre in a monodentate fashion at the N1 of the pyrazole moiety.

3.4. Mass spectrometry of the ruthenium-pyrazole complexes

The mass spectrometry results corroborate the theoretical predictions. Recall that these complexes are already positively charged, so the most intense peak in the mass spectrometry spectra is supposed to match the value of their theoretical exact mass. The ESI-MS data of compound **9a** shows the molecular cation as the most intense peak, at 657.1 m/z , which tallies well with the theoretical mass of 657. Regarding compound **9b**,

two intense peaks are present in its mass spectrometry spectrum. Since this compound has a chlorine atom, the two isotopes ^{35}Cl and ^{37}Cl may occur. The base peak at 693.0 m/z corresponds to the complex **9b** with the isotope ^{37}Cl and the peak with a slightly lower intensity at 691.0 m/z corresponds to the complex **9b** with the isotope ^{35}Cl . These results are in agreement with the theoretical exact mass of complex **9b** of 691.0. For complex **9c**, there is a base peak at 725.0 m/z, which matches with its exact mass of 725.0. Finally, complex **9d** mass spectrometry spectrum has a base peak at 687.1 m/z, which matches its exact mass of 687.1. The mass spectrometry analysis also allowed to confirm that the ruthenium coordination occurred by replacement of one chloride rather than the DMSO.

3.5. Fourier-transform infrared of the ruthenium-pyrazole complexes

The attribution of the bands associated with the pyrazole ligands was made with base on the report by Krishnakumar *et al*⁹⁷ (details in sub-chapter 5.2.2). The $\omega\text{C}\alpha=\text{C}\beta$ vibration, occurring at 960 – 966 cm^{-1} in compounds **4a-d**, appear in the 965 – 967 cm^{-1} region in the spectra of complexes **9a-d**, that is, this band is practically unshifted and it further indicates that the *trans* configuration of the vinylic system⁹⁸ was not altered upon coordination. The $\nu\text{C}=\text{C}$ stretching bands of the aromatic groups of the ligand, including pyrazole and aryl groups, are somewhat overlapped; nevertheless, a band at 1605 – 1639 cm^{-1} corresponding to the $\nu\text{C}=\text{N}$ vibration allows to confirm the presence of this ligand in the complexes. The spectra of the complexes **9a-d** also present, as expected, several vibrations associated with the macrocycle, such as the $\nu\text{C}-\text{H}$ vibration at 2961 – 2966 (except for complex **9c**), the $\nu\text{C}-\text{H}$ vibration at 2921 – 2926 and the $\rho\text{C}-\text{H}$ vibration at 908 – 910 cm^{-1} . The infrared spectra of complexes **9a-d** also present bands corresponding to the $\rho\text{C}-\text{H}_{(\text{DMSO})}$ vibrations at 908 – 910 cm^{-1} and 822 – 829 cm^{-1} . Complexes **9b** and **9d** infrared spectrum also present the $\nu\text{Ru}-\text{S}_{(\text{macrocycle})}$ vibration at 455 – 457 cm^{-1} . This vibration is also verified for complexes **9a** and **9d** at 493 cm^{-1} . Notice that complex **9c** didn't display any bands corresponding to the $\text{Ru}-\text{S}_{(\text{macrocycle})}$ vibration. Complexes **9a-d** display the $\nu\text{Ru}-\text{S}_{(\text{DMSO})}$ vibration at 424 – 425 cm^{-1} which in parallel with the $\rho\text{C}-\text{H}_{(\text{DMSO})}$ vibrations reassure the presence of DMSO in the ruthenium sphere. At last, the $\nu\text{Ru}-\text{N}$ stretching band is observed in the 373 – 377 cm^{-1} region, thus confirming the Ru coordination.

Chapter 4

Biological assays

The compounds **4a-d**, **7a-c**, **8a,b** and complexes **9a-d** were tested against the AGS cancer cell line. Compounds **4a-d**, **7b,c**, **8a,b** and **9d** were tested against the MRC-5 cell line. The results are discussed below. For experimental details refer to the sub-chapter 5.2.6.

4.1.1. AGS cancer cell line

The concentrations of the tested compounds were adjusted according to their activity. The compounds were initially tested at concentrations of 1:4 (0.39, 1.56, 6.25, 25 and 100 μM), however, in some cases these concentrations were not the most indicated to the IC_{50} calculation. Throughout this work it was clear that concentrations of 1:2 (6.25, 12.5, 25, 50 and 100 μM) fitted better the cytotoxic activity results of the tested compounds since they often presented IC_{50} values around 50 – 100 μM . Consequently, there are compounds tested in the 0.39 – 100 μM range and others tested in the 6.25 – 100 μM range. The attained cell viability results may be consulted in the Figure 4.1 and the general structure of the tested compounds and their corresponding IC_{50} values may be consulted in the Table 4.1.

Concerning compounds **4a-d**, the *-para*-Cl substituted compound **4b** is the only one to present a measurable IC_{50} under 100 μM , with an IC_{50} of 37 μM . Yet, even though the *-ortho*- CF_3 substituted compound **4c** has $\text{IC}_{50} > 100 \mu\text{M}$, it was more active than the non-substituted compound **4a** and the *-para*- OCH_3 substituted compound **4d**. Compounds **4a** and **4d** revealed to be inefficient against the AGS cancer cell line.

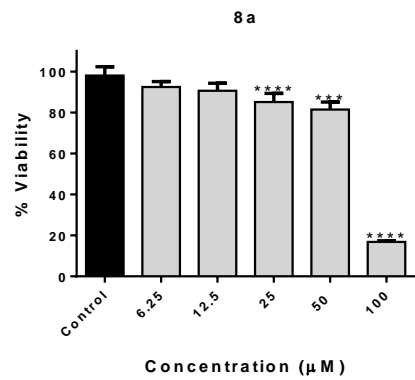
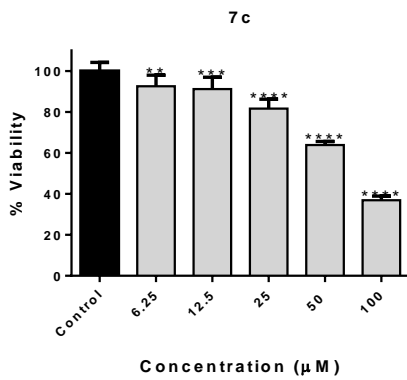
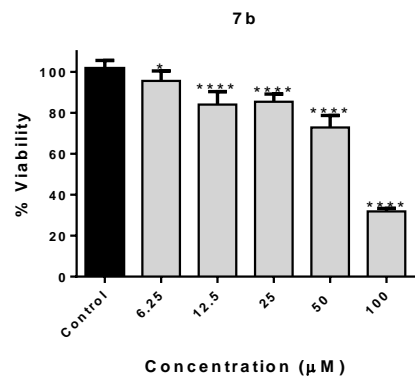
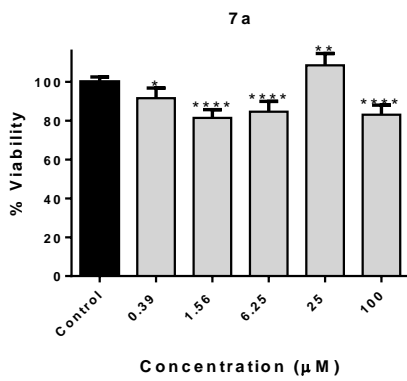
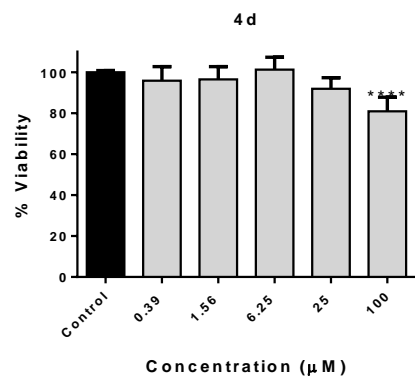
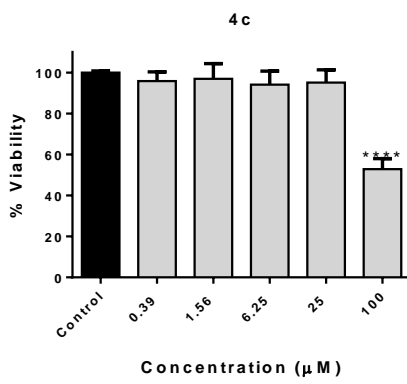
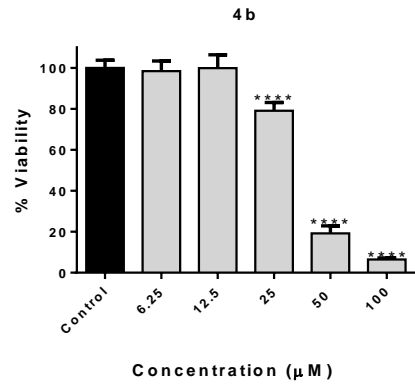
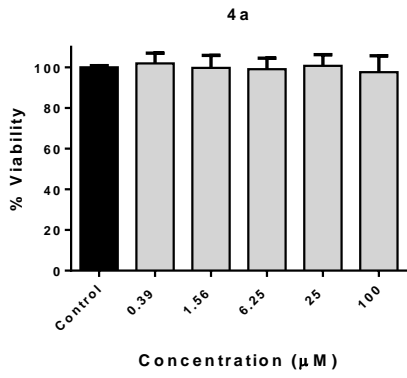
For compounds **7a-c** it's not possible to discuss the electron-donating group effect since these compounds are either non-substituted (**7a**), halogen substituted (**7b**) or substituted with an electron-withdrawing group in the phenyl ring (**7c**). The non-substitution of the phenyl ring had no benefit in the cytotoxic activity. In fact, at the concentration of 25 μM , compound **7a** appears to promote AGS cancer cells' metabolism. To inspect whether compound **7a** triggers cancer cells metabolism or proliferation at this concentration, in the future it is advisable to perform a Sulforhodamine B assay.⁹⁹ Regarding compounds **7b** and **7c**, their IC_{50} is quite similar (78.8 and 73.0 μM , respectively). Notice that the insertion of the $\text{R}^3 = \text{Glc}$ improved compound's **7c** IC_{50} when compared to its precursor, compound **4c**. However, the IC_{50} of **7b** is worse than its precursor, compound **4b**. Further studies should be conducted to understand if the insertion

of the $R^3 = \text{Glc}$ group is a good strategy for the enhancement of the *in vitro* cytotoxic activity.

Regarding compounds **8a,b**, compound **8a** afforded a poorer IC_{50} (74.2 μM) than its precursor, compound **4b**. Since compounds **7b** and **8a** revealed to be less potent than compound **4b**, the insertion of a glucose unit in the *-para*-Cl substituted compound **4b** doesn't seem to be beneficial for its cytotoxic activity. Still, the *-ortho*- CF_3 substituted compound **8b** disclosed an IC_{50} value of 41.3 μM and thus, it was more potent than its precursor, **4c**, which didn't present a measurable IC_{50} below 100 μM . Also, compound **8b** IC_{50} value was better than the other *-ortho*- CF_3 substituted compound, **7c**. So, in the case of *-ortho*- CF_3 substituted compounds, the insertion of $R^3 = \text{Dx}$ is better than the insertion of $R^3 = \text{Glc}$. Altogether, it's possible to verify that the insertion a sugar moiety ($R^3 = \text{Dx}$ or Glc) improves the cytotoxic activity of the *-ortho*- CF_3 substituted compounds **7c** and **8b**, when compared to **4c**, and jeopardizes the cytotoxic activity of the *-para*-Cl substituted compounds **7b** and **8a** when compared to **4b**. Due to these results, with would be interesting to study the cytotoxic activity of *-para*- CF_3 and *-ortho*-Cl substituted compounds.

The ruthenium complexes, **9a-d** comprise the most potent compound in the present study. Even though the non-substituted (**9a**), the halogen substituted (**9b**) and the electron-withdrawing substituted (**9c**) compounds did not afford cytotoxic activity below 100 μM , the *-para*- OCH_3 substituted compound (**9d**) presented an IC_{50} value of 18.3 μM . Note that the literature describes good inhibitory action for another ruthenium trithiacyclononane complex with a parent ligand, 3-(2-hydroxy)-phenyl-5-R-styryl pyrazole, in which the R-substituent was precisely a methoxyl group in the *-para* position of the aromatic ring of styryl.²⁰ This suggests that, when coordinated with $\text{Ru}([\text{9}]aneS_3)$, disubstituted pyrazoles bearing *-para*- OCH_3 groups promote a better cytotoxic activity *in vitro*. In the future it would be pertinent to study the effect of other electron-donating groups in the cytotoxic activity of $\text{Ru} [\text{9}]aneS_3$ complexes with disubstituted pyrazoles of the same family.

Cytotoxicity against AGS



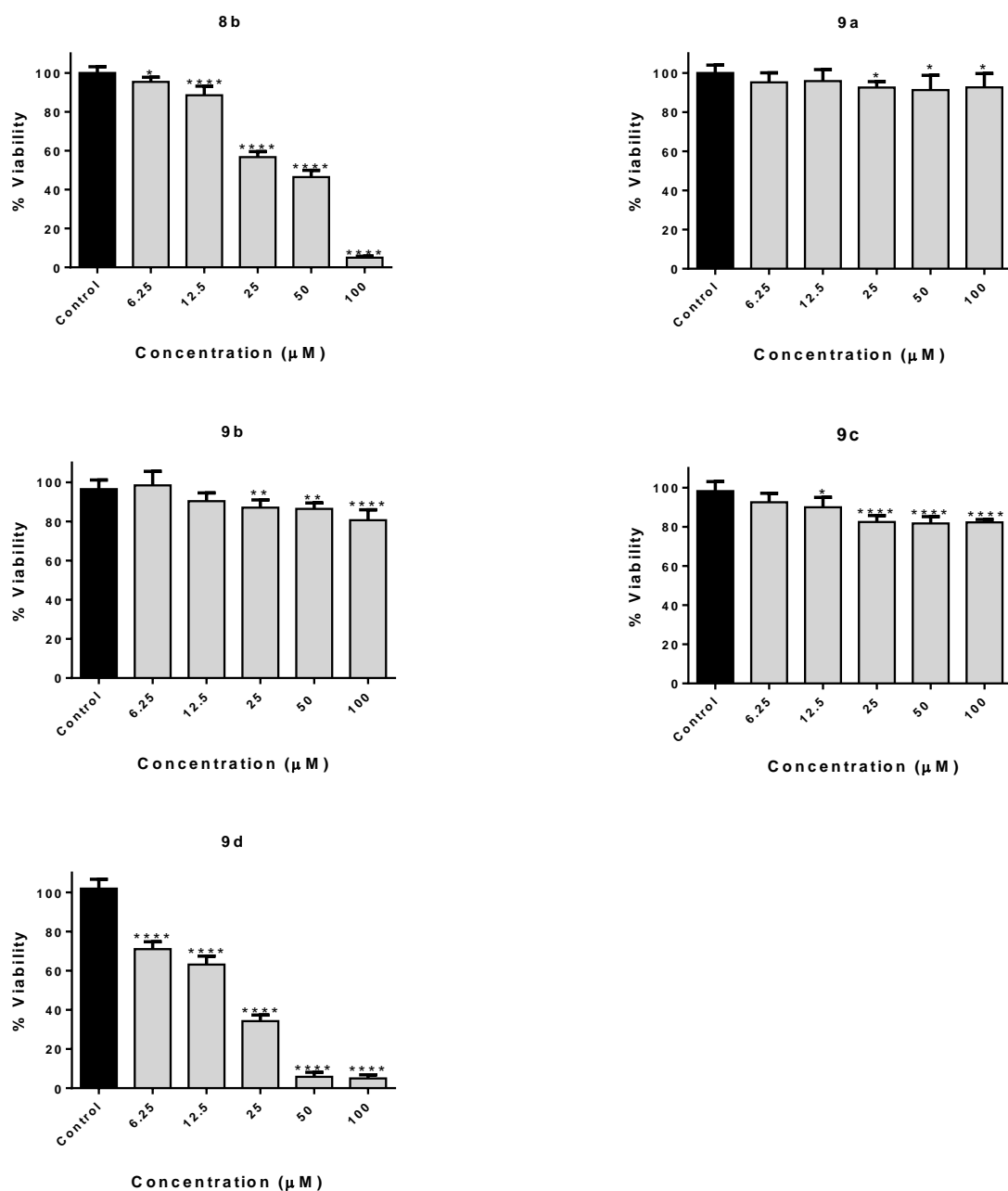
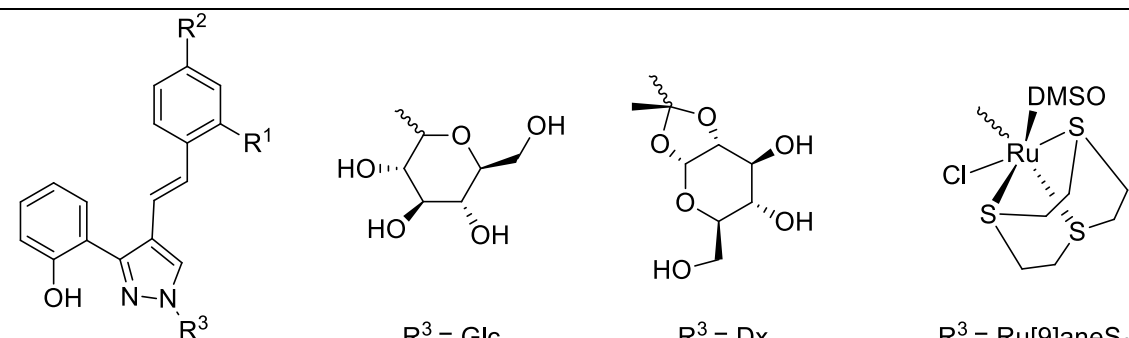


Figure 4.1 – Cytotoxic effect of compounds **4a-d**, **7a-c**, **8a,b** and **9a-d** against the AGS cancer cell line. The cells were incubated with five different concentrations of these compounds for 24h. The data is expressed as % of viability and represents the mean \pm mean standard deviation from three to four independent experiments run in triplicate. * denotes p -value < 0.05 , ** denotes p -value < 0.01 , *** denotes p -value < 0.001 and **** denotes p -value < 0.0001 .

Table 4.1 – Structural representation and cytotoxic activity of compounds **4a-d**, **7a-c**, **8a,b** and **9a-d** against the AGS cancer cell line. The results are expressed as IC₅₀ (μM).

Compound				
	R ¹	R ²	R ³	IC ₅₀ AGS
4a	H	H	H	>100
4b	H	Cl	H	37.0
4c	CF ₃	H	H	>100
4d	H	OCH ₃	H	>100
7a	H	H	Glc	>100
7b	H	Cl	Glc	78.8
7c	CF ₃	H	Glc	73.0
8a	H	Cl	Dx	74.2
8b	CF ₃	H	Dx	41.3
9a	H	H	Ru[9]aneS ₃	>100
9b	H	Cl	Ru[9]aneS ₃	>100
9c	CF ₃	H	Ru[9]aneS ₃	>100
9d	H	OCH ₃	Ru[9]aneS ₃	18.3

4.1.2. MRC-5 cell line

Due to the slow proliferation rate of the MRC-5 cell line, it wasn't possible to test all the compounds against this cell line (see Figure 4.2).

Compounds **4a-d** afforded measurable IC₅₀ values under 100 μM when tested against the MRC-5 cell line (see Table 4.1). With exception of compound **4b**, this set of compounds showed higher cytotoxicity against the MRC-5 than AGS cell line. Even though compound **4b** presented a better cytotoxic action against the AGS cell line than

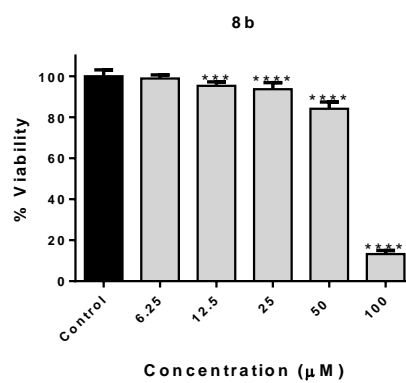
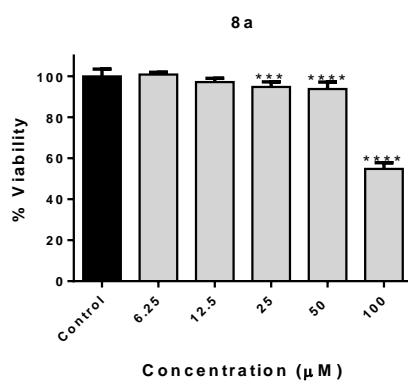
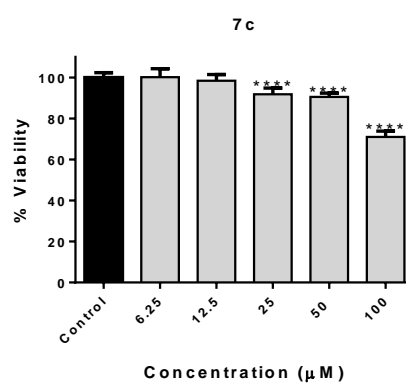
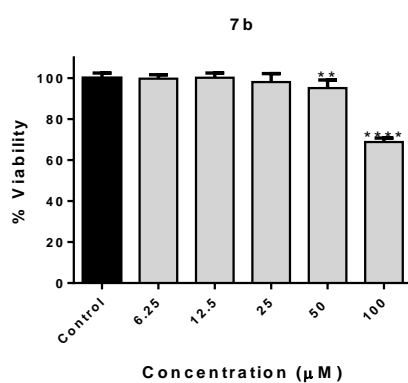
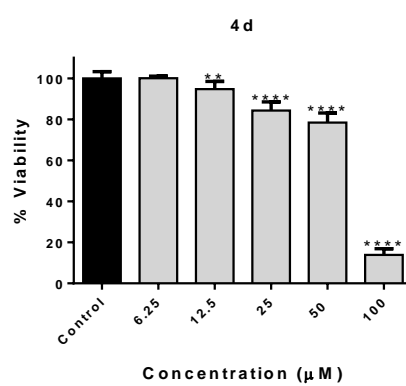
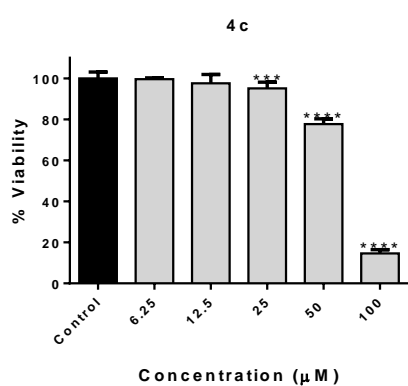
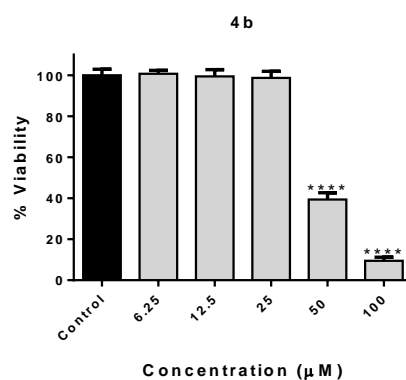
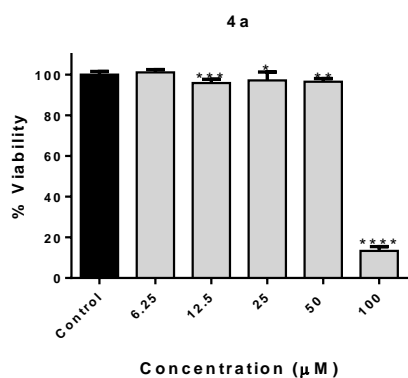
MRC-5, the safety range of this compound is quite narrow. Note that compound **4b** has IC_{50} values of 45.0 and 37.0 μM against MRC-5 and AGS, respectively, which demonstrates its lack of selectivity.

Regarding the glycosylated derivatives with $R^3 = \text{Glc}$, only compounds **7b** and **7c** were tested against MRC-5. None of these two exhibited a measurable IC_{50} value below 100 μM against this cell line. Since **7b** and **7c** had a IC_{50} of, respectively, 78.8 and 73.0 μM against AGS cell line, their safety margin is better than that of compound **4b**. Thus, the insertion of $R^3 = \text{Glc}$ may be a good strategy to afford pyrazole derivatives with a better selectivity towards the AGS cancer cell line.

Compounds **8a** and **8b** were also tested against the MRC-5 cell line. Compound **8a** didn't present a measurable IC_{50} under 100 μM . Still, even though it didn't compromise the MRC-5 viability by 50%, compound **8a** was rather cytotoxic to MRC-5 cell lines at the concentration of 100 μM (see Figure 4.2). Still, the insertion of the $R^3 = \text{Dx}$ increased the safety margin of compound **8a** when compared to its precursor, compound **4a**. Compound **8b** has an IC_{50} value of 73.8 μM against MRC-5 cell line, which is almost two-fold higher than the IC_{50} value obtained with the AGS cancer cell line (41.3 μM). Thus, compound **8b** presented a better selectivity than its precursor, compound **4c**. Altogether, these results indicate that the insertion of the $R^3 = \text{Dx}$ group improves the selectivity of the pyrazole derivatives towards this cancer cell line.

Finally, within the ruthenium complexes, (**9a-d**) only one, complex **9d**, was tested against the MRC-5 cell line, presenting a IC_{50} value of 62.2 μM . This result is approximately three-fold higher than the one obtained against the AGS cell line ($IC_{50} = 18.3 \mu\text{M}$). Moreover, complex **9d** also presented a better selectivity towards the AGS cancer cell line than its precursor, compound **4d**. The reasonable safety margin and the potency of complex **9d** against AGS cancer cell line makes it an interesting *in vitro* cytotoxic agent. Still, more tests need to be performed to evaluate unequivocally its safety toward healthy cell lines.

Cytotoxicity against MRC-5



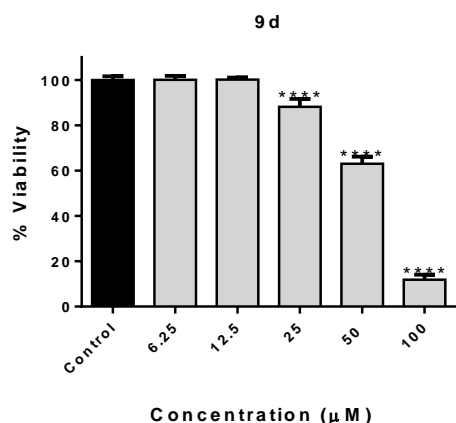


Figure 4.2 – Cytotoxic effect of compounds **4a-d**, **7b-c**, **8a,b** and **9d** against the MRC-5 cell line. The cells were incubated with five different concentrations of these compounds for 24h. The data is expressed as % of viability and represents the mean \pm mean standard deviation from three to four independent experiments run in triplicate. * denotes p -value < 0.05 , ** denotes p -value < 0.01 , *** denotes p -value < 0.001 and **** denotes p -value < 0.0001 .

Table 4.2 – Structural representation and cytotoxic activity of compounds **4a-d**, **7b-c**, **8a,b** and **9d** against the MRC-5 cell line. The results are expressed as IC_{50} (μM).

Compound	Structural representation			IC_{50} MRC-5
	R^1	R^2	R^3	
4a	H	H	H	77.9
4b	H	Cl	H	45.0
4c	CF_3	H	H	72.0
4d	H	OCH_3	H	72.4
7b	H	Cl	Glc	>100
7c	CF_3	H	Glc	>100
8a	H	Cl	Dx	>100
8b	CF_3	H	Dx	73.8
9d	H	OCH_3	Ru[9]aneS ₃	62.2

Chapter 5

Experimental section

5.1. Equipment, materials and solvents

Commercial reagents used in this study suffered no purification prior to their use.

All solvents were of analytical grade except when otherwise specified.

Pyridine was dried by reflux over sodium hydroxide and then it was distilled and kept in molecular sieves (MS) 4Å.

The acetone was dried with anhydrous sodium sulfate and kept in MS 4Å.

Dichloromethane was dried by reflux over calcium hydride and then it was distilled and kept in MS 4Å.

Progress of the reactions was monitored by TLC, using coated laminated sheets of silica gel 60 F254 plates from Riedel-de-Hans or silica gel 60 NHR / UV254 of Macherey Nigel.

The purifications by preparative TLC were carried out on glass plates (20 × 20 cm) previously coated with a layer of silica gel 60 GF254 Riedel-de-Hans, with a thickness of 0.5 mm and activated at 125°C for 12 hours. After elution of the compounds, the plates were observed under UV light at λ of 254 and / or 366 nm.

The purifications by column chromatography were performed in a glass column using silica gel 60, Riedel-de-Hans, particle size 70-230 mesh as a support. Fractions were monitored by TLC and visualized by UV light ($\lambda = 254$ and/or 366 nm).

The eluents used in either column chromatography or preparative TLC are mentioned in each case, as well as their volume ratio (proportion) in the case of mixtures of solvents.

The values of the m.p. were determined on a Büchi melting point apparatus B-540 and were not corrected.

NMR spectra were acquired on a Bruker Avance 300 instrument operating at a frequency of 300.13 MHz for ^1H and 75.47 MHz for ^{13}C , or a Bruker Avance 500 instrument operating at a frequency of 500.16 MHz for ^1H and 125.77 MHz for ^{13}C . Tetramethylsilane (TMS) was used as internal standard. The chemical shifts (δ , ppm) were obtained at r.t. and the deuterated solvent used is indicated in each case. For ^1H NMR characterization, chemical shifts, multiplicity and coupling constants (J , Hz) are presented.

The unequivocal assignment of the resonances of protons and carbons was performed using two-dimensional HSQC, HMBC, COSY and NOESY NMR experiments.

Fourier-transform infrared (FT-IR) spectra were collected as KBr pellets with typically 2 mg of sample and 200 mg of KBr using a Bruker Optics Tensor 27 FT-IR spectrophotometer (4000–400 cm^{-1} range, 64 scans, 2 cm^{-1} maximal resolution).

Positive-ion ESI mass spectra and high resolution mass spectra [ESI(+)-HRMS] were performed using a Q Exactive Orbitrap mass spectrometer (Thermo Fischer Scientific, Bremen, Germany) controlled by THERMO Xcalibur 4.1. The capillary voltage of the electrospray ionization (ESI) was set to 3000 V. The capillary temperature was 250°C. The sheath gas flow rate (nitrogen) was set to 5 (arbitrary unit as provided by the software settings).

The AGS cancer cell line was purchased from the American Type Culture Collection (Manassas, Virginia, USA). The MRC-5 cell line was acquired from ECACC (Porton Down Salisbury, UK).

The culture medium DMEM (1X) + GlutaMAXTM-1 (Dulbecco's Modified Eagle Medium) and MEM (1X) + GlutaMAXTM-1 were acquired at Gibco[®]. PBS and trypsin (0.25%) were also purchased at Gibco[®].

The MTT solution was prepared in culture medium (5 mg/mL) and sterilized by filtration.

The biological assays were performed on the ESCO[®] Airstream[®] Class II biological safety cabinet.

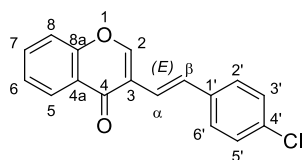
5.2. Protocols

5.2.1. Synthesis of (*E*)-3-styryl-4*H*-chromen-4-ones

Only the (*E*)-3-styryl-4*H*-chromen-4-one (**3a**), (*E*)-3-(4-chlorostyryl)-4*H*-chromen-4-one (**3b**) and (*E*)-3-(4-methoxystyryl)-4*H*-chromen-4-one (**3d**) were prepared in this work. The synthesis of these compounds was accomplished according to the procedure reported by Silva *et al.*⁹⁰ To a solution of 4-oxo-4*H*-chromene-3-carbaldehyde (**1**) (300 mg, 1.72 mmol) in dry pyridine (20 mL) were added 5 equiv. of the appropriate phenylacetic acid (**2a**, **2b** or **2d**) (8.60 mmol) and 1.5 equiv. of *tert*-BuOK (290 mg, 2.58 mmol). The mixture was stirred at 120 °C under a nitrogen atmosphere. After 24 hours the reaction was monitored by TLC, using CH_2Cl_2 as eluent, and then it was stopped. The reaction mixture was cooled down to r.t.. Afterwards, the mixture was acidified with an HCl solution until

pH 2 was reached. The compound was extracted from the aqueous phase with dichloromethane and the organic and aqueous phases were separated. The organic layer was dried over anhydrous sodium sulfate. The solvent was removed under reduced pressure and a light brown solid was obtained. The solid was dissolved in CH₂Cl₂ and purified by column chromatography using CH₂Cl₂ as eluent. Compounds **3a**, **3b** and **3d** were dried in a vacuum pump and were obtained as a beige, pale beige and yellow solids, respectively in 73 %, 82 % and 34 % yields.

(E)-3-(4-Chlorostyryl)-4H-chromen-4-one (3b)



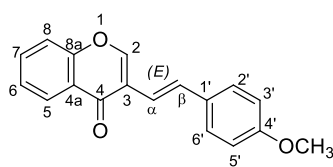
Pale beige solid, 82%, m.p. 152 – 154 °C, (Lit. 159 – 160 °C)⁹⁶

¹H NMR (CDCl₃, 300.13 MHz): δ = 6.93 (dd, 1 H, *J* = 16.3, 0.6 Hz, H-α), 7.32 (d, 2 H, *J* = 8.5 Hz, H-3', 5'), 7.41-7.49 (m, 2 H, H-6, 8), 7.45 (d, 2 H, *J* = 8.5 Hz, H-2', 6') 7.63 (d, 1 H, *J* = 16.3

Hz, H-β), 7.68 (ddd, 1 H, *J* = 8.5, 7.0, 1.7 Hz, H-7), 8.10 (s, 1 H, H-2), 8.30 (dd, 1 H, *J* = 8.0, 1.7 Hz, H-5) ppm.

¹³C NMR (CDCl₃, 75.47 MHz): δ = 118.1 (C-8), 119.7 (C-α), 121.5 (C-3), 124.1 (C-4a), 125.4 (C-6), 126.3 (C-5), 127.8 (C-2', 6'), 128.8 (C-3', 5'), 130.5 (C-β), 133.5 (C-4'), 133.6 (C-7), 135.9 (C-1'), 153.4 (C-2), 155.8 (C-8a), 176.6 (C-4) ppm.

(E)-3-(4-Methoxystyryl)-4H-chromen-4-one (3d)



Yellow solid, 34%.

¹H NMR (CDCl₃, 500.13 MHz): δ = 3.83 (s, 3 H, -OCH₃), 6.86 (dd, 1 H, *J* = 16.3, 0.7 Hz, H-α), 6.90 (d, 2 H, *J* = 8.7 Hz, H-3', 5'), 7.42 (ddd, 1 H, *J* = 8.2, 7.2, 1.0 Hz, H-6), 7.46-

7.48 (m, 1 H, H-8) 7.67 (d, 2 H, *J* = 8.7 Hz, H-2', 6'), 7.55 (d, 1 H, *J* = 16.3 Hz, H-β), 7.67 (ddd, 1 H, *J* = 8.5, 7.2, 1.5 Hz, H-7), 8.10 (d, 1 H, *J* = 0.7 Hz, H-2), 8.30 (dd, 1 H, *J* = 8.2, 1.5 Hz, H-5) ppm.

¹³C NMR [CDCl₃, 75.47 MHz]: δ = 55.3 (-OCH₃), 114.1 (C-3', 5'), 116.8 (C-α), 118.1 (C-8), 112.1 (C-3), 124.1 (C-4a), 125.2 (C-6), 126.3 (C-5), 127.9 (C-2', 6'), 130.2 (C-1'), 131.2 (C-β), 133.4 (C-7), 152.5 (C-2), 155.8 (C-8a), 159.5 (C-4'), 176.7 (C-4) ppm.

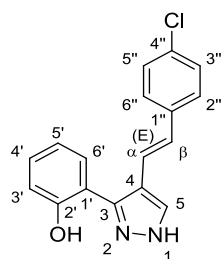
MS (ESI⁺) m/z (%): 279.1. [(M+H)⁺, 100].

HRMS (ESI⁺) m/z calcd for C₁₈H₁₄O₃ (M+H)⁺, 279.1016; found: 279.1011.

5.2.2. Synthesis of (*E*)-3(5)-(2-hydroxyphenyl)-4-styryl-1*H*-pyrazoles

The synthesis of (*E*)-3(5)-(2-hydroxyphenyl)-4-styryl-1*H*-pyrazoles (**4a**, **4b** and **4d**) was performed following a procedure described by Silva *et al.*⁸⁷ Briefly, 2 equiv of hydrazine hydrate, (0.15 mL, 2.66 mmol) were added to a solution of the appropriate (*E*)-3-styryl-4*H*-chromen-4-one (**3a**, **3b** or **3d**) (1.33 mmol) in methanol (80 mL). The reaction mixture was stirred at r.t., under nitrogen atmosphere, for 5h. The consumption of the starting material was monitored by TLC using CH₂Cl₂ as eluent. Then, the solvent was partially removed and the mixture was poured into 100 mL of CHCl₃ and washed with 2 × 100 mL of acidified water (pH 5). The organic layer was dried over anhydrous sodium sulfate and the solvent was evaporated to dryness. The (*E*)-3(5)-(2-hydroxyphenyl)-4-styryl-1*H*-pyrazoles (**4a**, **4b** and **4d**) were dried in a vacuum pump and were obtained as pale beige, white and pale beige solids, respectively in 74%, 92% and 95% yields.

(*E*)-4-(4-Chlorostyryl)-3(5)-(2-hydroxyphenyl)-1*H*-pyrazole (**4b**)



White solid, m.p. 169.4 – 169.9 °C, (Lit.: 163 – 164 °C),⁸⁷ 92%.

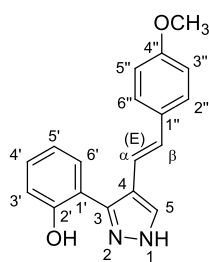
¹H NMR (CDCl₃, 300.13 MHz): δ = 6.84 (d, 1 H, *J* = 16.4 Hz, H-β), 6.97 (dt, 1 H, *J* = 7.6, 1.3 Hz, H-5'), 7.08 (dd, 1 H, *J* = 8.4, 1.3 Hz, H-3'), 7.12 (d, 1 H, *J* = 16.4 Hz, H-α), 7.28-7.35 (m, 1 H, H-4'), 7.32 (d, 2 H, *J* = 8.6 Hz, H-2'',6''), 7.39 (d, 2 H, *J* = 8.6 Hz, H-3'',5''), 7.58

(dd, 1 H, *J* = 7.6, 1.6 Hz, H-6'), 7.85 (broad s, 1 H, H-5) ppm.

¹³C NMR (CDCl₃, 75.47 MHz): δ = 117.0 (C-3'), 117.2 (C-1'), 120.5 (C-4), 119.5 (C-α), 119.6 (C-5'), 127.5 (C-2'',6''), 127.7 (C-5), 128.5 (C-6'), 128.7 (C-β), 128.9 (C-3'',5''), 129.6 (C-4'), 133.2 (C-4''), 135.8 (C-1''), 148.0 (C-3), 155.6 (C-2') ppm.

FT-IR (KBr, $\bar{\nu}_{\max}$ (cm⁻¹)): 3264 s (νN-H), 1635 m (νC=C), 1586 s (νC=N), 1154 w (νN-N), 1087 s (νC-OH), 966 s (ωCα=Cβ), 752 vs (νC-H), 709 s (νC-H).

(*E*)-3(5)-(2-Hydroxyphenyl)-4-(4-methoxystyryl)-1*H*-pyrazole (**4d**)



Pale beige solid, m.p. 157.3-158.5 °C, 95%.

¹H NMR [(CD₃)₂CO, 300.13 MHz]: δ = 3.83 (s, 3 H, -OCH₃), 6.84 (d, 1 H, *J* = 16.2, Hz, H-β), 6.91 (d, 2 H, *J* = 8.8 Hz, H-3'', 5''), 6.92-6.99 (m, 1 H, H-5'), 7.02 (d, 1 H, *J* = 16.2 Hz, H-α), 7.07 (dd, 1 H, *J* = 8.0, 1.2 Hz, H-3'), 7.26 (ddd, 1 H, *J* = 8.0, 7.7, 1.6 Hz, H-4'), 7.41 (d, 2 H, *J* = 8.8 Hz, H-2'', 6''), 7.64 (dd, 1 H, *J* = 7.8, 1.6 Hz, H-6'), 7.81 (s, 1 H, H-

5) ppm.

¹³C NMR [(CD₃)₂CO, 75.47 MHz]: δ = 55.4 (-OCH₃), 116.8 (C-3'', 5''), 116.8 (C-α), 117.0 (C-3'), 117.4 (C-1'), 118.8 (C-4), 119.5 (C-5'), 127.5 (C-2'',6'', 5), 128.5 (C-6'), 129.4 (C-4'), 129.6 (C-β), 130.1 (C-1''), 148.0 (C-3), 155.6 (C-2'), 159.3 (C-4'') ppm.

FT-IR (KBr, $\bar{\nu}_{\max}$ (cm⁻¹)): 3127 m (νN-H), 1601 m (νC=C), 1576 m (νC=N), 1152 m (νN-N), 1086 m (νC-OH), 960 s (ωCα=Cβ), 770 s (νC-H), 701 m (νC-H).

MS (ESI⁺) m/z (%): 293.1 [(M+H)⁺, 100].

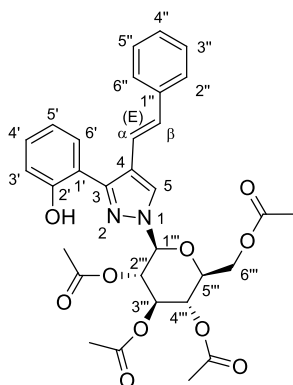
HRMS (ESI⁺) m/z calcd for C₁₈H₁₆N₂O₂ (M+H)⁺, 293.1277; found: 293.1285.

5.2.3. Glycosylation of (*E*)-3(5)-(2-hydroxyphenyl)-4-styryl-1*H*-pyrazoles

According to the Koenigs-Knorr method,⁸⁸ 3 equiv. of Ag₂CO₃ (278 mg, 1.02 mmol), 0.15 equiv. of AgOTf (12.9 mg, 0.05 mmol) and 1.5 equiv of 2,3,4,6-tetra-*O*-acetyl-α-D-glucopyranosyl bromide (213.8 mg, 0.52 mmol) were added to a solution of the appropriate (*E*)-3(5)-(2-hydroxyphenyl)-4-styryl-1*H*-pyrazole (0.34 mmol) (**4a-d**) in CH₂Cl₂ (8 mL). MS 4Å (3.4 g) were added to guarantee anhydrous conditions. The mixture was stirred at r.t., under a nitrogen atmosphere for 7 to 10 days. After that period, the reaction mixture was filtered, the solid was washed with CH₂Cl₂ and the solvent was evaporated to dryness. The organic residue was dissolved in CH₂Cl₂ and purified by TLC using CH₂Cl₂:acetone (9:1) as eluent. After purification the obtained compounds were dried in a vacuum pump and were analysed by ¹H NMR spectroscopy. According to the ¹H NMR data, the compound with lower r.f. corresponds to compound **5** and the compound with higher r.f. is compound **6**. Compounds **5a-d** were obtained as pale beige solids with respectively, 20 %, 19 %, 41 % and 12 % yields (see Table 2.1, entry 1, 3, 6 and 7). Compounds **6** were obtained as: pale yellow oil (**6a**), yellow oil (**6b**) and pale yellow oils

(**6c** and **6d**) with yields of 52 %, 50 %, 11 % and 39% (consult Table 2.1, entry 1, 3, 6 and 7).

(E)-1-[β-D-(2,3,4,6-tetra-O-acetylglycose-1-yl)]-3-(2-hydroxyphenyl)-4-styryl-1H-pyrazole (5a)

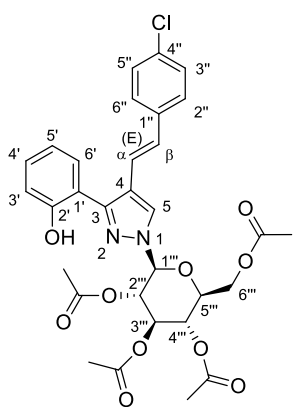


Pale beige solid, 20%.

¹H NMR [(CD₃)₂CO, 500.13 MHz]: δ = 1.98 (s, 3 H, -COCH₃), 2.01 (s, 3 H, -COCH₃), 2.04-2.10 (m, 6 H, 2 × -COCH₃), 3.81-4.34 (m, 3 H, 6'''-CH₂OCOCH₃, 5'''), 5.29 (t, 1 H, *J* = 9.5 Hz, H-4'''), 5.56 (t, 1 H, *J* = 9.5 Hz, H-3'''), 5.79 (t, 1 H, *J* = 9.5 Hz, H-2'''), 6.02 (d, 1 H, *J* = 9.5 Hz, H-1'''), 6.98 (ddd, 1 H, *J* = 7.5, 7.6, 1.0 Hz, H-5'), 7.02 (dd, 1 H, *J* = 7.7, 1.0 Hz, H-3'), 7.05 (d, 1 H, *J* = 16.3 Hz, H-β), 7.21 (d, 1 H, *J* = 16.3 Hz, H-α), 7.27-7.31 (m, 2 H, H-4', 4''), 7.38 (t, 2 H, *J* = 7.5 Hz, H-3'', 5''), 7.56 (d, 2 H, *J* = 7.5 Hz, H-2'', 6''), 7.64 (dd, 1 H, *J* = 7.6, 1.6 Hz, H-6'), 8.43 (s, 1 H, H-5), 9.68 (s, 1 H, 2'-OH) ppm.

¹³C NMR [(CD₃)₂CO, 75.47 MHz]: δ = 20.2 (-COCH₃), 20.5 (-COCH₃), 20.6 (2 × -COCH₃), 62.7 (C-6'''), 68.4 (C-4'''), 71.0 (C-2'''), 73.7 (C-3'''), 75.0 (C-5'''), 87.3 (C-1'''), 117.6 (C-3'), 118.3 (C-1'), 119.3 (C-α), 120.2 (C-5'), 120.7 (C-4), 127.1 (C-2'', 6''), 128.4 (C-4''), 129.5 (C-3'', 5''), 129.8 (C-6'), 129.9 (C-5), 130.5 (C-4'), 130.9 (C-β), 149.4 (C-1''), 156.7 (C-3), 156.7 (C-2'), 169.4 (-COCH₃), 170.0 (-COCH₃), 170.3 (-COCH₃), 170.7 (-COCH₃) ppm.

(E)-1-[β-D-(2,3,4,6-tetra-O-acetylglycose-1-yl)]-4-(4-chlorostyryl)-3-(2-hydroxyphenyl)-1H-pyrazole (5b)



Pale beige solid, 19%.

¹H NMR [(CD₃)₂CO, 300.13 MHz]: δ = 1.87 (s, 3 H, -COCH₃), 2.00 (s, 3 H, -COCH₃), 2.02 (s, 3 H, -COCH₃), 2.04-2.07 (m, 3 H, -COCH₃), 4.16-4.36 (m, 3 H, 6'''-CH₂OCOCH₃, 5'''), 5.28 (t, 1 H, *J* = 9.5 Hz, H-4'''), 5.55 (t, 1 H, *J* = 9.5 Hz, H-3'''), 5.78 (t, 1 H, *J* = 9.5 Hz, H-2'''), 6.01 (d, 1 H, *J* = 9.5 Hz, H-1'''), 6.97 (t, 1 H, *J* = 7.9 Hz, H-5'), 7.04 (d, 1 H, *J* = 16.3 Hz, H-β), 7.00-7.09 (m, 1 H, H-3'), 7.23 (d, 1 H, *J* = 16.3 Hz, H-α), 7.29 (ddd, 1 H, *J*

= 7.7, 7.9, 1.6 Hz, H-4'), 7.40 (d, 2 H, $J = 8.2$ Hz, H-3'',5''), 7.58 (d, 2 H, $J = 8.2$ Hz, H-2'',6''), 7.63 (dd, 1 H, $J = 7.9, 1.6$ Hz, H-6'), 8.43 (s, 1 H, H-5), 9.63 (s, 1 H, 2'-OH) ppm.

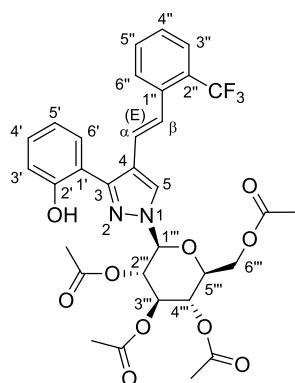
^{13}C NMR [(CD₃)₂CO, 75.47 MHz]: $\delta = 20.2$ (-COCH₃), 20.5 (-COCH₃), 20.6 (2 \times -COCH₃), 62.7 (C-6'''), 68.8 (C-4'''), 71.1 (C-2'''), 73.7 (C-3'''), 75.0 (C-5'''), 87.3 (C-1'''), 117.6 (C-3'), 118.3 (C-1'), 120.3 (C-5'), 120.3 (C- α), 120.5 (C-4), 128.7 (C-2'', 6''), 129.4 (C- β), 129.6 (C-3'', 5''), 130.0 (C-6'), 130.1 (C-5), 130.5 (C-4'), 133.3 (C-4''), 137.2 (C-1''), 149.4 (C-3), 156.6 (C-2'), 169.4 (-COCH₃), 170.0 (-COCH₃), 170.3 (-COCH₃), 170.7 (-COCH₃) ppm.

MS (ESI⁺) m/z (%): 627.2 [(M+H)⁺, ³⁵Cl] (100).

HRMS (ESI⁺) m/z calcd for C₃₁H₃₁ClN₂O₁₀ (M+H)⁺, 627.1736; found: 627.174

(E)-1-[β -D-(2,3,4,6-tetra-O-acetylglycose-1-yl)]-3-(2-hydroxyphenyl)-4-(2-trifluoromethylstyryl)-1H-pyrazole (5c)

Pale beige solid, m.p. 76.7-79.4 °C, 11%.



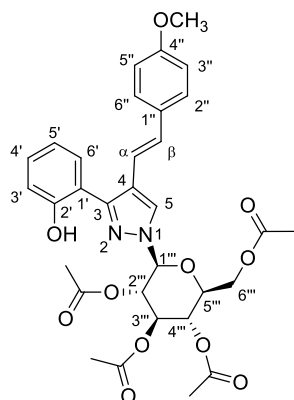
^1H NMR [(CD₃)₂CO, 500.16 MHz]: $\delta = 1.88$ (s, 3 H, -COCH₃), 1.98-2.10 (m, 9 H, 3 \times -COCH₃), 4.19-4.34 (m, 3 H, 6'''-CH₂OCOCH₃,5'''), 5.29 (t, 1 H, $J = 9.5$ Hz, H-4'''), 5.55 (t, 1 H, $J = 9.5$ Hz, H-3'''), 5.83 (t, 1 H, $J = 9.5$ Hz, H-2'''), 6.03 (d, 1 H, $J = 9.5$ Hz, H-1'''), 6.97 (dt, 1 H, $J = 7.6, 1.1$ Hz, H-5'), 7.02 (dd, 1 H, $J = 8.0, 1.1$ Hz, H-3'), 7.25 (d, 1 H, $J = 16.0$ Hz, H- α), 7.30 (ddd, 1 H, $J = 8.0, 7.6, 1.6$ Hz, H-4'), 7.32 (d, 1 H, $J = 16.0$ Hz,

H- β), 7.50 (t, 1 H, $J = 7.8$ Hz, H-4''), 7.59 (dd, 1 H, $J = 7.6, 1.6$ Hz, H-6'), 7.68 (t, 1 H, $J = 7.8$ Hz, H-5''), 7.75 (d, 1 H, $J = 7.8$ Hz, H-3''), 7.96 (d, 1 H, $J = 7.8$ Hz, H-6''), 8.52 (s, 1 H, H-5), 9.53 (s, 1 H, 2'-OH) ppm.

^{13}C NMR [(CD₃)₂CO, 75.47 MHz]: $\delta = 20.2$ (-COCH₃), 20.5 (-COCH₃), 20.6 (2 \times -COCH₃), 62.7 (C-6'''), 68.8 (C-4'''), 71.0 (C-2'''), 73.7 (C-3'''), 75.0 (C-5'''), 87.3 (C-1'''), 117.6 (C-3'), 118.3 (C-1'), 120.3 (C-5'), 124.0 (C- α), 125.5 (C-4), 126.6 (q, $J = 5.8$ Hz, C-3''), 127.4 (q, $J = 32.6$ Hz, C-2''), 128.1 (C-6''), 128.4 (C-4''), 130.1 (C-6'), 130.6 (C-5, 4'), 130.6 (C- β), 133.4 (C-5''), 137.1 (C-1''), 149.7 (C-3), 156.6 (C-2'), 169.5 (-COCH₃), 170.0 (-COCH₃), 170.3 (-COCH₃), 170.7 (-COCH₃) ppm.

Note: It was not possible to assign the CF₃ carbon resonance.

(E)-1-[β -D-(2,3,4,6-tetra-*O*-acetylglucose-1-yl)]-3-(2-hydroxyphenyl)-4-(4-methoxystyryl)-1*H*-pyrazole (5d)



Pale beige solid, 12%.

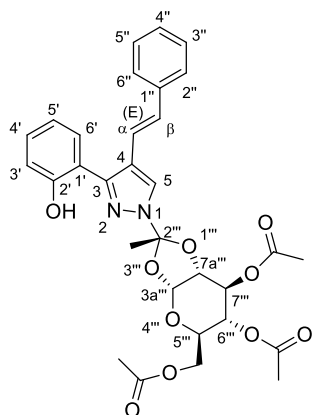
$^1\text{H NMR}$ [(CD_3) $_2\text{CO}$, 500.16 MHz]: δ = 1.87 (s, 3 H, -COCH $_3$), 2.00 (s, 3 H, -COCH $_3$), 2.02 (s, 3 H, -COCH $_3$), 2.04-2.07 (m, 3 H, -COCH $_3$), 3.83 (s, 3 H, 4''-OCH $_3$) 4.18-4.34 (m, 3 H, 6'''-CH $_2$ OCOCH $_3$,5'''), 5.29 (t, 1 H, J = 9.5 Hz, H-4'''), 5.48 (t, 1 H, J = 9.3 Hz, H-3'''), 5.55 (t, 1 H, J = 9.5 Hz, H-3'''), 5.68 (t, 1 H, J = 9.3 Hz, H-2'''), 5.78 (t, 1 H, J = 9.5 Hz, H-2'''), 5.94 (d, 1 H, J = 9.3 Hz, H-1'''), 6.00 (d, 1 H, J = 9.5 Hz, H-1'''), 6.70 (d, 1 H, J = 12.0 Hz, H- α/β *), 6.82 (d, 2 H, J = 8.9 Hz, H-3'',5''*), 6.87-6.90 (m, 1 H, H-5'*), 6.94-6.98 (m, 1 H, H-5'), 6.95 (d, 2 H, J = 8.7 Hz, H-3'',5''), 6.98-7.02 (m, 1 H, H-3'), 6.98 (d, 1 H, J = 16.2 Hz, H- α/β), 7.05 (d, 1 H, J = 16.2 Hz, H- α/β), 7.22-7.26 (m, 1 H, H-4'*), 7.26-7.30 (m, 1 H, H-4'), 7.50 (d, 2 H, J = 8.7 Hz, H-2'',6''), 7.65 (dd, 1 H, J = 7.8, 1.6 Hz, H-6'), 8.37 (s, 1 H, H-5), 9.74 (s, 1 H, 2'-OH) ppm.

MS (ESI $^+$) m/z (%): 693.2 [(M+H) $^+$, 100].

HRMS (ESI $^+$) m/z calcd for $\text{C}_{32}\text{H}_{34}\text{N}_2\text{O}_{11}$ (M+H) $^+$, 623.2239; found: 623.2235.

Note: the “*” symbol corresponds to the proton duplications correspondent to the minority *cis* isomer. A full NMR characterization wasn't presented due to the presence of the two isomers. The structure displayed here only represents the *trans* isomer.

1-[(2*R*,3*aR*,5*R*,6*S*,7*S*,7*aR*)-6,7-diacetoxy-5-acetoxymethyl-2-methyltetrahydro-5*H*-[1,3]dioxolo[4,5-*b*]pyran-2-yl]-(*E*)-3-(2-hydroxyphenyl)-4-styryl-1*H*-pyrazole (6a)



Pale yellow oil, 52%.

$^1\text{H NMR}$ [(CD_3) $_2\text{CO}$, 300.13 MHz]: δ = 2.05-2.10 (m, 6 H, 2 \times -COCH $_3$), 2.13 (br s, 3 H, -COCH $_3$), 2.19 (s, 3 H, 2'''-CH $_3$), 4.23 (t, 1 H, J = 5.2 Hz, H-7a'''), 4.26-4.31 (m, 2 H, 5'''-CH $_2$ OCOCH $_3$), 4.46 (ddd, 1 H, J = 5.2, 2.8, 0.9 Hz, H-5'''), 4.97 (ddd, 1 H, J = 9.1, 1.8, 0.9 Hz, H-6'''), 5.25 (t, 1 H, J = 2.8 Hz, H-7'''), 6.18 (d, 1 H, J = 5.2 Hz, H-3a'''), 6.96-6.98 (m, 1 H, H-

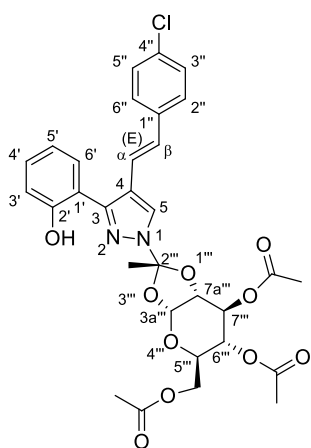
5'), 7.02 (dd, 1 H, $J = 7.8, 1.1$ Hz, H-3'), 7.07 (d, 1 H, $J = 16.5$ Hz, H- β), 7.24 (d, 1 H, $J = 16.5$ Hz H- α), 7.27-7.32 (m, 2 H, H-4',4''), 7.38 (t, 2 H, $J = 7.4$ Hz, H-3'',5''), 7.55 (d, 2 H, $J = 7.4$ Hz, H-2'',6''), 7.67 (dd, 1 H, $J = 7.8, 1.6$ Hz, H-6'), 8.37 (s, 1 H, H-5), 10.12 (s, 1 H, 2'-OH) ppm.

^{13}C NMR [(CD₃)₂CO, 75.47 MHz]: $\delta = 20.2$ (-COCH₃), 20.5 (-COCH₃), 20.6 (-COCH₃), 24.3 (2''''-CH₃), 63.9 (5''''-CH₂OCOCH₃), 68.4 (C-7a'''), 68.8 (C-6'''), 70.1 (C-7'''), 73.8 (C-5'''), 98.9 (C-3a'''), 114.5 (C-2'''), 117.6 (C-3'), 118.4 (C-4), 119.4 (C- α), 119.5 (C-1'), 120.2 (C-5'), 127.1 (C-2'',6''), 127.6 (C-5), 128.3 (C-4''), 129.5 (C-3'',5'',6'), 130.3 (C-4'), 130.7 (C- β), 138.4 (C-1''), 149.4 (C-3), 156.8 (C-2'), 169.5 (-COCH₃), 170.1 (-COCH₃), 170.8 (-COCH₃) ppm.

MS (ESI⁺) m/z (%): 593.2 [(M+H)⁺, 100].

HRMS (ESI⁺) m/z calcd for C₃₁H₃₂N₂O₁₀ (M+H)⁺, 593.2131; found: 593.213.

1-[(2*R*,3*aR*,5*R*,6*S*,7*S*,7*aR*)-6,7-diacetoxy-5-acetoxymethyl-2-methyltetrahydro-5*H*-[1,3]dioxolo[4,5-*b*]pyran-2-yl]-(*E*)-4-(4-chlorostyryl)-3-(2-hydroxyphenyl)-1*H*-pyrazole (6b)



Pale yellow oil, 50%.

^1H NMR [(CD₃)₂CO, 300.13 MHz]: $\delta = 2.05$ -2.07 (m, 6 H, 2 \times -COCH₃), 2.13 (br s, 3 H, -COCH₃), 2.19 (s, 3 H, 2''''-CH₃), 4.24 (t, 1 H, $J = 5.2$ Hz, H-7a'''), 4.25-4.33 (m, 2 H, 5''''-CH₂OCOCH₃), 4.46 (ddd, 1 H, $J = 5.2, 2.8, 0.9$ Hz, H-5'''), 4.99 (ddd, 1 H, $J = 9.8, 2.0, 0.9$ Hz, H-6'''), 5.26 (t, 1H, $J = 2.8$ Hz, H-7'''), 6.17 (d, 1 H, $J = 5.2$ Hz, H-3a'''), 6.97 (ddd, 1 H, $J = 7.7, 7.6, 1.1$ Hz, H-5'), 7.02 (dd, 1 H, $J = 8.0, 1.1$ Hz, H-3'), 7.05 (d, 1 H, $J = 16.2$ Hz, H- β), 7.26 (d, 1 H, $J = 16.2$ Hz, H- α), 7.29

(ddd, 1 H, $J = 8.0, 7.6, 1.6$ Hz, H-4'), 7.39 (d, 2 H, $J = 8.6$ Hz, H-3'',5''), 7.56 (d, 2 H, $J = 8.6$ Hz, H-2'',6''), 7.65 (dd, 1 H, $J = 7.7, 1.6$ Hz, H-6'), 8.38 (s, 1 H, H-5), 10.08 (s, 1 H, 2'-OH) ppm.

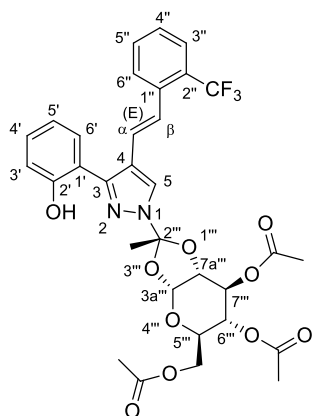
^{13}C NMR [(CD₃)₂CO, 75.47 MHz]: $\delta = 20.6$ (2 \times -COCH₃), 20.8 (-COCH₃), 24.3 (2''''-CH₃), 63.8 (5''''-CH₂OCOCH₃), 68.4 (C-7a'''), 68.8 (C-6'''), 70.1 (C-7'''), 73.8 (C-5'''), 98.9 (C-3a'''), 114.5 (C-2'''), 117.5 (C-3'), 118.4 (C-1'), 119.3 (C-4), 120.2 (C-5'), 120.4 (C- α), 127.7 (C-5), 128.5 (C-2'',6''), 129.2 (C- β), 129.5 (C-3'',5'',6'), 130. (C-4'), 133.2

(C-4''), 137.2 (C-1''), 149.5 (C-3), 156.7 (C-2'), 169.5 (7'''-COCH₃), 170.1 (6'''-COCH₃), 170.8 (5'''-CH₂OCOCH₃) ppm.

MS (ESI⁺) m/z (%) = 627.2 [(M+H)⁺, ³⁵Cl] (100), 629.2 [(M+H)⁺, ³⁷Cl]

HRMS (ESI⁺) m/z calcd for C₃₁H₃₁ClN₂O₁₀ (M+H)⁺, 627.1742; found: 627.174.

1-[(2*R*,3*aR*,5*R*,6*S*,7*S*,7*aR*)-6,7-diacetoxy-5-acetoxymethyl-2-methyltetrahydro-5*H*-[1,3]dioxolo[4,5-*b*]pyran-2-yl)-(E)-3-(2-hydroxyphenyl)-4-(2-trifluoromethylstyryl)-1*H*-pyrazole (6c)



Yellow oil, 41%.

¹H NMR [(CD₃)₂CO, 500.16 MHz]: δ = 2.05-2.07 (m, 6 H, 2 × -COCH₃), 2.13 (br s, 3 H, -COCH₃), 2.19 (s, 3 H, 2'''-CH₃), 4.21 (t, 1 H, *J* = 5.2 Hz, H-7a'''), 4.25-4.31 (m, 2 H, 5'''-CH₂OCOCH₃), 4.47 (ddd, 1 H, *J* = 5.2, 2.3, 0.8 Hz, H-5'''), 4.98 (ddd, 1 H, *J* = 8.5, 2.0, 0.8 Hz, H-6'''), 5.25 (t, 1 H, *J* = 2.3 Hz, H-7'''), 6.16 (d, 1 H, *J* = 5.2 Hz, H-3a'''), 6.96 (dt, 1 H, *J* = 7.6, 1.2 Hz, H-5'), 7.02 (dd, 1 H, *J* = 8.2, 1.2 Hz, H-3'), 7.26 (d, 1 H,

J = 16.0 Hz, H-α), 7.28-7.34 (m, 2 H, H-4', β), 7.50 (t, 1 H, *J* = 7.8 Hz, H-4''), 7.61 (dd, 1 H, *J* = 7.6, 1.6 Hz, H-6'), 7.68 (t, 1 H, *J* = 7.8 Hz, H-5''), 7.75 (d, 1 H, *J* = 7.8 Hz, H-3''), 7.93 (d, 1 H, *J* = 7.8 Hz, H-6''), 8.43 (s, 1 H, H-5) ppm.

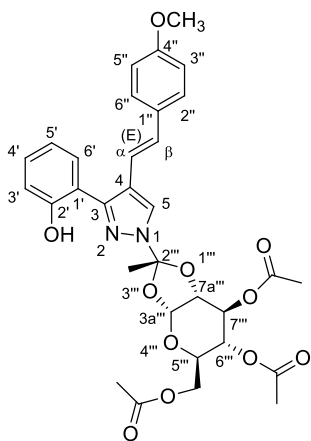
¹³C NMR [(CD₃)₂CO, 75.47 MHz]: δ = 20.6-20.8 (3 × CO₂CH₃), 24.4 (2'''-CH₃), 63.9 (CH₂CO₂CH₃), 68.4 (C-7a'''), 68.8 (C-6'''), 70.1 (C-7'''), 73.8 (C-5'''), 98.9 (C-3a'''), 114.6 (C-2'''), 117.5 (C-3'), 118.4 (C-1'), 119.1 (C-4), 120.3 (C-5'), 124.4 (C-α), 128.0 (C-5), 128.2 (C-6''), 128.4 (C-4''), 129.8 (C-6'), 130.5 (C-4', β), 133.4 (C-5''), 137.2 (C-1''), 149.8 (C-3), 156.7 (C-2'), 169.5 (7'''-COCH₃), 170.2 (6'''-COCH₃), 170.8 (5'''-CH₂OCOCH₃) ppm.

MS (ESI⁺) m/z (%): 661.2 [(M+H)⁺, 100].

HRMS (ESI⁺) m/z calcd for C₃₂H₃₁F₃N₂O₁₀ (M+H)⁺, 661.1998; found: 661.2004.

Note: It was not possible to unequivocally assign the resonances of C-2'', C-3'' and CF₃ carbons due to the very low intensity of the corresponding signals.

1-[(2*R*,3*aR*,5*R*,6*S*,7*S*,7*aR*)-6,7-diacetoxy-5-acetoxymethyl-2-methyltetrahydro-5*H*-[1,3]dioxolo[4,5-*b*]pyran-2-yl]-(*E*)-3-(2-hydroxyphenyl)-4-(4-methoxystyryl)-1*H*-pyrazole (6d)



Pale beige solid, 77%

¹H NMR [(CD₃)₂CO, 300.13 MHz]: δ = 3.83 (s, 3 H, 4'''-OCH₃), 3.99-4.07 (m, 2 H, 5''''*-CH₂OCOCH₃), 4.24-4.31 (m, 2 H, 5''''-CH₂OCOCH₃), 4.42 (ddd, 1 H, *J* = 5.4, 3.1, 0.8 Hz, H-5'''), 4.89 (ddd, 1 H, *J* = 9.6, 3.1, 0.8 Hz, H-6'''), 5.14 (t, 1 H, *J* = 2.9 Hz, H-7'''), 5.64 (d, 1 H, *J* = 5.6 Hz, H-3*a*'''*), 5.75 (d, 1 H, *J* = 5.4 Hz, H-3a'''), 6.93-7.01 (m, 2 H, H-3',5'), 6.95 (d, 2 H, *J* = 8.7 Hz, H-3'',5''), 6.96 (d, 1 H, *J* = 16.2 Hz, H-α/β), 7.15 (d, 1 H, *J* = 16.2 Hz, H-α/β), 7.25 (ddd, 1 H, *J* = 8.2, 7.7, 1.5 Hz, H-4'), 7.50 (d, 2 H, *J* = 8.7 Hz, H-2'',6''), 7.69 (d, 1 H, *J* = 7.5 Hz, H-6'), 8.16 (s, 1 H, H-5), 9.74 (s, 1 H, 2'-OH) ppm.

HRMS (ESI⁺) *m/z* calcd for C₃₂H₃₄N₂O₁₁ (M+H)⁺, 623.2237; found: 623.2235.

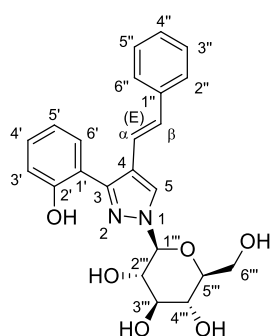
Note: the “*” symbol indicates the resonances of the protons correspondent to the less abundant isomer. The full NMR characterization wasn't presented due to the presence of the two isomers. The structure presented here only represents the *trans* isomer.

5.2.4. Deprotection of the glycosylated products 5 and 6

The deprotection of the sugar moiety of compounds **5a-d** and **6a, 6c** and **6d** was achieved using the Amberlite[®] IRA-400(OH) resin, as reported by Pathak *et al.*⁹⁵ However, we only had access to Amberlite[®] IRA-400(Cl) resin. Consequently, a pre-treatment of this resin was required prior to its use in the reaction. Amberlite[®] IRA-400(Cl) (110.3 mg) was rinsed with 6 mL of a NaOH 1M solution, 6 mL of H₂O and 6 mL of MeOH, in this order, under reduced pressure. These volumes were added 2 mL at the time, to ensure the resin was properly treated. In some cases, the volume of H₂O was increased, to guarantee that the resin was properly washed and the pH of H₂O after passing through the resin was around 7. Afterwards, to a solution of **5a-d** or **6a-d** (0.070 mmol) in 11 mL of MeOH, it was added the Amberlite[®] IRA-400(OH) resin (110.3 mg). The reaction was kept at 30 °C,

under constant stirring for 4 hours or 21 hours. The reaction was monitored by TLC, using CH₂Cl₂:acetone (9:1) as eluent. The resin was removed through a filtration unit and washed with MeOH. Compounds **7a-d** and **8a,b** were dried in a vacuum pump. Compounds **7a-d** were obtained as pale beige solids with a 68 %, 67 %, 77 % and 30% of yield, respectively. Compound **8b** was obtained as a pale beige solid in a quantitative yield.

(E)-1-[β-D-(glycose-1-yl)]-3-(2-hydroxyphenyl)-4-styryl-1H-pyrazole (7a)



Pale beige solid, m.p. 114.4-118.4 °C, 68%

¹H NMR [(CD₃)₂CO, 500.16 MHz]: δ = 3.58 (t, 1 H, *J* = 9.3 Hz, H-4'''), 3.63 (ddd, 1 H, *J* = 9.3, 4.8, 1.8 Hz, H-5'''), 3.67 (t, 1 H, *J* = 9.3 Hz, H-3'''), 3.73 (dd, 1 H, *J* = 11.9, 4.8 Hz, 6'''-CH₂OH), 3.89 (dd, 1 H, *J* = 11.9, 1.8 Hz, 6'''-CH₂OH), 4.07 (t, 1 H, *J* = 9.3 Hz, H-2'''), 5.44 (d, 1 H, *J* = 9.3 Hz, H-1'''), 6.98 (t, 1 H, *J* = 7.6 Hz, H-5'), 7.00 (d, 1 H, *J* = 8.4 Hz, H-3'), 7.07 (d, 1 H, *J* = 16.2 Hz, H-β),

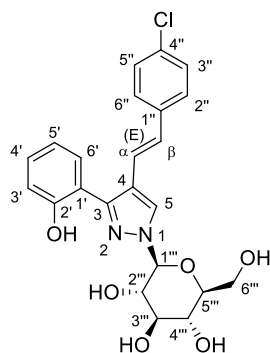
7.25-7.29 (m, 3 H, H-4', 4'', α), 7.38 (t, 2 H, *J* = 7.6 Hz, H-3'', 5''), 7.56 (d, 2 H, *J* = 7.6 Hz, H-2'', 6''), 7.68 (dd, 1 H, *J* = 7.6, 1.2 Hz, H-6'), 8.35 (s, 1 H, H-5) ppm.

¹³C NMR [(CD₃)₂CO, 75.47 MHz]: δ = 62.5 (C-6'''), 71.0 (C-4'''), 73.3 (C-2'''), 78.5 (C-3'''), 80.4 (C-5'''), 90.4 (C-1'''), 117.5 (C-3'), 118.6 (C-1'), 119.6 (C-α), 119.8 (C-5'), 120.7 (C-4), 127.1 (C-2'', 6''), 128.2 (C-4''), 129.5 (C-6'), 129.5 (C-3'', 5''), 130.0 (C-5), 130.2 (C-4'), 130.5 (C-β), 148.5 (C-1''), 151.7 (C-3), 156.8 (C-2') ppm.

MS (ESI⁺) m/z (%): 425.2 [(M+H)⁺, 100].

HRMS (ESI⁺) m/z calcd for C₂₃H₂₄N₂O₆ (M+H)⁺, 425.1706; found: 425.1707.

(E)-4-(4-Chlorostyryl)-1-[β-D-(glycose-1-yl)]-3-(2-hydroxyphenyl)-1H-pyrazole (7b)



Pale beige solid, 67%.

¹H NMR [(CD₃)₂CO, 500.16 MHz]: δ = 3.57 (t, 1 H, *J* = 9.1 Hz, H-4'''), 3.63 (ddd, 1 H, *J* = 9.1, 5.3, 2.2 Hz, H-5'''), 3.67 (t, 1 H, *J* = 9.1 Hz, H-3'''), 3.72 (dd, 1 H, *J* = 12.0, 5.3 Hz, 6'''-CH₂OH), 3.89 (dd, 1 H, *J* = 12.0, 2.2 Hz, 6'''-CH₂OH), 4.06 (t, 1 H, *J* = 9.1 Hz, H-2'''), 5.44 (d, 1 H, *J* = 9.1 Hz, H-1'''), 6.97 (ddd, 1 H, *J* = 7.8, 7.5, 1.0 Hz, H-5'), 7.00 (dd, 1 H, *J* = 7.8, 1.0 Hz, H-3'), 7.07 (d, 1 H, *J* =

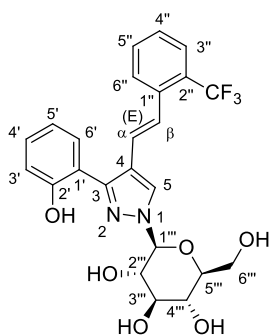
16.3 Hz, H-β), 7.26-7.30 (m, 1 H, H-4'), 7.29 (d, 1 H, $J = 16.3$ Hz, H-α), 7.40 (d, 2 H, $J = 8.5$ Hz, H-3'',5''), 7.59 (d, 2 H, $J = 8.5$ Hz, H-2'',6''), 7.67 (dd, 1 H, $J = 7.8, 1.5$ Hz, H-6'), 8.37 (s, 1 H, H-5) ppm.

^{13}C NMR [$(\text{CD}_3)_2\text{CO}$, 75.47 MHz]: $\delta = 62.5$ (C-6'''), 71.0 (C-4'''), 73.3 (C-2'''), 78.5 (C-3'''), 80.4 (C-5'''), 90.4 (C-1'''), 117.5 (C-3'), 118.5 (C-1'), 119.6 (C-5'), 120.1 (C-α), 120.6 (C-4), 128.6 (C-2'',6''), 129.0 (C-β), 129.5 (C-3'',5'',6'), 130.1 (C-4'), 130.2 (C-5), 137.2 (C-4''), 137.4 (C-1''), 148.6 (C-3), 156.8 (C-2') ppm.

MS (ESI⁺) m/z (%): 459.1 [(M+H)⁺, ^{35}Cl] (100), 461.1 [(M+H)⁺, ^{37}Cl].

HRMS (ESI⁺) m/z calcd for $\text{C}_{23}\text{H}_{23}\text{ClN}_2\text{O}_6$ (M+H)⁺, 459.1314; found: 459.1317.

(E)-1-[β-D-(glycose-1-yl)]-3-(2-hydroxyphenyl)-4-(2-trifluoromethylstyryl)-1H-pyrazole (7c)



Pale beige solid, 77%.

^1H NMR [$(\text{CD}_3)_2\text{CO}$, 500.16 MHz]: $\delta = 3.56$ (t, 1 H, $J = 9.1$ Hz, H-4'''), 3.62 (ddd, 1 H, $J = 9.1, 5.3, 2.0$ Hz, H-5'''), 3.66 (t, 1 H, $J = 9.1$ Hz, H-3'''), 3.72 (dd, 1 H, $J = 12.0, 5.3$ Hz, 6'''-CH₂OH), 3.89 (dd, 1 H, $J = 12.0, 2.0$ Hz, 6'''-CH₂OH), 4.09 (t, 1 H, $J = 9.1$ Hz, H-2'''), 5.47 (d, 1 H, $J = 9.1$ Hz, H-1'''), 6.97 (dt, 1 H, $J = 7.6, 1.0$ Hz, H-5'), 7.01 (dd, 1 H, $J = 8.0, 1.0$ Hz, H-3'), 7.28 (ddd, 1 H, $J = 8.0, 7.6, 1.7$ Hz, H-4'), 7.30-7.33 (m, 2 H, H-α,β), 7.50 (t, 1 H, $J = 7.8$ Hz, H-4''), 7.65 (dd, 1 H, $J = 7.6, 1.7$ Hz, H-6'), 7.68 (t, 1 H, $J = 7.8$ Hz, H-5''), 7.75 (d, 1 H, $J = 7.8$ Hz, H-3''), 7.97 (d, 1 H, $J = 7.8$ Hz, H-6''), 8.45 (s, 1 H, H-5) ppm.

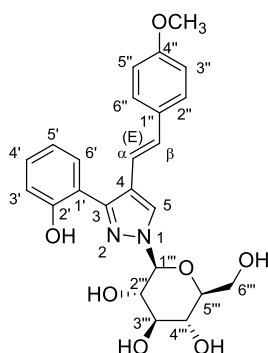
^{13}C NMR [$(\text{CD}_3)_2\text{CO}$, 75.47 MHz]: $\delta = 62.5$ (C-6'''), 71.0 (C-4'''), 73.2 (C-2'''), 78.5 (C-3'''), 80.5 (C-5'''), 90.4 (C-1'''), 117.5 (C-3'), 118.4 (C-1'), 119.4 (C-4), 120.2 (C-4), 124.4 and 125.1 (C-α,β), 126.6 (q, $J = 5.7$ Hz, C-3''), 126.9 (q, $J = 29.6$ Hz, C-2''), 128.2 (C-6''), 128.3 (C-4''), 129.7 (C-6'), 130.3 (C-4'), 131.0 (C-5), 137.2 (C-5''), 144.7 (C-1'), 148.9 (C-3), 156.7 (C-2') ppm.

MS (ESI⁺) m/z (%): 493.2 [(M+H)⁺, 100].

HRMS (ESI⁺) m/z calcd for $\text{C}_{24}\text{H}_{23}\text{F}_3\text{N}_2\text{O}_6$ (M+H)⁺, 493.1579; found: 493.1581.

Note: It was not possible to unequivocally assign the resonance of CF_3 carbon due to the very low intensity of the signals.

(E)-1-[β-D-(glycose-1-yl)]-3-(2-hydroxyphenyl)-4-(4-methoxystyryl)-1H-pyrazole (7d)



Pale beige solid, 30 %.

¹H NMR [(CD₃)₂CO, 500.16 MHz]: δ = 3.42 (t, 1 H, *J* = 8.9 Hz, H-4'''), 3.47-3.61 (m, 1 H, H-5'''), 3.63-3.69 (m, 1 H, H-3'''), 3.69 (s, 3 H, 4''-OCH₃), 3.69-3.79 (m, 2 H, 6'''-CH₂OH), 3.91 (t, 1 H, *J* = 8.9 Hz, H-2'''), 4.08 (t, 1 H, *J* = 4.9 Hz, H-2'''), 5.28 (d, 1 H, *J* = 8.9 Hz, H-1'''), 5.57 (d, 1 H, *J* = 4.9 Hz, H-1'''), 6.32 (d, 1 H, *J* = 11.9 Hz, H-α/β*), 6.52 (d, 1 H, *J* = 11.9 Hz, H-α/β*), 6.81 (d, 2

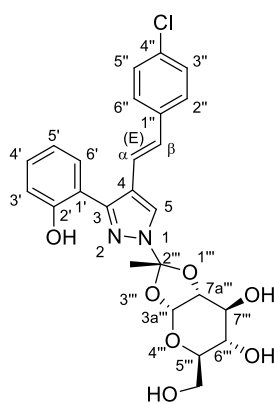
H, *J* = 8.7 Hz, H-3'',5''), 6.82-6.86 (m, 2 H, H-3',5'), 6.86 (d, 1 H, *J* = 16.4 Hz, H-α/β), 6.98 (d, 1 H, *J* = 16.4 Hz, H-α/β), 7.12 (dt, 1 H, *J* = 7.8, 1.6 Hz, H-4'), 7.36 (d, 2 H, *J* = 8.7 Hz, H-2'',6''), 7.54 (dd, 1 H, *J* = 7.8, 1.6 Hz, H-6'), 8.15 (s, 1 H, H-5) ppm.

MS (ESI⁺) m/z (%): 455.2 [(M+H)⁺, 100].

HRMS (ESI⁺) m/z calcd for C₂₄H₂₆N₂O₇ (M+H)⁺, 455.1803; found: 455.1813.

Note: the “*” symbol indicates the resonances of the protons correspondent to the less abundant *cis* isomer. A full NMR characterization wasn't presented due to the presence of the two isomers. The structure displayed here only represents the *trans* isomer.

(E)-4-(4-Chlorostyryl)-1-[(2R,3aR,5R,6S,7S,7aR)-6,7-dihydroxy-5-hydroxymethyl-2-methyltetrahydro-5H-[1,3]dioxolo[4,5-*b*]pyran-2-yl]-3-(2-hydroxyphenyl)-1H-pyrazole (8a)



White solid, quantitative.

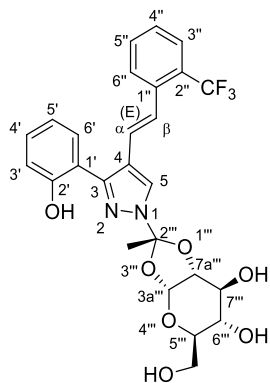
¹H NMR [(CD₃)₂CO, 500.16 MHz]: δ = 2.19 (s, 3 H, 2'''-CH₃), 3.66 (dd, 1 H, *J* = 8.5, 3.9 Hz, H-6'''), 3.73-3.78 (m, 2 H, H-5'''), 5'''-CH₂OH), 3.86 (d, 1 H, *J* = 10.0 Hz, 5'''-CH₂OH), 4.03 (t, 1 H, *J* = 3.9 Hz, H-7'''), 4.30 (t, 1 H, *J* = 4.6 Hz, H-7a'''), 5.98 (d, 1 H, *J* = 4.6 Hz, H-3a'''), 6.97 (t, 1 H, *J* = 7.6 Hz, H-5'), 7.01 (d, 1 H, *J* = 8.3 Hz, H-3'), 7.10 (d, 1 H, *J* = 16.1 Hz, H-β), 7.27-7.30 (m, 1 H, H-4'), 7.29 (d, 1 H, *J* = 16.1 Hz, H-α), 7.40 (d, 2 H, *J* = 8.5 Hz, H-

3'', 5''), 7.58 (d, 2 H, $J = 8.5$ Hz, H-2'', 6''), 7.67 (dd, 1 H, $J = 7.6, 1.1$ Hz, H-6'), 8.38 (s, 1 H, H-5), 10.25 (br s, 1 H, 2'-OH) ppm.

^{13}C NMR [$(\text{CD}_3)_2\text{CO}$, 75.47 MHz]: $\delta = 24.9$ (2'''-CH₃), 63.0 (5'''-CH₂OH), 70.4 (C-6'''), 73.7 (C-7'''), 74.9 (C-5'''), 78.2 (C-7a'''), 99.5 (C-3a'''), 113.8 (C-2'''), 117.5 (C-3'), 118.4 (C-1'), 119.0 (C-4), 120.2 (C-5'), 120.5 (C- α), 127.6 (C-5), 128.6 (C-2'', 6''), 129.1 (C- β), 129.5 (C-6'), 129.6 (C-3'', 5''), 130.3 (C-4'), 133.2 (C-4''), 137.4 (C-1''), 149.2 (C-3), 156.8 (C-2'), ppm.

1-[(2*R*,3*aR*,5*R*,6*S*,7*S*,7*aR*)-6,7-dihydroxy-5-hydroxymethyl-2-methyltetrahydro-5*H*-[1,3]dioxolo[4,5-*b*]pyran-2-yl]-(*E*)-3-(2-hydroxyphenyl)-4-(2-trifluoromethylstyryl)-1*H*-pyrazole (8b)

Pale beige solid, m.p. 75.1-76.1 °C, 66%.



^1H NMR [$(\text{CD}_3)_2\text{CO}$, 500.16 MHz]: $\delta = 2.13$ (s, 3 H, 2'''-CH₃), 3.66 (dd 1 H, $J = 8.9, 4.4$ Hz, H-6'''), 3.73 (t, 1 H, $J = 5.6$ Hz, CH₂OH), 3.78 (dd, 1 H, $J = 5.6, 2.3$ Hz, H-5'''), 3.86 (dd, 1 H, $J = 11.2, 2.3$ Hz, CH₂OH), 4.03 (t, 1 H, $J = 4.4$ Hz, H-7'''), 4.31 (t, 1 H, $J = 4.8$ Hz, H-7a'''), 5.97 (d, 1 H, $J = 4.8$ Hz, H-3a'''), 6.96 (ddd, 1 H, $J = 7.5, 7.7, 1.1$ Hz, H-5'), 7.02 (dd, 1 H, $J = 8.2, 1.1$ Hz, H-3'), 7.27-7.37 (m, 1 H, H-4'), 7.30 (d, 1 H, $J = 16.0$ Hz, H- α), 7.31 (d, 1

H, $J = 16.0$ Hz, H- β), 7.50 (t, 1 H, $J = 7.8$ Hz, H-4''), 7.64 (dd, 1 H, $J = 7.7, 1.6$ Hz, H-6'), 7.68 (t, 1 H, $J = 7.8$ Hz, H-5''), 7.75 (d, 1 H, $J = 7.8$ Hz, H-3''), 7.95 (d, 1 H, $J = 7.8$ Hz, H-6''), 8.43 (s, 1 H, H-5) ppm.

^{13}C NMR [$(\text{CD}_3)_2\text{CO}$, 75.47 MHz]: $\delta = 25.0$ (2'''-CH₃), 63.0 (CH₂OH), 70.4 (C-6'''), 73.8 (C-7'''), 74.9 (C-5'''), 78.3 (C-7a'''), 99.6 (C-3a'''), 113.9 (C-2'''), 117.5 (C-3'), 118.4 (C-1'), 118.8 (C-4), 120.2 (C-5'), 124.2 (C- α), 127.9 (C-5), 128.2 (C-6''), 128.3 (C-4''), 129.6 (C-6'), 130.4 (C-4', β), 133.4 (C-5''), 137.4 (C-1''), 149.5 (C-3), 156.7 (C-2'), ppm.

MS (ESI⁺) m/z (%): 535.2 [(M+H)⁺, 100].

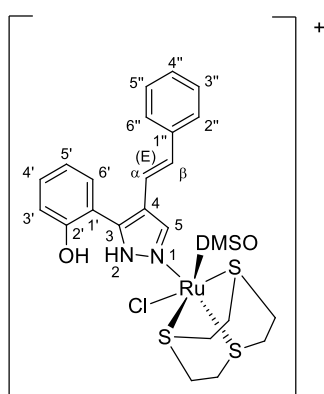
HRMS (ESI⁺) m/z calcd for C₂₆H₂₅F₃N₂O₇ (M+H)⁺, 535.1677; found: 535.1687.

Note: It was not possible to unequivocally assign the resonance of C-2'', C-3'' and CF₃ carbons.

5.2.5. Synthesis of the complexes [Ru([9]aneS₃)((*E*)-3(5)-(2-hydroxyphenyl)-4-styryl-1*H*-pyrazole)(DMSO)Cl]Cl

The procedure employed for the synthesis of the complexes of ruthenium and pyrazoles was adopted from Silva *et al.*²⁰ To a solution of compound **4** (0.22 mmol) in 25 mL of MeOH, it was added 0.8 equiv. of Ru([9]aneS₃)(DMSO)Cl₂ (75 mg, 0.17 mmol). The reaction mixture was refluxed under nitrogen, at 60 °C and constant stirring for 18h. After that period, the obtained solution was evaporated until one-third of the initial volume of methanol was left. To that solution, a large volume of diethyl ether was added. To aid the formation of the precipitate, the solution was kept under a cool temperature using ice. Whenever the precipitation process was concluded, the solid was filtered, washed with diethyl ether and immediately dried in the vacuum pump. The desired complexes **9a-d** were obtained as yellow solids, with 30 %, 72 % and 51% of yield. The yield of the complex **9d** was not calculated. Depending on the solubility of the compounds, some precipitates were easier to form than others. For that reason, for obtaining the precipitates of **9a** and **9d** it was necessary to resort to liquid nitrogen to cool down the solution.

[Ru([9]aneS₃)((*E*)-3(5)-(2-hydroxyphenyl)-4-styryl-1*H*-pyrazole)(DMSO)Cl]Cl (**9a**)



Yellow solid, 30%.
¹H NMR [DMSO-D₆, 500.16 MHz][§]: δ = 2.57-2.85 (m, 12 H, CH₂, [9]aneS₃), 2.95-3.06 (m, 6 H, 2 × CH₃, DMSO), 6.91-6.98 (m, 2 H, H-3''*,5''*), 7.00-7.05 (m, 1 H, H-5'), 7.03 (d, 1 H, *J* = 16.2 Hz, H-α), 7.07-7.08 (m, 1 H, H-3'), 7.10 (d, 1 H, *J* = 16.2 Hz, H-β), 7.19-7.31 (m, 4 H, H-4',4''*,4'',4''*), 7.33-7.36 (m, 2 H, H-3''',5'''), 7.38 (t, 2 H, *J* = 7.6 Hz, H-3'',5''), 7.40 (dd, 1 H, *J* = 8.1, 1.8 Hz, H-

[§] The “*” symbol present in the complexes **9a-d** NMR characterization indicates the resonance of the protons correspondent to the less abundant complex. The stereochemistry depicted for complexes **9a-d** is merely representative.

6'*), 7.50 (d, 2 H, $J = 7.4$ Hz, H-2''*,6''*), 7.52 (dd, 1 H, $J = 7.8, 1.6$ Hz, H-6'), 7.55 (d, 2 H, $J = 7.6$ Hz, H-2'',6''), 8.29 (d, 1 H, $J = 2.0$ Hz, H-5), 8.34 (d, 1 H, H-5*), 10.65 (s, 1 H, 2'-OH*), 10.90 (s, 1 H, 2'-OH), 12.90 (s, 1 H, NH*), 12.93 (s, 1 H, NH) ppm.

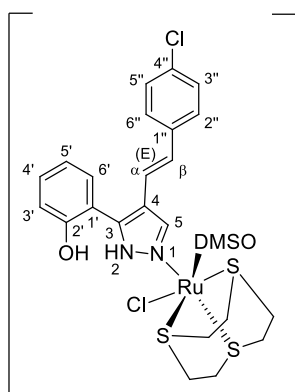
^{13}C NMR [DMSO-D₆, 75.47 MHz]: $\delta = 30.1\text{-}35.2$ ($\underline{\text{C}}\text{H}_2$, [9]aneS₃), 114.1 (C-1'), 114.5 (C-1'*), 116.3 (C-3',3'*), 117.3-120.0 (C-4,4*,5',5'*, α , α *), 125.7 (C-2''*,6''*), 126.2 (C-2'',6''), 127.5 (C-4''*), 127.7 (C-4''), 128.7 (C- β *), 128.8 (C- β), 128.9 (C-3'',3''*,5'',5''*), 129.8 (C-6'), 130.0 (C-6'*), 130.6 (C-4'*), 130.9 (C-4'*), 137.0 (C-1''*), 137.1 (C-1''), 138.9 (C-3*), 139.0 (C-3), 140.6 (C-5*), 141.3 (C-5), 154.8 (C-2', 2'*) ppm.

FT-IR (KBr, $\bar{\nu}_{\text{max}}$ (cm⁻¹)): 2961 m ($\nu\text{C-H}$ macro), 2921 s ($\nu\text{C-H}$ macro), 1635 m ($\nu\text{C=N}$), 1108 vs ($\nu\text{C-OH}$), 967 m ($\omega\text{C}\alpha=\text{C}\beta$), 908 m ($\rho\text{C-H}$ (DMSO)), 826 m ($\rho\text{C-H}$ (DMSO)), 760 vs ($\nu\text{C-H}$), 697 vs ($\nu\text{C-H}$), 493 w ($\nu\text{Ru-S}$ (macro)), 425 m ($\nu\text{Ru-S}$ (DMSO)), 377 w ($\nu\text{Ru-N}$).

MS (ESI⁺) m/z (%): 657.1 (M⁺, 100).

Anal. Calcd. for (Ru(C₆H₁₂S₃)(C₁₇H₁₄N₂O)(C₂H₆SO)Cl₂)·0.3H₂O (698.2) (%): C, 43.01; H, 4.706; N, 4.012; S, 18.37. Found: C, 43.05; H, 4.632; N, 4.031; S, 16.14.

[Ru([9]aneS₃)(*E*)-4-(4-chlorostyryl)-3(5)-(2-hydroxyphenyl)-1*H*-pyrazole)(DMSO)Cl]Cl (9b)



Yellow solid, 72%.

^1H NMR [DMSO-D₆, 500.16 MHz]: $\delta = 2.59\text{-}2.88$ (m, 12 H, $\underline{\text{C}}\text{H}_2$, [9]aneS₃), 2.91-3.10 (m, 6 H, 2 \times $\underline{\text{C}}\text{H}_3$, DMSO), 6.89-6.98 (m, 2 H, H-3''*,5''*), 7.01 (t, 1 H, $J = 7.6$ Hz, H-5'), 7.04-7.11 (m, 1 H, H-3'), 7.08 (d, 1 H, $J = 16.2$ Hz, H- α), 7.23 (d, 1 H, $J = 16.2$ Hz, H- β), 7.26-7.41 (m, 2 H, H-4',4'*), 7.43 (d, 2 H, $J = 8.5$ Hz, H-3'',5''), 7.51 (dd, 1 H, $J = 7.6, 1.4$ Hz, H-6'), 7.57 (d, 2 H, $J = 8.5$ Hz, H-2''*,6''*),

8.30 (d, 1 H, $J = 1.9$ Hz, H-5), 8.33 (d, 1 H, $J = 1.3$ Hz, H-5*), 10.65 (s, 1 H, 2'-OH*), 10.90 (s, 1 H, 2'-OH), 12.91 (s, 1 H, NH*), 12.95 (s, 1 H, NH) ppm.

^{13}C NMR [DMSO-D₆, 75.47 MHz]: $\delta = 30.2\text{-}35.2$ ($\underline{\text{C}}\text{H}_2$, [9]aneS₃), 114.1 (C-1'*), 116.1 (C-1'), 116.3 (C-3',3'*), 118.2 (C- α), 118.5 (C- α *), 118.8 (C-4*), 119.2 (C-4), 119.7 (C-5'*), 119.9 (C-5'), 127.8 (C-2''*,6''*), 127.9 (C-2'',6''), 128.7 (C- β), 128.8 (C-

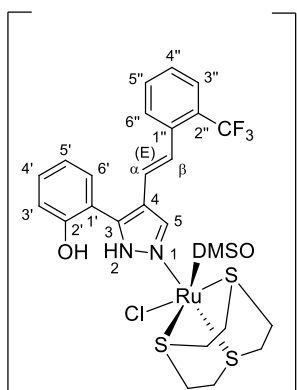
3'',3''*,5'',5''*), 129.9 (C-6'), 130.1 (C-6'*), 130.7 (C-4'*), 130.9 (C-4'), 131.7 (C-4''*), 131.2 (C-4''), 136.0 (C-1''), 136.1 (C-1''*), 139.1 (C-3*), 139.2 (C-3), 140.7 (C-5*), 141.4 (C-5), 154.8 (C-2', 2'*) ppm.

FT-IR (KBr, $\bar{\nu}_{\max}$ (cm⁻¹)): 2961 m (νC–H macro), 2926 s (νC–H macro), 1639 m (νC=N), 1108 s (νC–OH), 967 m (ωCα=Cβ), 909 m (ρC–H (DMSO)), 826 m (ρC–H (DMSO)), 759 m (νC–H), 686 m (νC–H), 455 w (νRu–S (macro)), 425 m (νRu–S (DMSO)), 373 w (νRu–N).

MS (ESI⁺) m/z (%): 693.0 (M⁺, ³⁷Cl) (100), 691.0 (M⁺, ³⁵Cl).

Anal. Calcd. for (Ru(C₆H₁₂S₃)(C₁₇H₁₃N₂OCl)(C₂H₆SO)Cl₂) (727.2) (%): C, 41.32; H, 4.304; N, 3.858; S, 17.61. Found: C, 42.13; H, 4.607; N, 4.057; S, 15.48.

[Ru([9]aneS₃)((E)-3(5)-(2-hydroxyphenyl)-4-(2-trifluoromethylstyryl)-1H-pyrazole)(DMSO)Cl]Cl (9c)



Yellow solid, 51%.

¹H NMR [DMSO-D₆, 500.16 MHz]: δ = 2.59-2.86 (m, 12 H, CH₂, [9]aneS₃), 2.88-3.04 (m, 6 H, 2 × CH₃, DMSO), 6.90-6.91 (m, 1 H, H-3''*), 6.94 (t, 1 H, *J* = 7.5 Hz, H-5''*), 6.98 (t, 1 H, *J* = 7.5 Hz, H-5'), 7.03 (d, 1 H, *J* = 15.8 Hz, H-β), 7.06-7.07 (m, 1 H, H-3'), 7.10 (d, 1 H, *J* = 15.8 Hz, H-α), 7.24 (d, 1 H, *J* = 15.7 Hz, H-α/β*), 7.30-7.36 (m, 2 H, H-4',4'*), 7.49 (t, 1 H, *J* = 7.7 Hz, H-4''), 7.46 (d, 1 H, *J* = 7.5,

H-6'), 7.61-7.64 (m, 1 H, H-5''*), 7.67 (t, 1 H, *J* = 7.7 Hz, H-5''), 7.71 (d, 1 H, *J* = 8.0 Hz, H-3''*), 7.73 (d, 1 H, *J* = 7.7 Hz, H-3''), 7.83 (d, 1 H, *J* = 8.0 Hz, H-6''*), 7.89 (d, 1 H, *J* = 7.7 Hz, H-6''), 8.30 (d, 1 H, *J* = 1.9 Hz, H-5), 8.32 (d, 1 H, H-5*), 10.58 (s, 1 H, 2'-OH*), 10.80 (s, 1 H, 2'-OH), 13.09 (s, 1 H, NH), 13.10 (s, 1 H, NH*) ppm.

¹³C NMR [DMSO-D₆, 75.47 MHz]: δ = 30.3-35.1 (CH₂, [9]aneS₃), 114.0 (C-1'*), 114.3 (C-1'), 116.3 (C-3',C-3''*), 118.1 (C-4*), 118.7 (C-4), 119.5 (C-5'*), 119.6 (C-5'), 112.5 (C-α), 122.9 (C-β), 124.2 (C-α/β*), 127.1 (C-6''*), 127.4 (C-6''), 127.6 (C-4''*), 127.8 (C-4''), 130.1 (C-6'), 130.4 (C-6'*), 130.8 (C-4'*), 131.0 (C-4'), 132.8 (C-5''*), 132.9 (C-5''), 135.7 (C-1''*), 135.8 (C-1''), 140.0 (C-3*), 140.2 (C-3), 140.9 (C-5*), 141.7 (C-5), 155.0 (C-2'*), 155.1 (C-2'*) ppm.

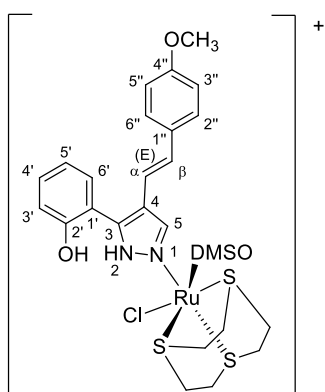
FT-IR (KBr, $\bar{\nu}_{\max}$ (cm⁻¹)): 2923 m (νC–H macro), 1637 m (νC=N), 1107 vs (νC–OH), 965 m (ωCα=Cβ), 910 w (ρC–H (DMSO)), 829 w (ρC–H (DMSO)), 762 m (νC–H), 682 m (νC–H), 425 m (νRu–S (DMSO)), 375 w (νRu–N).

MS (ESI⁺) m/z (%): 725.1 (M⁺, 100).

Anal. Calcd. for (Ru(C₆H₁₂S₃)(C₁₈H₁₃N₂OF₃)(C₂H₆SO)Cl₂)·0.2H₂O (764.4) (%): C, 40.85; H, 4.140; N, 3.665; S, 16.78. Found: C, 40.91; H, 4.134; N, 3.831; S, 15.97.

Note: It was not possible to unequivocally assign the resonances of C-2'', C-3'' and CF₃ carbons.

[Ru([9]aneS₃)((E)-3(5)-(2-hydroxyphenyl)-4-(4-methoxystyryl)-1H-pyrazole)(DMSO)Cl]Cl (9d)



Yellow solid.

¹H NMR [DMSO-D₆, 500.16 MHz]: δ = 2.59-2.87 (m, 12 H, CH₂, [9]aneS₃), 2.95-3.14 (m, 6 H, 2 × CH₃, DMSO), 3.76 (s, 3 H, 4''-OCH₃*), 3.77 (s, 3 H, 4''-OCH₃), 6.84 (d, 1 H, *J* = 16.3 Hz, H-α), 6.92 (d, 2 H, *J* = 8.9 Hz, H-3''*,5''*), 6.95 (d, 2 H, *J* = 8.8 Hz, H-3'',5''), 6.99-7.05 (m, 1 H, H-5'), 7.01 (d, 1 H, *J* = 7.8 Hz, H-3'*), 7.06 (d, 1 H, *J* = 7.9 Hz, H-3'), 7.17 (d, 1 H, *J* = 16.3 Hz, H-β), 7.28 (dt, 1 H, *J* =

7.8, 1.4 Hz, H-4'*), 7.32 (ddd, 1 H, *J* = 7.9, 7.8, 1.3 Hz, H-4'), 7.41 (dd, 1 H, *J* = 7.8 Hz, H-6'*), 7.44 (d, 2 H, *J* = 8.9 Hz, H-2''*,6''*), 7.49 (d, 2 H, *J* = 8.8 Hz, H-2'',6''), 7.53 (dd, 1 H, *J* = 7.8, 1.3 Hz, H-6'), 8.24 (d, 1 H, *J* = 2.1 Hz, H-5*), 8.26 (d, 1 H, *J* = 1.9 Hz, H-5), 10.65 (s, 1 H, 2'-OH*), 10.90 (s, 1 H, 2'-OH), 12.85 (s, 1 H, NH*), 12.90 (s, 1 H, NH) ppm.

¹³C NMR [DMSO-D₆, 75.47 MHz]: δ = 30.1-35.2 (CH₂, [9]aneS₃), 55.1 (4''-OCH₃) 114.1 (C-3''*,5''*), 114.2 (C-3'',5''), 114.9 (C-1'), 115.6 (C-α), 116.3 (C-3',3'*), 118.9 (C-4), 119.6 (C-4*), 119.7 (C-5'), 119.8 (C-5*), 127.4 (C-2''*,6''*), 127.5 (C-2'',6''), 128.8 (C-1''), 129.6 (C-6'*), 129.8 (C-6'), 129.9 (C-β), 130.4 (C-4'), 130.7 (C-4'*), 138.4 (C-3), 138.6 (C-3*), 140.3 (C-5*), 141.0 (C-5), 154.7 (C-2',2'*), 158.8 (C-4''), 158.9 (C-4''*) ppm.

FT-IR (KBr, $\bar{\nu}_{\max}$ (cm⁻¹)): 2966 m (νC–H macro), 2926 m (νC–H macro), 1605 m (νC=N), 1110 m (νC–OH), 966 m (ωCα=Cβ), 908 m (ρC–H (DMSO)), 822 m (ρC–H (DMSO)), 760 m (νC–H), 687 m (νC–H), 493 w (νRu–S (macro)), 457 w (νRu–S (macro)), 424 m (νRu–S (DMSO)), 373 w (νRu–N).

MS (ESI⁺) m/z (%): 687.1 (M⁺, 100).

Anal. Calcd. for (Ru(C₆H₁₂S₃)(C₁₈H₁₆N₂O₂)(C₂H₆SO)Cl₂) (722.8) (%): C, 43.21; H, 4.741; N, 3.876; S, 17.74. Found: C, 43.38; H, 4.747; N, 4.090; S, 15.40.

5.2.6. Biological assays

5.2.6.1. Preparation of the stock solutions

All the stock solutions were freshly prepared in 100% DMSO, at a concentration of 20 mM. Since DMSO is toxic to cells at certain concentrations,¹⁰⁰ the dilutions, which were performed with the appropriate cell culture medium, were arranged so that the maximum concentration of DMSO in each well was 0.5% (v/v). Parallel experiments, which are not presented here, revealed that the cell viability was not compromised upon exposure to 0.5% (v/v) DMSO for both cell lines studied.

5.2.6.2. Thaw of the cell lines

The cell lines, which were provided by the Faculty of Pharmacy of University of Porto, were preserved at –80 °C. The thaw of the cells was accomplished by resuspending them in 45 mL of previously heated culture medium at 37 °C. Then, a centrifugation at 210 g was performed for 5 minutes, at 37 °C. The supernatant was discarded and the pellet was resuspended in 15 mL of culture medium at 37 °C. This volume was added to a 75 cm² flask, where the cells were allowed to grow, as intended.

5.2.6.3. Cell culture

Two human cell lines were tested in the present work: the human lung fibroblast cell line (MRC-5) and the human gastric adenocarcinoma cell line (AGS). The cells were cultured as monolayers and maintained at 37 °C, in a humidified incubator under 5% of CO₂. The AGS cancer cell line was maintained in DMEM (1X) + GlutaMAX™-1 (Dulbecco's Modified Eagle Medium) and the MRC-5 cell line was maintained in MEM

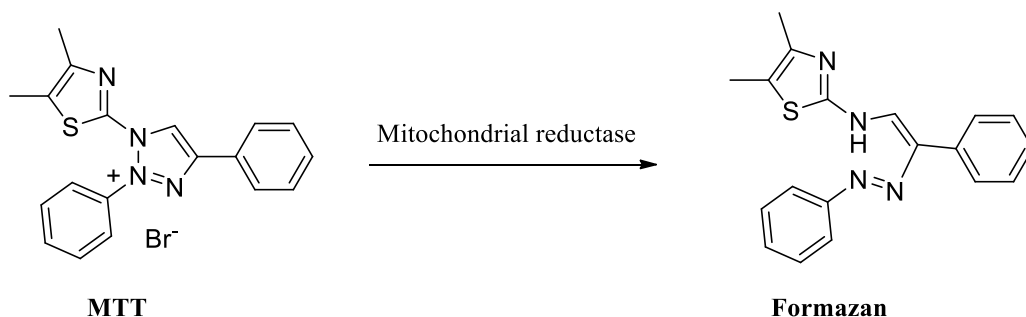
(1X) + GlutaMAX™-1 (Minimum Essential Medium). Each culture medium was previously supplemented with 10% of FBS (fetal bovine serum) and 1% of penicillin-streptomycin.

Whenever the cells reached 80% of confluence, the cell culture medium was rejected and the 75 cm² flask was washed twice with 8 mL of PBS (phosphate-buffered saline). Afterwards, 2.5 mL of trypsin (0.25%) were added and the flask was placed in the incubator for 3 minutes. After that period, 5 mL of the proper culture medium was added and the obtained mixture was transferred to a centrifuge tube and centrifuged for 3 minutes, at 1300 rpm and 37 °C. The supernatant was discarded and the pellet was resuspended in 4 mL of culture medium. The desired volume of this mixture was then transferred to a new 75 cm² flask, already containing 13 mL of the adequate culture medium.

The number of cells was assessed by transferring 10 µL of the solution of the resuspended cells in 4 mL of culture medium to an eppendorf with 90 µL of trypan blue. The number of cells was counted resorting to a Neubauer chamber.

5.2.6.4. MTT assay

The assessment of the cytotoxic activity of the compounds was performed by the MTT assay. This colorimetric assay is widely used to quantify the cell viability.¹⁰¹ This assay is based on the reduction of MTT [3-(4,5-dimethylthiazol-2-yl)-2,5-diphenyltetrazolium bromide] into the insoluble purple formazan. The reduction of MTT is caused by the enzymatic activity of the mitochondria, *via* the cleavage of the tetrazolium ring (see Scheme 4.1).



Scheme 4.1 – Mitochondrial reduction of MTT to formazan, adapted from Präbst *et al.*¹⁰¹

The formed formazan crystals are impermeable to cell membranes, so, they hoard inside the viable cells. Therefore, the amount of formazan crystals is a good marker for the

cellular viability. After solubilization, the formazan is spectrophotometrically measured at its absorbance maximum (570 nm).

The MTT assay was performed following the adaptation of Videira *et al.*¹⁰² The cells were plated at the density of 1.5×10^4 cells/cm² for AGS and 2.0×10^4 cells/cm² for MRC-5, in 96-well microplates. After 24 hours, the culture medium of the wells was aspirated and 100 μ L of the proper compound dilution was added in triplicate. The 96-well microplates were incubated at 37 °C and 5% of CO₂ for 24 hours. After that period, the solutions of the testing compounds were removed and a solution of 100 μ L of MTT:culture medium (1:10) was added to each well. After 2 hours of incubation, the MTT:culture medium solution was removed and the formed formazan was dissolved in 200 μ L of DMSO:isopropanol (3:1). The optical absorbance was measured at 570 nm, using a microplate reader Thermo Scientific™ Multiskan™ GO.

5.2.6.5. Statistical analysis

The statistical analysis of the cell viability data was made using the GrapPad Prism® 6 software. The measured absorbance was converted into percentage of cell viability relative to the control, according to the formula presented in the Equation 5.1. The OD sample is the absorbance measure for wells containing drug-treated cells and the OD control represents the absorbance measured for the wells with untreated cells. The percentage of cell viability of the control was calculated as seen in the Equation 5.2, where \bar{x} OD control represents the mean of the absorbance measured for the wells with untreated cells.

$$\frac{\text{OD sample}}{\text{OD control}} \times 100 \quad (5.1)$$

$$\frac{\text{OD control}}{\bar{x} \text{ OD control}} \times 100 \quad (5.2)$$

The results (chapter 4) are expressed as the mean \pm mean standard deviation obtained from three to four independent experiments, each comprising three replicate

measurements performed for each concentration of each compound tested, plus the untreated control.

The significant outliers of the cell viability data were excluded resorting to Grubb's test, also known as the extreme studentized deviate method from GraphPad. The distribution of the data was evaluated by the D'Agostino-Pearson normality test. According to this test, the cell viability data for both AGS and MRC-5 cell line presented a normal distribution. The statistical analysis was performed by one-way ANOVA, followed by the Dunnetts's *post hoc* test for statistical comparison between the experimental data, the *p*-values minor than 0.05 were deemed significant.

The IC₅₀ values were determined by fit spline, using the method point-to-point to create a curve. To avoid redundancy the curves were not shown in this work.

Conclusions and future perspectives

The glycosylation of (*E*)-3(5)-(2-hydroxyphenyl)-4-styryl-1*H*-pyrazoles **4a-d** via the Koenigs-Knorr reaction afforded new (*E*)-1-[β -D-(2,3,4,6-tetra-*O*-acetylglycose-1-yl)]-3-(2-hydroxyphenyl)-4-styryl-1*H*-pyrazoles **5a-d**, and 1-[(2*R*,3*aR*,5*R*,6*S*,7*S*,7*aR*)-6,7-diacetoxy-5-acetoxymethyl-2-methyltetrahydro-5*H*-[1,3]dioxolo[4,5-*b*]pyran-2-yl]-(*E*)-3-(2-hydroxyphenyl)-4-styryl-1*H*-pyrazoles **6a-d**. Generally, compounds **6** were the main reaction product. However, the yield of compounds **6** was particularly affected by the presence of water in the reaction solvent – dichloromethane. The global yield of the glycosylation reaction is increased when dichloromethane is dried over calcium hydride, distilled and kept stored with molecular sieves. Furthermore, longer reaction times (10 days) also seem to increase the global yield of the glycosylation reaction.

The cleavage of the acetyl protecting groups of the sugar moiety of compounds **5** and **6** resulted in the novel compounds (*E*)-1-[β -D-(glycose-1-yl)]-3-(2-hydroxyphenyl)-4-styryl-1*H*-pyrazoles **7a-d** and compounds 1-[(2*R*,3*aR*,5*R*,6*S*,7*S*,7*aR*)-6,7-dihydroxy-5-hydroxymethyl-2-methyltetrahydro-5*H*-[1,3]dioxolo[4,5-*b*]pyran-2-yl]-(*E*)-3-(2-hydroxyphenyl)-4-styryl-1*H*-pyrazoles **8a,b**. The structure of all the mentioned compounds was determined by 1D and 2D NMR techniques and by mass spectrometry. These analyses disclosed that all the obtained products are *N*-glycosylated.

The Ru[9]aneS₃ coordination with (*E*)-3(5)-(2-hydroxyphenyl)-4-styryl-1*H*-pyrazoles afforded the novel complexes [Ru([9]aneS₃)(*E*)-3(5)-(2-hydroxyphenyl)-4-styryl-1*H*-pyrazole)(DMSO)Cl]Cl **9a-d**. The purity and structure of the ruthenium-pyrazoles was determined by 1D and 2D NMR techniques, infrared spectroscopy (FT-IR), mass spectrometry and elemental analysis. Coordination of the pyrazole derivatives to ruthenium occurred *via* the replacement of one chloride rather than the DMSO, as confirmed by the mass spectrometry results, NMR and FT-IR.

The cytotoxic activity of compounds **4a-d**, **7a-c**, **8a,b** and **9a-d** was evaluated by the MTT colorimetric assay on the cancer AGS and healthy MRC-5 cell lines. The most potent compounds against the AGS cancer cell line are **4b** and **9d** with IC₅₀ values of 37.0 and 18.3 μ M, respectively. Among these two compounds, **4b** has less selectivity than **9d**. In fact, compound **4b** presents high cytotoxicity against the MRC-5 cell line (IC₅₀ = 45.0 μ M) and, consequently, it has a narrow safety margin. Complex **9d** has an IC₅₀ value of

62.2 μM against MRC-5 cell line, which is approximately three-fold higher than the one obtained against the AGS cancer cell line. Complex **9d** is more selective than the pure ligand, **4d**, which suggests that the Ru coordination improves the selectivity. The insertion of a sugar moiety into the pyrazole scaffold also increased the selectivity of the compounds when compared to their precursors. Concerning the cytotoxic activity, the insertion of the sugar moiety was beneficial for the *ortho*-CF₃ compounds but jeopardized the cytotoxic activity of the *para*-Cl compounds. In the future, it is appropriate to finish the studies for the remaining compounds against the MRC-5 cell line. Also, the compounds should be tested against other cancer and healthy cell lines.

Hereafter, it is also worth exploring the effect of an electron-donating group in the phenyl ring of the glycosylated products and to test the influence of the substituent position by synthesizing these glycosylated products substituted with *-ortho*-Cl or *-para*-CF₃ in the phenyl ring. Furthermore, it is also envisioned to expand the Ru([9]aneS₃)(pyrazole) family by substituting the phenyl ring with other electron-donating groups.

References

- (1) Ferlay, J.; Soerjomataram, I.; Dikshit, R.; Eser, S.; Mathers, C.; Rebelo, M.; Parkin, D. M.; Forman, D.; Bray, F. Cancer Incidence and Mortality Worldwide: Sources, Methods and Major Patterns in GLOBOCAN 2012. *Int. J. Cancer* **2015**, *136* (5), E359–E386.
- (2) Cooper, G. M.; Hausman, R. E. *The Cell: A Molecular Approach*, 2nd edition; *Sinauer Associates*, **2013**.
- (3) Lee, E. Y. H. P.; Muller, W. J. Oncogenes and Tumor Suppressor Genes. *Cold Spring Harb. Perspect. Biol.* **2010**, *2* (10), a003236.
- (4) Miranda, N.; Portugal, C. Doenças Oncológicas em Números – 2015, Available online at: <https://www.dgs.pt/em-destaque/portugal-doencas-oncologicas-em-numeros-201511.aspx> (accessed March 13, 2018).
- (5) Yasbin, R. E.; Matthews, C. R.; Clarke, M. J. Mutagenic and Toxic Effects of Ruthenium. *Chem. Biol. Interact.* **1980**, *31* (3), 355–365.
- (6) Chauhan, S.; Paliwal, S.; Chauhan, R. Anticancer Activity of Pyrazole via Different Biological Mechanisms. *Synth. Commun.* **2014**, *44* (10), 1333–1374.
- (7) Purandare, A. V.; Chen, Z.; Huynh, T.; Pang, S.; Geng, J.; Vaccaro, W.; Poss, M. A.; Oconnell, J.; Nowak, K.; Jayaraman, L. Pyrazole Inhibitors of Coactivator Associated Arginine Methyltransferase 1 (CARM1). *Bioorg. Med. Chem. Lett.* **2008**, *18* (15), 4438–4441.
- (8) Hassan, G. S.; Kadry, H. H.; Abou-Seri, S. M.; Ali, M. M.; Mahmoud, A. E. E.-D. Synthesis and in Vitro Cytotoxic Activity of Novel pyrazolo[3,4-*d*]pyrimidines and Related Pyrazole Hydrazones toward Breast Adenocarcinoma MCF-7 Cell Line. *Bioorg. Med. Chem.* **2011**, *19* (22), 6808–6817.
- (9) Abd-El Gawad, N. M.; Georgey, H. H.; Ibrahim, N. A.; Amin, N. H.; Abdelsalam, R. M. Synthesis of Novel Pyrazole and Dihydropyrazoles Derivatives as Potential Anti-Inflammatory and Analgesic Agents. *Arch. Pharm. Res.* **2012**, *35* (5), 807–821.
- (10) Sun, J.; Zhou, Y. Synthesis and Antifungal Activity of the Derivatives of Novel Pyrazole Carboxamide and Isoxazolol Pyrazole Carboxylate. *Molecules* **2015**, *20* (3), 4383–4394.
- (11) Hu, D.-Y.; Wan, Q.-Q.; Yang, S.; Song, B.-A.; Bhadury, P. S.; Jin, L.-H.; Yan, K.;

- Liu, F.; Chen, Z.; Xue, W. Synthesis and Antiviral Activities of Amide Derivatives Containing the α -Aminophosphonate Moiety. *J. Agric. Food Chem.* **2008**, *56* (3), 998–1001.
- (12) Raffa, D.; Maggio, B.; Raimondi, M. V.; Cascioferro, S.; Plescia, F.; Cancemi, G.; Daidone, G. Recent Advanced in Bioactive Systems Containing Pyrazole Fused with a Five Membered Heterocycle. *Eur. J. Med. Chem.* **2015**, *97* (1), 732–746.
- (13) Havrylyuk, D.; Roman, O.; Lesyk, R. Synthetic Approaches, Structure Activity Relationship and Biological Applications for Pharmacologically Attractive Pyrazole/pyrazoline-Thiazolidine-Based Hybrids. *Eur. J. Med. Chem.* **2016**, *113*, 145–166.
- (14) Clemett, D.; Goa, K. L. Celecoxib: A Review of Its Use in Osteoarthritis, Rheumatoid Arthritis and Acute Pain. *Drugs* **2000**, *59* (4), 957–980.
- (15) Deneke, J.; Luckow, V.; Guserle, R.; Passler, H. H. Transsynovial Kinetics of Lonazolac and Its Hydroxy Metabolite in Synovitis Patients. *Int. J. Clin. Pharmacol. Ther.* **1998**, *36* (8), 418–424.
- (16) Elkady, M.; Nieß, R.; Schaible, A. M.; Bauer, J.; Luderer, S.; Ambrosi, G.; Werz, O.; Laufer, S. A. Modified Acidic Nonsteroidal Anti-Inflammatory Drugs as Dual Inhibitors of mPGES-1 and 5-LOX. *J. Med. Chem.* **2012**, *55* (20), 8958–8962.
- (17) Schenone, S.; Bruno, O.; Ranise, A.; Bondavalli, F.; Brullo, C.; Fossa, P.; Mosti, L.; Menozzi, G.; Carraro, F.; Naldini, A.; Bernini, C.; Manetti, F.; Botta, M. New pyrazolo[3,4-D]pyrimidines Endowed with A431 Antiproliferative Activity and Inhibitory Properties of Src Phosphorylation. *Bioorg. Med. Chem. Lett.* **2004**, *14* (10), 2511–2517.
- (18) Zheng, L. W.; Li, Y.; Ge, D.; Zhao, B. X.; Liu, Y. R.; Lv, H. S.; Ding, J.; Miao, J. Y. Synthesis of Novel Oxime-Containing Pyrazole Derivatives and Discovery of Regulators for Apoptosis and Autophagy in A549 Lung Cancer Cells. *Bioorg. Med. Chem. Lett.* **2010**, *20* (16), 4766–4770.
- (19) Daidone, G.; Maggio, B.; Raffa, D.; Plescia, S.; Schillaci, D.; Raimondi, M. V. Synthesis and in Vitro Antileukemic Activity of New 4-Triazenopyrazole Derivatives. *Farmaco* **2004**, *59* (5), 413–417.
- (20) Marques, J.; Silva, V. L. M.; Silva, A. M. S.; Marques, M. P. M.; Braga, S. S. Ru(II) Trithiacyclononane 5-(2-Hydroxyphenyl)-3-[(4-Methoxystyryl)pyrazole], a

- Complex with Facile Synthesis and High Cytotoxicity against PC-3 and MDA-MB-231 Cells. *Complex Met.* **2014**, *1* (1), 7–12.
- (21) Wang, M.; Xu, S.; Lei, H.; Wang, C.; Xiao, Z.; Jia, S.; Zhi, J.; Zheng, P.; Zhu, W. Design, Synthesis and Antitumor Activity of Novel Sorafenib Derivatives Bearing Pyrazole Scaffold. *Bioorg. Med. Chem.* **2017**.
- (22) Angelucci, A.; Schenone, S.; Gravina, G. L.; Muzi, P.; Festuccia, C.; Vicentini, C.; Botta, M.; Bologna, M. Pyrazolo[3,4-*d*]pyrimidines c-Src Inhibitors Reduce Epidermal Growth Factor-Induced Migration in Prostate Cancer Cells. *Eur. J. Cancer* **2006**, *42* (16), 2838–2845.
- (23) Luo, Y.; Zhang, S.; Qiu, K. M.; Liu, Z. J.; Yang, Y. S.; Fu, J.; Zhong, W. Q.; Zhu, H. L. Synthesis, Biological Evaluation, 3D-QSAR Studies of Novel Aryl-2*H*-Pyrazole Derivatives as Telomerase Inhibitors. *Bioorg. Med. Chem. Lett.* **2013**, *23* (4), 1091–1095.
- (24) Hanke, J. H.; Gardner, J. P.; Dow, R. L.; Changelian, P. S.; Brissette, W. H.; Weringer, E. J.; Pollok, B. A.; Connelly, P. A. Discovery of a Novel, Potent, and Src Family-Selective Tyrosine Kinase Inhibitor: Study of Lck- and FynT-Dependent T Cell Activation. *J. Biol. Chem.* **1996**, *271* (2), 695–701.
- (25) Wright, W. E.; Shay, J. W. Cellular Senescence as a Tumor-Protection Mechanism: The Essential Role of Counting. *Curr. Opin. Genet. Dev.* **2001**, *11* (1), 98–103.
- (26) Bernardes de Jesus, B.; Blasco, M. A. Telomerase at the Intersection of Cancer and Aging. *Trends Genet.* **2013**, *29* (9), 513–520.
- (27) Blasco, M.; Lee, H. W.; Hande, M. P.; Samper, E.; Lansdorp, P. M.; DePinho, R. a; Greider, C. W. Telomere Shortening and Tumor Formation by Mouse Cells Lacking Telomerase RNA. *Cell* **1997**, *91* (1), 25–34.
- (28) Kim, N. W.; Piatyszek, M. A.; Prowse, K. R.; Harley, C. B.; West, M. D.; Ho, P. L. C.; Coviello, G. M.; Wright, W. E.; Weinrich, S. L.; Shay, J. W. Specific Association of Human Telomerase Activity with Immortal Cells and Cancer. *Science*. **1994**, *266*, 2011–2015.
- (29) Hahn, W. C.; Meyerson, M. Telomerase Activation, Cellular Immortalization and Cancer. *Ann. Med.* **2001**, *33* (2), 123–129.
- (30) Wang, Y.; Cheng, F. X.; Yuan, X. L.; Tang, W. J.; Shi, J. B.; Liao, C. Z.; Liu, X. H. Dihydropyrazole Derivatives as Telomerase Inhibitors: Structure-Based Design,

- Synthesis, SAR and Anticancer Evaluation *in Vitro* and *in Vivo*. *Eur. J. Med. Chem.* **2016**, *112*, 231–251.
- (31) Shi, J. B.; Tang, W. J.; Qi, X. B.; Li, R.; Liu, X. H. Novel Pyrazole-5-Carboxamide and Pyrazole-Pyrimidine Derivatives: Synthesis and Anticancer Activity. *Eur. J. Med. Chem.* **2015**, *90*, 889–896.
- (32) Yadav, N.; Lee, J.; Kim, J.; Shen, J.; Hu, M. C.-T.; Aldaz, C. M.; Bedford, M. T. Specific Protein Methylation Defects and Gene Expression Perturbations in Coactivator-Associated Arginine Methyltransferase 1-Deficient Mice. *Proc. Natl. Acad. Sci.* **2003**, *100* (11), 6464–6468.
- (33) Bedford, M. T.; Clarke, S. G. Protein Arginine Methylation in Mammals: Who, What, and Why. *Mol. Cell* **2009**, *33* (1), 1–13.
- (34) Cheng, D.; Côté, J.; Shaaban, S.; Bedford, M. T. The Arginine Methyltransferase CARM1 Regulates the Coupling of Transcription and mRNA Processing. *Mol. Cell* **2007**, *25* (1), 71–83.
- (35) Covic, M.; Hassa, P. O.; Saccani, S.; Buerki, C.; Meier, N. I.; Lombardi, C.; Imhof, R.; Bedford, M. T.; Natoli, G.; Hottiger, M. O. Arginine Methyltransferase CARM1 Is a Promoter-Specific Regulator of NF- κ B-Dependent Gene Expression. *EMBO J.* **2005**, *24* (1), 85–96.
- (36) An, W.; Kim, J.; Roeder, R. G. Ordered Cooperative Functions of PRMT1, p300, and CARM1 in Transcriptional Activation by p53. *Cell* **2004**, *117* (6), 735–748.
- (37) Zhang, M.; Wu, W.; Gao, M.; Zhang, J.; Ding, X.; Zhu, R.; Chen, H.; Fei, Z. Coactivator-Associated Arginine Methyltransferase 1 Promotes Cell Growth and Is Targeted by microRNA-195-5p in Human Colorectal Cancer. *Tumor Biol.* **2017**, *39* (3), 101042831769430.
- (38) Elakoum, R.; Gauchotte, G.; Oussalah, A.; Wissler, M. P.; Clément-Duchêne, C.; Vignaud, J. M.; Guéant, J. L.; Namour, F. CARM1 and PRMT1 Are Dysregulated in Lung Cancer without Hierarchical Features. *Biochimie* **2014**, *97* (1), 210–218.
- (39) Ye, F.; Zhang, W.; Lu, W.; Xie, Y.; Jiang, H.; Jin, J.; Luo, C. Identification of Novel Inhibitors against Coactivator Associated Arginine Methyltransferase 1 Based on Virtual Screening and Biological Assays. *Biomed Res. Int.* **2016**, *2016*, 7086390.
- (40) Kaniskan, H. Ü.; Eram, M. S.; Liu, J.; Smil, D.; Martini, M. L.; Shen, Y.; Santhakumar, V.; Brown, P. J.; Arrowsmith, C. H.; Vedadi, M.; Jin, J. Design and

- Synthesis of Selective, Small Molecule Inhibitors of Coactivator-Associated Arginine Methyltransferase 1 (CARM1). *Med. Chem. Commun.* **2016**, 7 (9), 1793–1796.
- (41) Sack, J. S.; Thieffine, S.; Bandiera, T.; Fasolini, M.; Duke, G. J.; Jayaraman, L.; Kish, K. F.; Klei, H. E.; Purandare, A. V.; Rosettani, P.; Troiani, S.; Xie, D.; Bertrand, J. A. Structural Basis for CARM1 Inhibition by Indole and Pyrazole Inhibitors. *Biochem. J.* **2011**, 436 (2), 331–339.
- (42) Huynh, T.; Chen, Z.; Pang, S.; Geng, J.; Bandiera, T.; Bindi, S.; Vianello, P.; Roletto, F.; Thieffine, S.; Galvani, A.; Vaccaro, W.; Poss, M. A.; Trainor, G. L.; Lorenzi, M. V.; Gottardis, M.; Jayaraman, L.; Purandare, A. V. Optimization of Pyrazole Inhibitors of Coactivator Associated Arginine Methyltransferase 1 (CARM1). *Bioorg. Med. Chem. Lett.* **2009**, 19 (11), 2924–2927.
- (43) Therrien, E.; Larouche, G.; Manku, S.; Allan, M.; Nguyen, N.; Styhler, S.; Robert, M. F.; Goulet, A. C.; Besterman, J. M.; Nguyen, H.; Wahhab, A. 1,2-Diamines as Inhibitors of Co-Activator Associated Arginine Methyltransferase 1 (CARM1). *Bioorg. Med. Chem. Lett.* **2009**, 19 (23), 6725–6732.
- (44) Boggon, T. J.; Eck, M. J. Structure and Regulation of Src Family Kinases. *Oncogene* **2004**, 23 (48), 7918–7927.
- (45) Roskoski, R. Src Protein-Tyrosine Kinase Structure, Mechanism, and Small Molecule Inhibitors. *Pharmacol. Res.* **2015**, 94, 9–25.
- (46) Kravchenko, D. S.; Frolova, E. I.; Kravchenko, J. E.; Chumakov, S. P. Role of PDLIM4 and c-Src in Breast Cancer Progression. *Mol. Biol.* **2016**, 50 (1), 59–68.
- (47) Shukla, D.; Meng, Y.; Roux, B.; Pande, V. S. Activation Pathway of Src Kinase Reveals Intermediate States as Targets for Drug Design. *Nat. Commun.* **2014**, 5, 3397.
- (48) Yeatman, T. J. A Renaissance for SRC. *Nat. Rev. Cancer* **2004**, 4 (6), 470–480.
- (49) Ito, H.; Gardner-Thorpe, J.; Zinner, M. J.; Ashley, S. W.; Whang, E. E. Inhibition of Tyrosine Kinase Src Suppresses Pancreatic Cancer Invasiveness. *Surgery* **2003**, 134 (2), 221–226.
- (50) Verbeek, B. S.; Vroom, T. M.; Adriaansen-Slot, S. S.; Ottenhoff-Kalff, A. E.; Geertzema, J. G. N.; Hennipman, A.; Rijksen, G. C-Src Protein Expression Is Increased in Human Breast Cancer. An Immunohistochemical and Biochemical

- Analysis. *J. Pathol.* **1996**, *180* (4), 383–388.
- (51) Wiener, J. R.; Windham, T. C.; Estrella, V. C.; Parikh, N. U.; Thall, P. F.; Deavers, M. T.; Bast, R. C.; Mills, G. B.; Gallick, G. E. Activated SRC Protein Tyrosine Kinase Is Overexpressed in Late-Stage Human Ovarian Cancers. *Gynecol. Oncol.* **2003**, *88* (1), 73–79.
- (52) Mao, W.; Irby, R.; Coppola, D.; Fu, L.; Wloch, M.; Turner, J.; Yu, H.; Garcia, R.; Jove, R.; Yeatman, T. J. Activation of c-Src by Receptor Tyrosine Kinases in Human Colon Cancer Cells with High Metastatic Potential. *Oncogene* **1997**, *15* (25), 3083–3090.
- (53) Lorente, D.; De Bono, J. S. Molecular Alterations and Emerging Targets in Castration Resistant Prostate Cancer. *Eur. J. Cancer* **2014**, *50* (4), 753–764.
- (54) Carraro, F.; Pucci, A.; Naldini, A.; Schenone, S.; Bruno, O.; Ranise, A.; Bondavalli, F.; Brullo, C.; Fossa, P.; Menozzi, G.; Mosti, L.; Manetti, F.; Botta, M. Pyrazolo[3,4-D]pyrimidines Endowed with Antiproliferative Activity on Ductal Infiltrating Carcinoma Cells. *J. Med. Chem.* **2004**, *47* (7), 1595–1598.
- (55) Kaur, G.; Dufour, J. M. Cell Lines: Valuable Tools or Useless Artifacts. *Spermatogenesis* **2012**, *2* (1), 1–5.
- (56) Pan, C.; Kumar, C.; Bohl, S.; Klingmueller, U.; Mann, M. Comparative Proteomic Phenotyping of Cell Lines and Primary Cells to Assess Preservation of Cell Type-Specific Functions. *Mol. Cell. Proteomics* **2009**, *8* (3), 443–450.
- (57) Antonini, I.; Polucci, P.; Magnano, A.; Martelli, S. Synthesis, Antitumor Cytotoxicity, and DNA-Binding of Novel *N*-5,2-Di(omega-Aminoalkyl)-2,6-dihydropyrazolo[3,4,5-*Kl*]acridine-5-Carboxamides. *J. Med. Chem.* **2001**, *44* (20), 3329–3333.
- (58) Abadi, A. H.; Eissa, A. A. H.; Hassan, G. S. Synthesis of Novel 1,3,4-Trisubstituted Pyrazole Derivatives and Their Evaluation as Antitumor and Antiangiogenic Agents. *Chem. Pharm. Bull. (Tokyo)*. **2003**, *51* (7), 838–844.
- (59) Shaw, A. Y.; Liao, H. H.; Lu, P. J.; Yang, C. N.; Lee, C. H.; Chen, J. Y.; Xu, Z.; Flynn, G. 3,5-Diaryl-1H-Pyrazole as a Molecular Scaffold for the Synthesis of Apoptosis-Inducing Agents. *Bioorg. Med. Chem.* **2010**, *18* (9), 3270–3278.
- (60) D'Alessio, R.; Bargiotti, A.; Metz, S.; Brasca, M. G.; Cameron, A.; Ermoli, A.; Marsiglio, A.; Polucci, P.; Roletto, F.; Tibolla, M.; Vazquez, M. L.; Vulpetti, A.;

- Pevarello, P. Benzodipyrzoles: A New Class of Potent CDK2 Inhibitors. *Bioorg. Med. Chem. Lett.* **2005**, *15* (5), 1315–1319.
- (61) Hansen, R. D. Molecular Epidemiology of Colorectal Cancer. *Int. J. Mol. Epidemiol. Genet.* **2007**, *7* (3), 105–114.
- (62) Zhang, K.; Civan, J.; Mukherjee, S.; Patel, F.; Yang, H. Genetic Variations in Colorectal Cancer Risk and Clinical Outcome. *World J. Gastroenterol.* **2014**, *20* (15), 4167–4177.
- (63) Abdelgawad, M. A.; Bakr, R. B.; Alkhoja, O. A.; Mohamed, W. R. Design, Synthesis and Antitumor Activity of Novel pyrazolo[3,4-*d*]pyrimidine Derivatives as EGFR-TK Inhibitors. *Bioorg. Chem.* **2016**, *66*, 88–96.
- (64) Lukasik, P. M.; Elabar, S.; Lam, F.; Shao, H.; Liu, X.; Abbas, A. Y.; Wang, S. Synthesis and Biological Evaluation of imidazo[4,5-*b*]pyridine and 4-Heteroaryl-Pyrimidine Derivatives as Anti-Cancer Agents. *Eur. J. Med. Chem.* **2012**, *57*, 311–322.
- (65) Furrakh, M. Tobacco Smoking and Lung Cancer: Perception-Changing Facts. *Sultan Qaboos Univ. Med. J.* **2013**, *13* (3), 345–358.
- (66) Zappa, C.; Mousa, S. A. Non-Small Cell Lung Cancer: Current Treatment and Future Advances. *Transl. Lung Cancer Res.* **2016**, *5* (3), 288–300.
- (67) Xia, Y.; Dong, Z. W.; Zhao, B. X.; Ge, X.; Meng, N.; Shin, D. S.; Miao, J. Y. Synthesis and Structure-Activity Relationships of Novel 1-Arylmethyl-3-Aryl-1*H*-Pyrazole-5-Carbohydrazide Derivatives as Potential Agents against A549 Lung Cancer Cells. *Bioorg. Med. Chem.* **2007**, *15* (22), 6893–6899.
- (68) Lian, S.; Su, H.; Zhao, B. X.; Liu, W. Y.; Zheng, L. W.; Miao, J. Y. Synthesis and Discovery of Pyrazole-5-Carbohydrazide *N*-Glycosides as Inducer of Autophagy in A549 Lung Cancer Cells. *Bioorg. Med. Chem.* **2009**, *17* (20), 7085–7092.
- (69) Plummer, M.; Franceschi, S.; Vignat, J.; Forman, D.; De Martel, C. Global Burden of Gastric Cancer Attributable to *H. Pylori*. *Int. J. Cancer* **2015**, *136* (2), 487–490.
- (70) Webb, P. M.; Law, M.; Varghese, C.; Forman, D. Gastric Cancer and *Helicobacter Pylori*: A Combined Analysis of 12 Case Control Studies Nested within Prospective Cohorts. *Gut* **2001**, *49* (3), 347–353.
- (71) Zhang, D.; Wang, G.; Zhao, G.; Xu, W.; Huo, L. Synthesis and Cytotoxic Activity of Novel 3-(1*H*-Indol-3-yl)-1*H*-Pyrazole-5- Carbohydrazide Derivatives. *Eur. J.*

- Med. Chem.* **2011**, *46* (12), 5868–5877.
- (72) Yao, Y.; Liao, C.; Li, Z.; Wang, Z.; Sun, Q.; Liu, C.; Yang, Y.; Tu, Z.; Jiang, S. Design, Synthesis, and Biological Evaluation of 1,3-Disubstituted-Pyrazole Derivatives as New Class I and IIb Histone Deacetylase Inhibitors. *Eur. J. Med. Chem.* **2014**, *86*, 639–652.
- (73) Rockwell, S.; Dobrucki, I. T.; Kim, E. Y.; Marrison, S. T.; Vu, V. T. Hypoxia and Radiation Therapy: Past History, Ongoing Research, and Future Promise. *Curr. Mol. Med.* **2009**, *9* (4), 442–458.
- (74) Sabari, C. L.; Sivakumar, K.; Rajamohan, R. Improvement of Cytotoxic Activity of Local Anesthetics against Human Breast Cancer Cell Line through the Cyclodextrin Complexes. *J. Macromol. Sci. Part A Pure Appl. Chem.* **2017**, *54* (6), 402–410.
- (75) Ringhieri, P.; Morelli, G.; Accardo, A. Supramolecular Delivery Systems for Non-Platinum Metal-Based Anticancer Drugs. *Crit. Rev. Ther. Drug Carr. Syst.* **2017**, *34* (2), 149–183.
- (76) Messori, L.; Gonzales Vilchez, F.; Vilaplana, R.; Piccioli, F.; Alessio, E.; Keppler, B. Binding of Antitumor Ruthenium(III) Complexes to Plasma Proteins. *Met. Based. Drugs* **2000**, *7* (6), 335–342.
- (77) Allardyce, C. S.; Dyson, P. J. Ruthenium in Medicine: Current Clinical Uses and Future Prospects. *Platin. Met. Rev.* **2001**, *45* (2), 62–69.
- (78) Klein, A. V.; Hambley, T. W. Platinum Drug Distribution in Cancer Cells and Tumors. *Chem. Rev.* **2009**, *109* (10), 4911–4920.
- (79) Frik, M.; Martínez, A.; Elie, B. T.; Gonzalo, O.; Ramírez De Mingo, D.; Sanaú, M.; Sánchez-Delgado, R.; Sadhukha, T.; Prabha, S.; Ramos, J. W.; Marzo, I.; Contel, M. *In Vitro* and *in Vivo* Evaluation of Water-Soluble Iminophosphorane Ruthenium(II) Compounds. A Potential Chemotherapeutic Agent for Triple Negative Breast Cancer. *J. Med. Chem.* **2014**, *57* (23), 9995–10012.
- (80) Antonarakis, E. S.; Emadi, A. Ruthenium-Based Chemotherapeutics: Are They Ready for Prime Time? *Cancer Chemother. Pharmacol.* **2010**, *66* (1), 1–9.
- (81) Hartinger, C. G.; Zorbas-Seifried, S.; Jakupec, M. A.; Kynast, B.; Zorbas, H.; Keppler, B. K. From Bench to Bedside - Preclinical and Early Clinical Development of the Anticancer Agent Indazolium *Trans*-[tetrachlorobis(1*H*-indazole)ruthenate(III)] (KP1019 or FFC14A). *J. Inorg. Biochem.* **2006**, *100* (5–6),

- 891–904.
- (82) Flocke, L. S.; Trondl, R.; Jakupec, M. A.; Keppler, B. K. Molecular Mode of Action of NKP-1339 – a Clinically Investigated Ruthenium-Based Drug – Involves ER- and ROS-Related Effects in Colon Carcinoma Cell Lines. *Invest. New Drugs* **2016**, *34* (3), 261–268.
- (83) Seelig, M. H.; Berger, M. R.; Keppler, B. K. Antineoplastic Activity of Three Ruthenium Derivatives against Chemically Induced Colorectal Carcinoma in Rats. *J. Cancer Res. Clin. Oncol.* **1992**, *118* (3), 195–200.
- (84) Lentz, F.; Drescher, A.; Lindauer, A.; Henke, M.; Hilger, R. a; Hartinger, C. G.; Scheulen, M. E.; Dittrich, C.; Keppler, B. K.; Jaehde, U. Pharmacokinetics of a Novel Anticancer Ruthenium Complex (KP1019, FFC14A) in a Phase I Dose-Escalation Study. *Anticancer. Drugs* **2009**, *20* (2), 97–103.
- (85) Hartinger, C. G.; Jakupec, M. A.; Zorbas-Seifried, S.; Groessl, M.; Egger, A.; Berger, W.; Zorbas, H.; Dyson, P. J.; Keppler, B. K. KP1019, a New Redox-Active Anticancer Agent - Preclinical Development and Results of a Clinical Phase I Study in Tumor Patients. *Chem. Biodivers.* **2008**, *5* (10), 2140–2155.
- (86) Trondl, R.; Heffeter, P.; Kowol, C. R.; Jakupec, M. A.; Berger, W.; Keppler, B. K. NKP-1339, the First Ruthenium-Based Anticancer Drug on the Edge to Clinical Application. *Chem. Sci.* **2014**, *5* (8), 2925–2932.
- (87) Silva, V. L. M.; Silva, A. M. S.; Pinto, D. C. G. A.; Cavaleiro, J. A. S.; Elguero, J. Synthesis of (*E*)- and (*Z*)-3(5)-(2-Hydroxyphenyl)-4-Styrylpyrazoles. *Monatsh. Chem.* **2009**, *140* (1), 87–95.
- (88) Koenigs, W.; Knorr, E. Ueber Einige Derivate Des Traubenzuckers Und Der Galactose. *Berichte der Dtsch. Chem. Gesellschaft* **1901**, *34* (1), 957–981.
- (89) Leigh, G. J.; Favre, H. A.; Metanomski, W. V. Principles of Chemical Nomenclature 2011: A Guide to IUPAC Recommendations; 1998.
- (90) Silva, V. L. M.; Silva, A. M. S.; Pinto, D. C. G. A.; Cavaleiro, J. A. S.; Patonay, T. Condensation of Chromone-3-Carboxaldehyde with Phenylacetic Acids: An Efficient Synthesis of (*E*)-3-Styrylchromones. *Synlett* **2004**, *15*, 2717–2720.
- (91) Silva, V. L. M. “Síntese E Transformação de 3-Estirilcromonas E 3-(2-Hidroxifenil)pirazóis Com Potencial Atividade Analgésica.” *Universidade de Aveiro* **2006**.

- (92) Crich, D. Mechanism of a Chemical Glycosylation Reaction. *Acc. Chem. Res.* **2010**, *43* (8), 1144–1153.
- (93) Hung, S. C.; Zulueta, M. M. L. *Glycochemical Synthesis: Strategies and Applications*, 1st edition; *Wiley*, **2016**.
- (94) Demchenko, A. V. *Handbook of Chemical Glycosylation: Advances in Stereoselectivity and Therapeutic Relevance*, 1st edition; *Wiley-VCH*, **2008**.
- (95) Pathak, V. P. A Convenient Method for *O*-Deacetylation Using Ira-400(OH) Resin. *Synth. Commun.* **1993**, *23* (1), 83–85.
- (96) Sandulache, A.; Silva, A. M. S.; Pinto, D. C. G. a.; Almeida, L. M. P. M.; Cavaleiro, J. a. S. Wittig Reactions of Chromone-3-Carboxaldehydes with Benzylidenetriphenyl Phosphoranes: A New Synthesis of 3-Styrylchromones. *New J. Chem.* **2003**, *27* (11), 1592.
- (97) Krishnakumar, V.; Jayamani, N.; Mathammal, R. Molecular Structure, Vibrational Spectral Studies of Pyrazole and 3,5-Dimethyl Pyrazole Based on Density Functional Calculations. *Spectrochim. Acta A* **2011**, *79* (5), 1959–1968.
- (98) Nava, D.; de Parada, T. R.; González, E.; Boscàn, N.; De La Cruz, C. An Infrared Spectroscopic Comparison of Cis- and Trans-CH=CH and Vinyl CH=CH₂ Group Frequencies of Some Hexenes, Heptenes, and Stereospecific and Non-Stereospecific Polybutadienes. *Spectrochim. Acta A* **1996**, *52* (10), 1201–1210.
- (99) Orellana, E.; Kasinski, A. Sulforhodamine B (SRB) Assay in Cell Culture to Investigate Cell Proliferation. *Bio-Protocol* **2016**, *6* (21).
- (100) Da Violante, G.; Zerrouk, N.; Richard, I.; Provot, G.; Chaumeil, J. C.; Arnaud, P. Evaluation of the Cytotoxicity Effect of Dimethyl Sulfoxide (DMSO) on Caco2/TC7 Colon Tumor Cell Cultures. *Biol. Pharm. Bull.* **2002**, *25* (12), 1600–1603.
- (101) Präbst, K.; Engelhardt, H.; Ringgeler, S.; Hübner, H. Basic Colorimetric Proliferation Assays: MTT, WST, and Resazurin; *Methods in Molecular Biology* **2017**, *1601*, 1–17.
- (102) Videira, R. A.; Andrade, P. B.; Monteiro, L. S.; Valentão, P.; Ferreira, P. M. T.; Pereira, D. M. Toxicity and Structure-Activity Relationship (SAR) of α,β -Dehydroamino Acids against Human Cancer Cell Lines. *Toxicol. In Vitro* **2018**, *47*, 26–37.